Article

Application of Structure-Based Design and Parallel Chemistry to Identify a Potent, Selective, and Brain Penetrant Phosphodiesterase 2A Inhibitor

Christopher J. Helal, Eric P Arnold, Tracey L Boyden, Cheng Chang, Thomas A. Chappie, Kimberly F. Fennell, Michael D Forman, Mihaly Hajós, John F. Harms, William E. Hoffmann, John M. Humphrey, Zhijun Kang, Robin J. Kleiman, Bethany L. Kormos, Che-Wah Lee, Jiemin Lu, Noha Maklad, Laura McDowell, Scot Mente, Rebecca E O'Connor, Jayvardhan Pandit, Mary Piotrowski, Anne W. Schmidt, Christopher J. Schmidt, Hirokazu Ueno, Patrick R. Verhoest, and Edward X. Yang

J. Med. Chem., **Just Accepted Manuscript** • Publication Date (Web): 02 Jun 2017

Application of Structure-Based Design and Parallel Chemistry to Identify a Potent, Selective, and Brain Penetrant Phosphodiesterase 2A Inhibitor

Christopher J. Helal,*[a] Eric P. Arnold,[a] Tracey L. Boyden,[a] Cheng Chang,[d] Thomas A. Chappie,[b] Kimberly F. Fennell,[a] Michael D. Forman,[a] Mihaly Hajos,[b] John F. Harms,[b] William E. Hoffman,[b] John M. Humphrey,[a] Zhijun Kang,[a] Robin J. Kleiman,[b] Bethany L. Kormos,[b] Che-Wah Lee,[a] , Jiemin Lu,[a] Noha Maklad,[a] Laura McDowell,[a] Scot Mente,[b] Rebecca E. O'Connor,[a] Jayvardhan Pandit,[a] Mary Piotrowski,[a] Anne W. Schmidt,[a] Christopher J. Schmidt,[b] Hirokazu Ueno,[a] Patrick R. Verhoest,[b] and Edward X. Yang[a]

[a]Pfizer Worldwide Research and Development, Eastern Point Road, Groton, CT 06340
[b]Pfizer Worldwide Research and Development, 610 Main Street, Cambridge, MA 02139

KEYWORDS: phosphodiesterase, parallel chemistry, structure-based drug design, protein x-ray crystallography, brain penetration, schizophrenia, cognition, radio ligand, cyclic guanosine monophosphate, ketamine, MK-801, radial arm maze, electroencephalogram

ABSTRACT: Phosphodiesterase 2A (PDE2A) inhibitors have been reported to demonstrate *in vivo* activity in preclinical models of cognition. In order to more fully explore the biology of PDE2A inhibition we sought to identify potent PDE2A inhibitors with improved brain penetration as compared to current literature compounds. Applying estimated human dose

calculations while simultaneously leveraging synthetically enabled chemistry and structure-based drug design has resulted in a highly potent, selective, brain penetrant compound **71** (PF-05085727) that effects *in vivo* biochemical changes commensurate with PDE2A inhibition along with behavioral and electrophysiological reversal of the effects of NMDA antagonists in rodents. This data supports the ability of PDE2A inhibitors to potentiate NMDA signaling and their further development for clinical cognition indications.

Introduction

Phosphodiesterases (PDEs) are enzymes that catalyze the hydrolysis of the key second messenger cyclic nucleotides cAMP and cGMP to their respective acyclic variants (AMP, GMP). PDE inhibitors have demonstrated therapeutic potential for a range of conditions such as pulmonary hypertension (sildenafil, PDE5 inhibitor), erectile dysfunction (sildenafil, vardenafil, tadalafil, PDE5 inhibitors), chronic obstructive pulmonary disease (roflumilast, PDE4 inhibitor), psoriasis and psoriatic arthritis (apremilast, PDE4 inhibitor), and heart failure (milrinone, PDE3 inhibitor) reflecting the wide range of biological functions regulated by cyclic nucleotide signaling. The abundant expression of PDEs in the human brain, coupled with a requisite role for cyclic nucleotides in neurotransmission and synaptic plasticity, has prompted efforts to discover PDE selective inhibitors with brain penetration suitable for treating neurological and psychiatric disorders. Brain penetrant clinical candidates have been disclosed as inhibitors for PDE10A for the treatment of schizophrenia and Huntington's Disease[1,2] as well as PDE9A inhibitors for treatment of cognitive disorders.[3,4]

Inhibitors of PDE2A have been reported to demonstrate activity in a variety of pre-clinical models that are suggestive of cognitive improvement. This includes enhanced performance in

rodent novel object recognition and social recognition tasks and a reversal of performance deficits produced by treatment with the N-methyl-D-aspartate (NMDA) antagonist MK-801 in the alternating T-maze.[5] These behavioral effects are consistent with reports of enhanced hippocampal long-term potentiation, a measure of synaptic plasticity thought to underpin some forms of learning and memory. Additional data suggests that PDE2A inhibitors can reverse anxiolytic behavior in mice via cGMP-mediated processes.[6] This aggregate information encouraged our investment in the discovery of potent, selective, and brain penetrant PDE2A inhibitors to more effectively probe the potential of this class of molecules to treat a range of neurological disorders. For medicinal chemistry lead optimization, tracking binding efficiency and minimizing estimated human dose were supported by structure-based drug design and parallel synthesis strategies.

Results

The potent imidazotriazinone PDE2A inhibitor **1** (BAY 60-7550), PDE2A IC_{50} = 0.5 nM (our assay), 4.7 nM (literature assay)[5]) has most often been used to explore the pharmacology of PDE2A inhibition[7] (Table 1). A ligand efficiency (LE)[8] of 0.37 (based upon our assay) indicated a high binding efficiency, and a lipophilic ligand efficiency (LLE)[9] of 6.7 placed **1** in a range comparable to clinical candidates with a desirable balance between potency and lipophilicity. Selectivity of **1** for PDE2A as compared to PDE1B (PDE1B IC_{50}/PDE2A IC_{50}) was ca. 500-fold and significantly higher for all other PDEs (PDE3A/4D/5-11). ADME measurements revealed **1** to have high human liver microsome (HLM) clearance as represented by the apparent intrinsic clearance (HLM CL_{int}), short half-life ($t_{1/2}$) in rat liver microsomes (3 min) and significant efflux in a P-glycoprotein (P-gP) multidrug resistance protein (MDR1) over expressing cell line which is indicative of high probability of impaired brain penetration.[10]

Table 1: Potency, selectivity, and *in vitro* ADME properties of PDE2A inhibitor **1** (**1**)

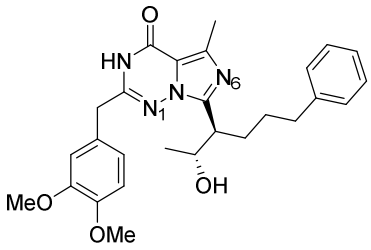

1

PDE2A IC_{50} (nM)	0.5
PDE Selectivity	534x (PDE1B) ≥1000x (PDE3A/4D/5-11)
LE (LipE)	0.37 (6.9)
HLM, CL_{int}[a]	219
MDR1 BA/AB[b]	16.2
# RB	10

a) values represent the HLM Clint,apparent scaled (μΛ/min/kg).; *b)* AB = Apical to basolateral; BA = Basolateral to apical; *c)* cpKa = calculated acid dissociation constant;

While **1** is a sufficient PDE2A inhibitor tool compound for *in vitro* studies, *in vivo* exposure both peripherally and in brain would be predicted to be poor. Indeed, low *in vivo* brain exposure has been reported recently[11] and was corroborated in similar experiments by us (see Supporting Information).

An x-ray crystal structure of **1** bound to PDE2A was determined which showed the binding mode in the active site, and allowed development of a plausible hypothesis to explain the selectivity profile of **1** (Figure 1). This crystal structure, determined independently, is isomorphous to the one described by Zhu et al, [12] with an r.m.s. deviation of 0.39 angstroms for

all backbone Cα atoms. We highlight here the critical features of the structure that we exploited in our subsequent medicinal chemistry design strategy. An induced pocket is seen, formed by the movement of Leu770, which accommodates binding of the propylphenyl group. The induced pocket, lined by mainly hydrophobic residues (Leu770, Leu809, Ile870, His773 and Leu774) had not previously been observed in any PDE structure, and is absent in all the previous PDE2 crystal structures we had determined. We hypothesized that compounds capable of inducing this conformational change in PDE2 would retain the relatively high PDE selectivity of **1**. The conserved glutamine at the back of the binding pocket (Gln859) makes a pair of hydrogen bonds with the imidazotriazinone core C=O(NH). Gln859 assumes the same rotamer as it would if bound to cGMP. A water molecule that is bound by the sidechain of Tyr655 and backbone carbonyl of Asp808 donates a hydrogen bond to N-6 of **1**.

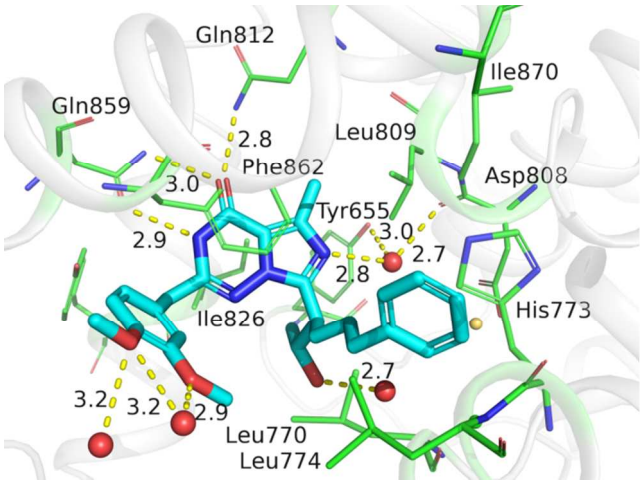

Figure 1. X-ray structure of **1** bound to PDE2A cyclic nucleotide binding site (hydrogen bond distances in angstroms). Polar hydrogen atoms used in *in silico* docking calculations have been indicated in their modeled positions in this and all other figures.

Based upon the challenges with modifying **1** to attain the desired alignment of potency, selectivity, and ADME parameters, alternative PDE2A inhibitor lead matter was sought. High-

throughput screening identified two novel series of PDE2A inhibitors: a pyrazolo[3,4-*d*]pyrimidine series (**2**) and a [1,2,4]triazolo[4,3-a]pyrazine series (**3**) (Tables 2 and 3). Both **2** and **3** lacked the HBDs in **1** that potentially contributed to the observed efflux in the MDR1 BA/AB assay, resulting in poor *in vivo* brain penetration. Our goal was to achieve equivalent potency to **1** and equally high (or higher PDE selectivity) with these new series during lead development while maintaining the CNS-penetration favoring physical properties.

Table 2. Potency, selectivity, *in vitro* ADME and physical properties of series **2** and **3** identified via a PDE2A high throughput screen

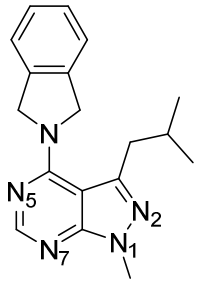

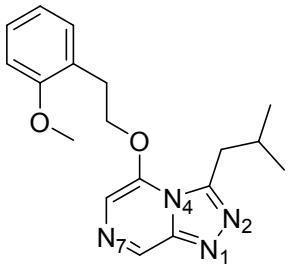

	2	**3**
PDE2A IC_{50} (nM)	146.4	389.6
LE (LipE)	0.42 (3.9)	0.37 (2.7)
HLM Cl_{int}	123	>287
MDR1 BA/AB	1.6	1.2
# RB	3	7
estimated human dose (mg/day)[a]	8787	>44142

a) estimated human dose (mg/day) = (10 x PDE2A IC_{50} x HLM CL_{int} x 24h x 70 kg) / (MDR1 BA/AB); see Equation 1.

Table 3. PDE Selectivity Profiles of **2** and **3**[a]

	1B	3A	4D	5A	6	7B	8B	9A	10A	11A
2	42	23	23	3	17	69	>615	>615	0.05	0.3
3	7	6	29	71	69	16	206	>231	5	0.4

a) PDE selectivity is measured as the ratio of PDEX IC_{50} / PDE2A IC_{50}.

Another goal of the lead optimization process was to minimize the estimated human dose since higher human drug dosages are strongly correlated with idiosyncratic adverse drug reactions.[13] The equation used for estimating the human dose for a brain targeted compound is shown in Equation 1 (see Supporting Information for derivation).

$$Dose\ (mg/day) = 10 * PDE2A\ IC50 * Tau * HLM\ CL\_int * BW * MDR\ BA/AB$$

Equation 1. Human dose equation for a brain targeting compound based upon *in vitro* data. Legend: PDE2A IC_{50}: compound *in vitro* potency at the PDE2A enzyme; Tau: dosing duration (24 h was used assuming once a day dosing); HLM CL_{int} was used as a surrogate for CLint,u (unbound intrinsic clearance); BW: typical human body weight, 70 kg was used; MDR1 BA/AB: The BA/AB ratio from the MDR1 assay was used as a surrogate for brain availability.

In the case of **2**, the estimated human dose projected by using this method afforded a value of 8787 mg/day. For **3** the estimated human dose was >44142 mg/day. In both cases it was clear that significant reductions in PDE2A IC_{50} and HLM Cl_{int} would be necessary while minimizing MDR1 BA/AB values to get to the desired target of estimated human dose <100 mg/day.

In order to understand the critical binding elements for each series, PDE2A protein x-ray crystal structures were sought with compounds **2** and **3** bound. Compound **3** yielded a high-resolution crystal structure with PDE2A (Figure 2a), but attempts at obtaining an x-ray crystal structure of **2** with PDE2A were not successful. Efforts with a related compound **4** (Table 4), with a similar PDE inhibition profile as **2** that was identified via initial lead optimization efforts, were successful (Figure 2b).

Table 4: PDE2A potency and PDE selectivity profile of **4**

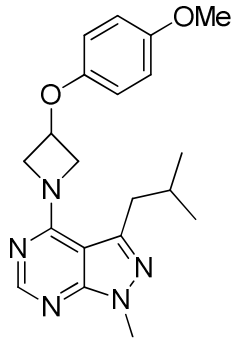

4

PDE2A IC_{50} (nM): 66.6

Fold PDE Selectivity (PDEX IC_{50}/ PDE2A IC_{50})				
1B	3B	4D	5A	6
64	4	112	11	58
7B	8B	9A	10A	11A
104	>1000	>1000	0.1	3

a) b)

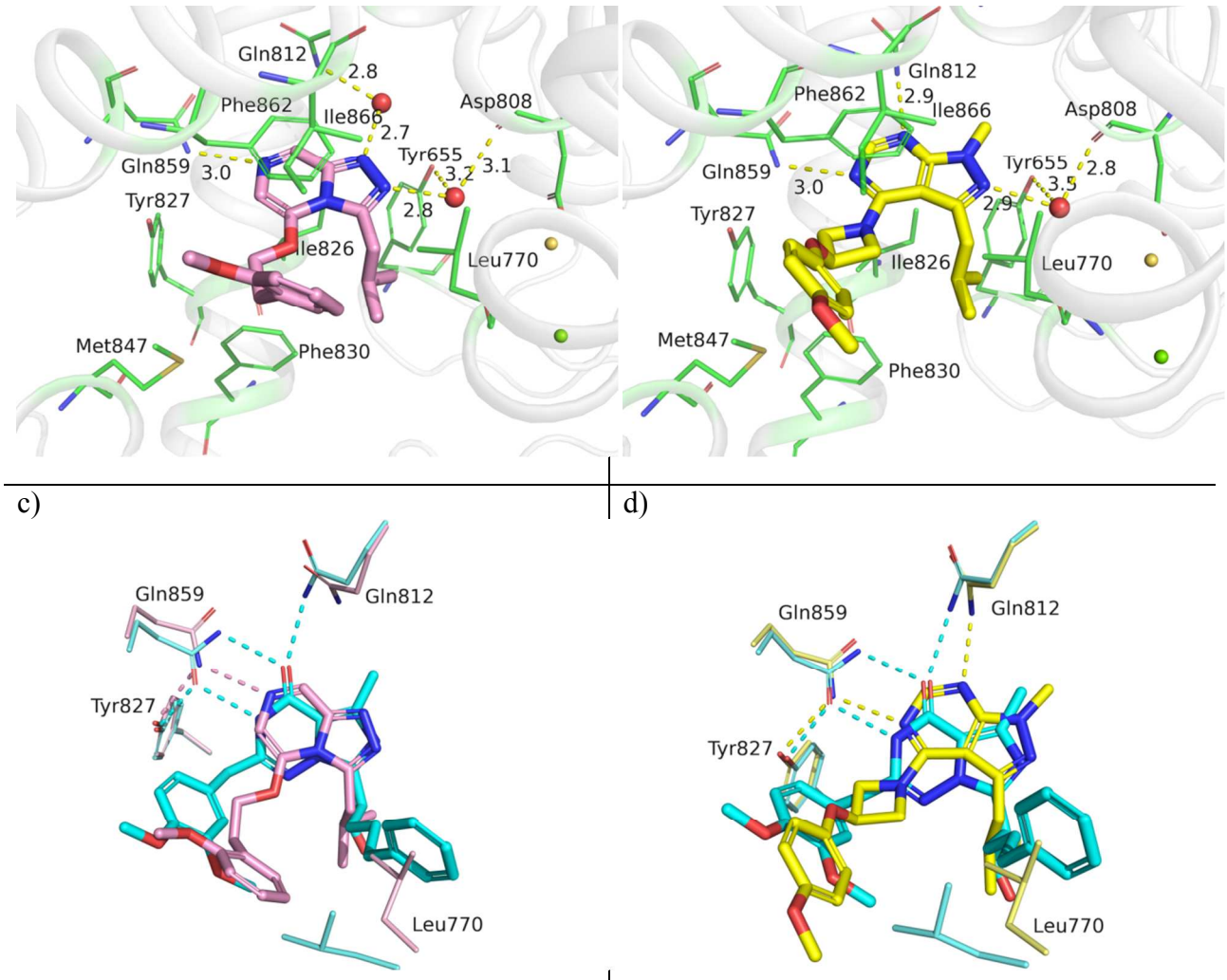

Figure 2. a) X-ray crystal structure of **3** bound to PDE2A cyclic nucleotide binding site (hydrogen bond distances in angstroms); b) X-ray crystal structure of **4** bound to PDE2A cyclic nucleotide binding site (hydrogen bond distances in angstroms); c) Overlap of PDE2A x-ray crystal structures of **3** (cyan) and **1** (blue); d) Overlap of PDE2A x-ray crystal structures of **4** (yellow) and **1** (blue).

The core heteroaromatic ring systems of **3** and **4** occupy roughly the same space as the corresponding imidazotriazinone ring system in **1** (Figures 2c and 2d). For a dual-specificity phosphodiesterase such as PDE2A, Gln859 is proposed to act as a switch, capable of freely rotating so as to form hydrogen bonds either with the exocyclic amino group of cAMP or the exocyclic carbonyl oxygen of cGMP.[14] In the structures of **3** and **4**, Gln859 must be in a flipped

orientation relative to that seen in the structure of **1** to allow for optimal protein-ligand interactions with N-7 of **3** and N-5 of **4**.

A second major difference is that **3** and **4** do not induce the conformational change in Leu770 which leads to the formation of the selectivity pocket, occupied by the phenpropyl moiety in **1**.

In all three crystal structures, substituents on the core extend towards the protein surface. The methoxy phenyl groups in **3** and **4** extend out of the substrate-binding site, and are oriented approximately perpendicular to the core ring, making an edge-to-face interaction with Phe862. These hydrophobic groups occupy a shallow channel on the surface of the protein, sandwiched between the side chains of Phe862 and Ile866 on one side and Phe830 and Met847 on the other side (Figures 2a and 2b). An important observation is that the methoxy phenyl substituents on **3** and **4** would clash with Leu770 if it were to assume the 'out' rotamer needed to create the selectivity pocket (Figures 2c and 2d).

Another common interaction is that of a core ring nitrogen (**1** – N6, **3** – N7, **4** – N2) with the structural water molecule which interacts with the sidechain of Tyr655 and the backbone carbonyl of Asp808. All three compounds also have substituents (**1** - 2-hydroxyethyl, **3** and **4** – *i*Bu) which occupy a pocket that is filled by the ribose of cyclic nucleotides.

Binding features unique to **1** and **4** relative to **3** are the interaction of C(4)=O and N-7, respectively, with Gln812. Comparatively, N-1 of **3** binds to a water molecule in the back of the pocket whereas both **1** and **4** displace the water with a methyl group (**1** – C5, **4** – N1).

The synthetic route to the pyrazolopyrimidine series (Scheme 2) entailed acylation of malonitrile (**5**) with isobutyryl chloride (**6**) as the first step to afford **7**. O-alkylation yielded **8** followed by condensation with N-methyl hydrazine to afford aminopyrazole **9**. Acidic hydrolysis of the

nitrile to primary amide (**10**) followed by condensation with formic acid yielded pyrazolopyrimidinone **11**, that was chlorinated with $POCl_3$ to yield penultimate chloro pyrazolopyrimidine **12**. S_NAr reaction of **12** with amines afforded analogs of general structure **13**.

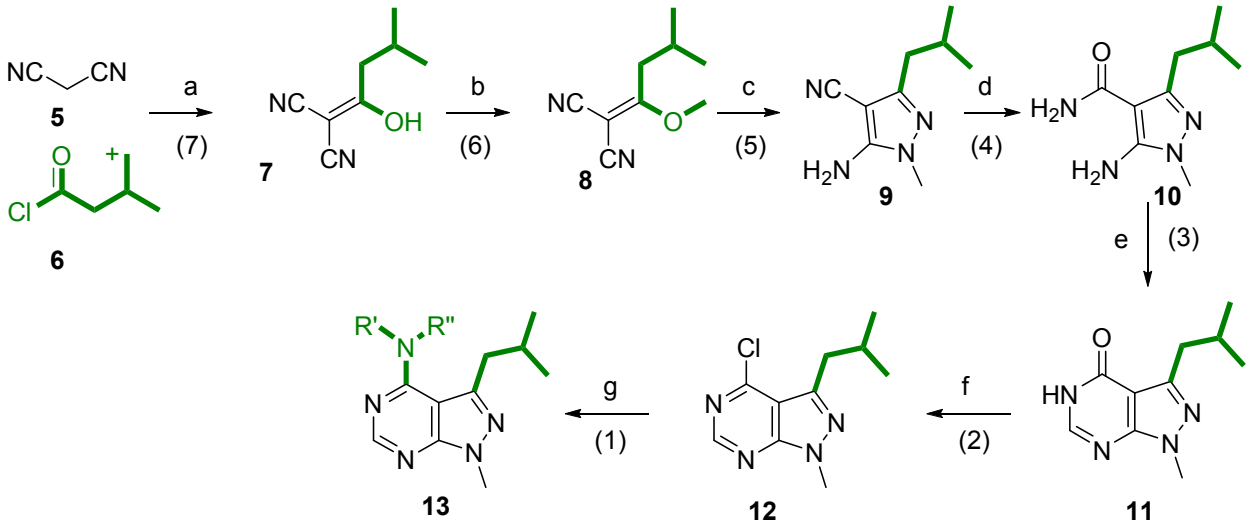

Scheme 2. Synthetic route to pyrazolo[3,4-*d*]pyrimidine targets of general structure **13** with key diversity points highlighted in green. a) NaH, THF; acid chloride, 76% b) Me_2SO_4, $NaHCO_3$, dioxane, water, 56% c) $MeNHNH_2$, EtOH, 35% d) H_2SO_4 , 68% e) HCO_2H, 71% f) $POCl_3$, crude g) R'R''NH, K_2CO_3, THF, H_2O (75% for **2**).

The synthetic route to the triazolopyrazines started with a selective S_NAr reaction between an alkoxide **14** and 2,6-dichloropyrazine (**15**) in Step 1 to afford the ether **16** (Scheme 3). A second S_NAr with hydrazine yielded **17** (Step 2). A one-pot hydrazone formation with isobutyraldehyde (**18**) followed by oxidative triazole formation with phenyl-iodoacetate in Step 3 yielded **19**. Of particular note in contrasting the synthetic routes to **13** and **19**, is that the isobutyl group in **19**,

which overlays with that of **13** in the ribose region and with the potential to access the selectivity pocket, is introduced in the last step of the synthetic sequence and is amenable to variation via parallel synthesis which is not the case for the isobutyl vector in **13**.

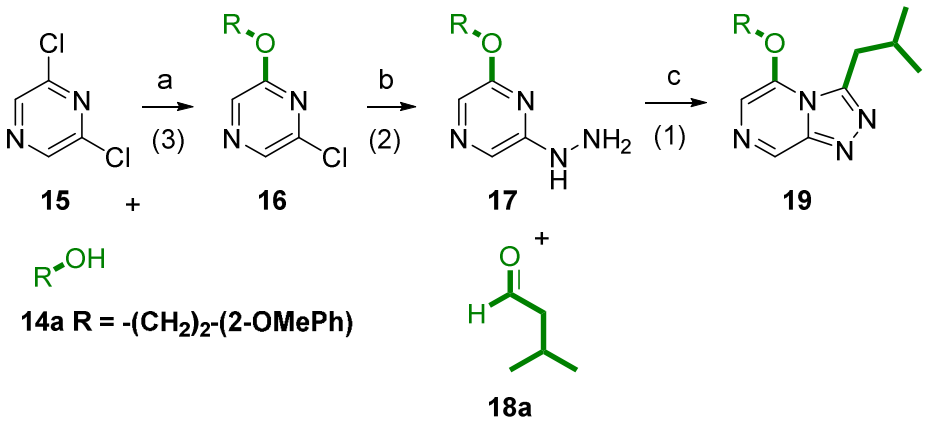

Scheme 3. Synthetic route to [1,2,4]triazolo[4,3-a]pyrazine targets of general structure **3** with key diversity points highlighted in green. a) KOtBu, CH_2Cl_2 b) NH_2NH_2, EtOH c) i. **17** + **18**, $ClCH_2CH_2Cl$; ii. (Diacetoxy)iodobenzene.

The starting hypothesis was that growing the isobutyl group of either **2** or **3** could lead to formation and filling of the PDE2A induced pocket with significant increases in both PDE2A potency and overall selectivity over other PDEs while maintaining low MDR1 BA/AB. The highly enabled nature of the isobutyl in **3** led to a parallel synthesis effort in this series. A key concern from a structural perspective during the design of the initial parallel synthesis compound sets was the observed movement of Leu770 towards the 2-methoxyphenyl group of **3** when the induced pocket is formed and the potential for negative protein-ligand interactions which could reduce potency as previously mentioned (Figure 2d).

In order to address this concern, removal of the ether substituent in the initial parallel synthesis to afford compounds of general formula **21** was undertaken, realizing that potency losses could be addressed in follow-up compounds by reincorporating ether substituents (Scheme 4).

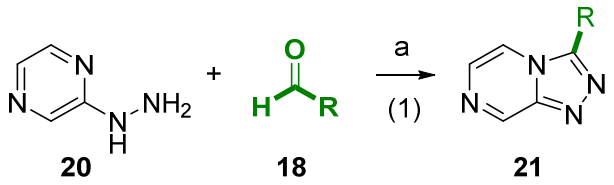

Scheme 4. One-step synthetic scheme to vary vector headed towards induced pocket. a) i. **20** + **18**, $ClCH_2CH_2Cl$; ii. (Diacetoxy)iodobenzene

More than 2000 virtual compounds were enumerated by using the available aldehydes in the Pfizer monomer file which were docked into the PDE2A x-ray crystal structure. Compounds were chosen for synthesis by using the following criteria:

1. Potential for accessing deep into the induced pocket in a manner analogous to the pendant phenyl of **1.**
2. Possible hydrogen bond interactions were observed in the ribose region, similar to the hydroxyl of **1.**

   If there were highly similar aldehyde monomers available, a representative was chosen to minimize duplication and maximize diversity of the parallel synthesis library. Compounds were removed from consideration if clear negative interactions with the protein existed.

   This lead to 484 compounds being chosen for actual synthesis in a parallel format. From this set, 283 were successfully purified by HPLC (283/484 = 58% success rate) and were screened in the PDE2A inhibition assay. From this effort one compound (**22**) was identified with μM potency and favorable physicochemical properties (Table 5).

Table 5. PDE2A potency, lipophilicity and binding efficiency of **22**

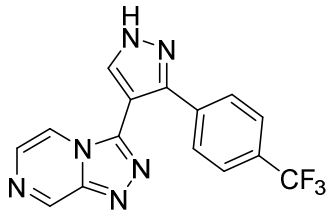

22

PDE2A IC_{50} (nM)	2107.4
clogP	2.2
LE	0.27
LipE	2.5

Computational docking of **22** in the PDE2A protein and overlay with **1** (Figure 3) suggested that the trifluoromethyl group was positioned in the same space as the pendant phenyl of **1** and that the pyrazole could engage in hydrogen-bonding interactions with tightly bound waters around the catalytic metals in a similar manner to the hydroxyl of **1**. The preferred pyrazole tautomer was not clearly defined, with the pyrazole having the potential to be either a hydrogen bond donor or acceptor. In order to further optimize this promising hit, three different approaches were explored: 1) reintroduction of the ether at the 5-position of the [1,2,4]triazolo[4,3-a]pyrazine core, 2) variation of the pyrazole nitrogen substituents to lock out a specific tautomer, and 3) evaluation of alternative aryl groups to the para-trifluoromethyl phenyl.

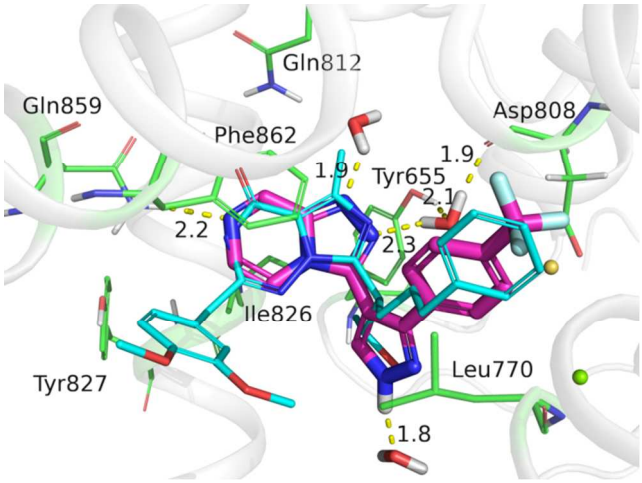

Figure 3. Modeled pose of **22** (cyan) overlayed with **1** (blue).

In the next rounds of parallel synthesis, two different parallel-enabled synthetic routes were used. The 3-step synthetic route in Scheme 3 was employed to introduce different alcohols (**14a-b**) at the 5-position to see if potency could be increased while concurrently using pyrazolo-aldehydes (**23**) from the Pfizer monomer store affording compounds of structure **24** (Scheme 5).

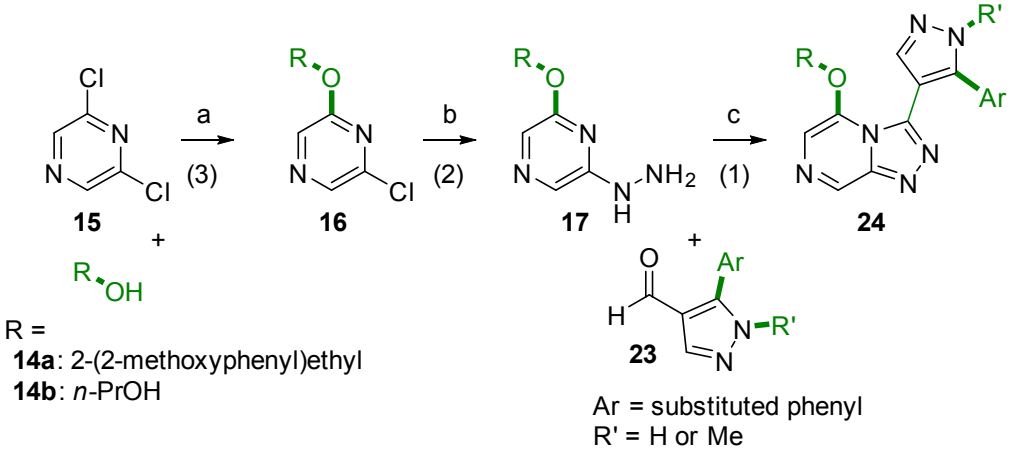

Scheme 5. Parallel synthesis route to introduce different ether substituents and substituted pyrazoles using methods of Scheme 3. a) KOtBu, CH_2Cl_2 b) NH_2NH_2, EtOH c) i. **17** + **18**, $ClCH_2CH_2Cl$; ii. (Diacetoxy)iodobenzene.

In the second library, the aryl group attached to the pyrazole was varied via a 4-step sequence wherein the ether substituent was fixed as *n*-propyl (Scheme 6). Starting with iodopyrazole **25**, Suzuki coupling with aryl boronates afforded **26**. Selective C-4 iodination gave **27** that could be carbonylated in the presence of triethylsilane to yield **23**. Condensation of **23** with **17a** followed by oxidative cyclization gave analogs **24a**. Compounds derived from both routes were resynthesized on larger scale for more thorough characterization via the route shown in Scheme 7.

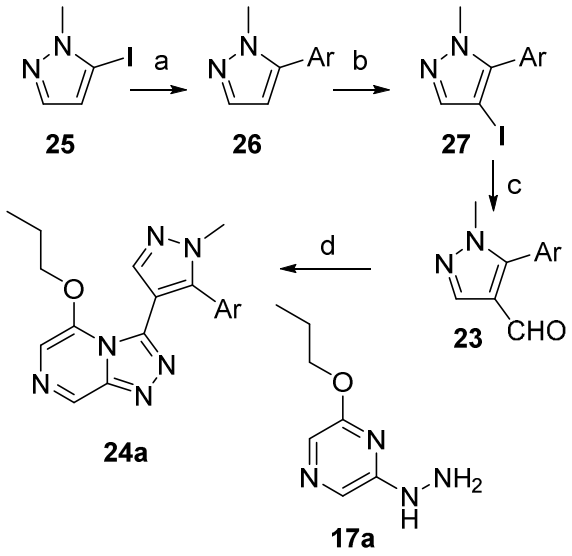

Scheme 6. a) $ArB(OH)_2$, $Pd(dppf)Cl_2$, Cs_2CO_3, DMF b) NIS, MeCN c) $Pd(OAc)_2$, dppf. CO, TEA, $SiHEt_3$ d) 2-hydrazinyl-6-propoxypyrazine **17a**, EtOH; (diacetoxyiodo)benzene, EtOH

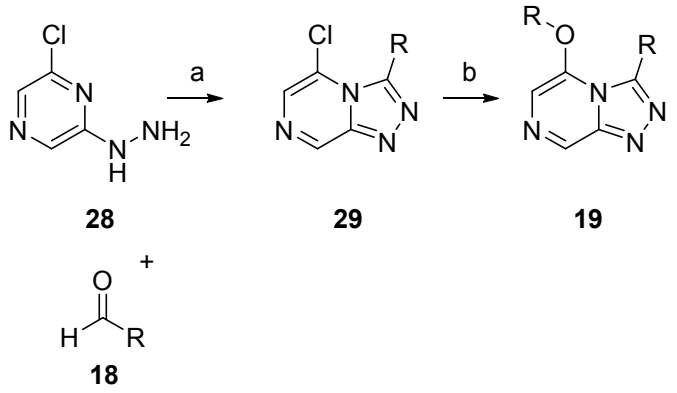

Scheme 7. Re-synthesis route for key library compounds. a) i. **28** + **18**, $ClCH_2CH_2Cl$; ii. (Diacetoxy)iodobenzene b) ROH, NaH, THF

Two different alcohol starting materials were employed in Scheme 5: 2-(2-methoxyphenyl)ethanol which is in **3**, along with the lower molecular weight alcohol *n*-propanol which was expected to have reduced steric interactions with Leu770 due to its smaller size. As a direct comparator to **3**, 3-isobutyl-5-propoxy analog **30** was prepared and a 5-fold decrease in PDE2A potency was observed but LipE remained essentially equivalent due to reduced lipophilicity (Table 6). LE increased, indicating more optimal interactions of **30** with protein relative to **3** on a per atom basis.

Table 6. PDE2A potency, physical properties and binding efficiencies of **3** and **30**

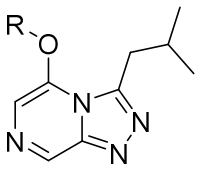

Cpd. ID	R	PDE2A IC_{50} (nM)	clogP	LE	LipE
30	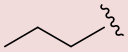	5323.8	2.7	0.43	2.5
3	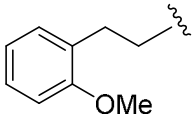	389.6	3.7	0.37	2.7

Reincorporating the 5-ether substituent made a significant impact on potency (Table 7). For example, the *n*-propoxy group (**31**) afforded a >10-fold increase in potency over the parent **22**. Lipophilicity was significantly higher for **31** vs. **22** (clogP = 3.8 vs. 2.2), yet LipE values were equivalent and LE was improved for **31**. As the ether substituent size and lipophilicity increased in **32**, potency values increased slightly relative to **31** with concomitant decreases in LE and LipE indicating more efficient binding of **31**.

Table 7. Impact of 5-position substitution on PDE2A potency and binding efficiency measures

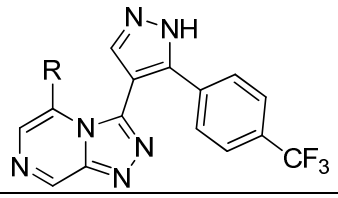

Cpd. ID	R	PDE2A IC_{50} (nM)[a]	clogP	LE	LipE
22	H	2107.4	2.2	0.27	2.5
31	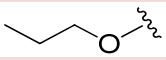	115.0	3.8	0.35	3.1
32	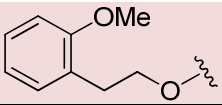	24.4	4.8	0.30	2.8

a) PDE2A IC_{50} data is from resynthesized samples, not from initial library compounds.

The next key finding was that methylation of the pyrazole nitrogen adjacent to the aromatic ring afforded >10-fold increase in PDE2A inhibitory potency when compared to **33** and **34** (Table 8). In order to provide a second example of this trend, **35**, the N-methylated version of library compound **31**, was prepared and the matched pair (**31** and **35)** showed the same relative potency increase. This result was critical in that not only was potency improved, but a HBD was removed that resulted in reduced MDR1 BA/AB efflux. The increased lipophilicity due to the methylation, however, increased HLM Cl_{int}.

Table 8. Impact of pyrazole N-substitution on PDE2A potency, MDR1 BA/AB, and HLM Cl_{int}

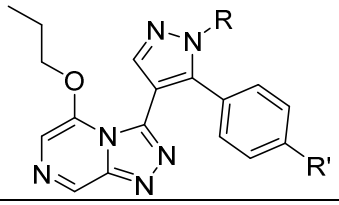

Cpd. ID	R	R'	PDE2A IC_{50} (nM)[a]	IC_{50} ratio R=H/Me	MDR1 BA/AB	HLM Cl_{int}
33	H	Me	297.8		5.6	102
34	Me	Me	27.7	11	1.8	232
31	H	CF_3	115.0		3.9	198
35	Me	CF_3	9.7	13	1.6	>300

a) PDE2A IC_{50} data is from resynthesized samples, not from initial library compounds.

A number of analogs wherein the 5-aryl pyrazole group had differing substitution at the para-position were prepared in the library which showed larger substituents provided increased potency (Table 9). These compounds were resynthesized and two additional compounds (**35** and **36**) were prepared. The unsubstituted phenyl (**36**) had PDE2A IC_{50} = 566.1 nM. Progressively larger substituent size led to significant increases in potency. For example, addition of a fluoro (**37**) gave a 2-fold potency increase, methyl (**38**) yielded a 20-fold potency increase, while the larger trifluoromethyl (**35**) and ethyl (**40**) resulted in 57-fold and 80-fold potency increases, respectively. Both LE and LipE increased with increasing substituent size, suggesting that the potency was being driven by more than non-specific lipophilic interactions which would result in lower LE and LipE values.

Table 9. Impact of 5-aryl para-position substitution and impact on PDE2A potency and binding efficiency measures

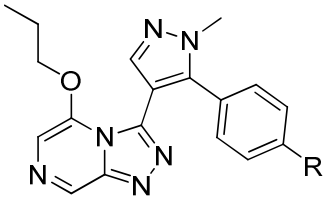

Cpd. ID	R	PDE2A IC_{50} (nM)[a]	clogP	LE	LipE
36	H	566.1	2.8	0.34	3.4
37	F	240.8	3.0	0.35	3.6
38	MeO-	108.5	2.8	0.35	4.2
34	Me	27.7	3.3	0.4	4.2
35	CF_3	9.7	3.7	0.38	4.3
39	Et	7.1	3.8	0.41	4.3

a) PDE2A IC_{50} data is from resynthesized samples, not from initial library compounds.

A protein x-ray crystal structure of **39** bound to PDE2A was obtained to help clarify the roles that the ether, methylated pyrazole, and phenyl para-substitution all play in potency enhancement (Figure 4a). First, the triazolopyrazine core of **39** maintains the same interactions with the enzyme as **3**. The *n*-propyl ether occupies the same space as the dimethoxyphenyl group in **1**, while avoiding deleterious interactions with Leu770. The 1-methyl-5-arylpyrazole in **39** overlaps with the 2-hydroxy-6-phenylhexan-3-yl sidechain in **1**. The sp2 nitrogen (N-2) of the pyrazole is well-aligned with the hydroxyl in **1**, accepting a hydrogen bond from a water molecule**.** The vector to access the induced pocket off the pyrazole 5-position with a rigid phenyl linker allows para substituents to reach the deep recesses of the pocket, with a lower entropic penalty than in the conformationally flexible sidechain of **1**.

a) b)

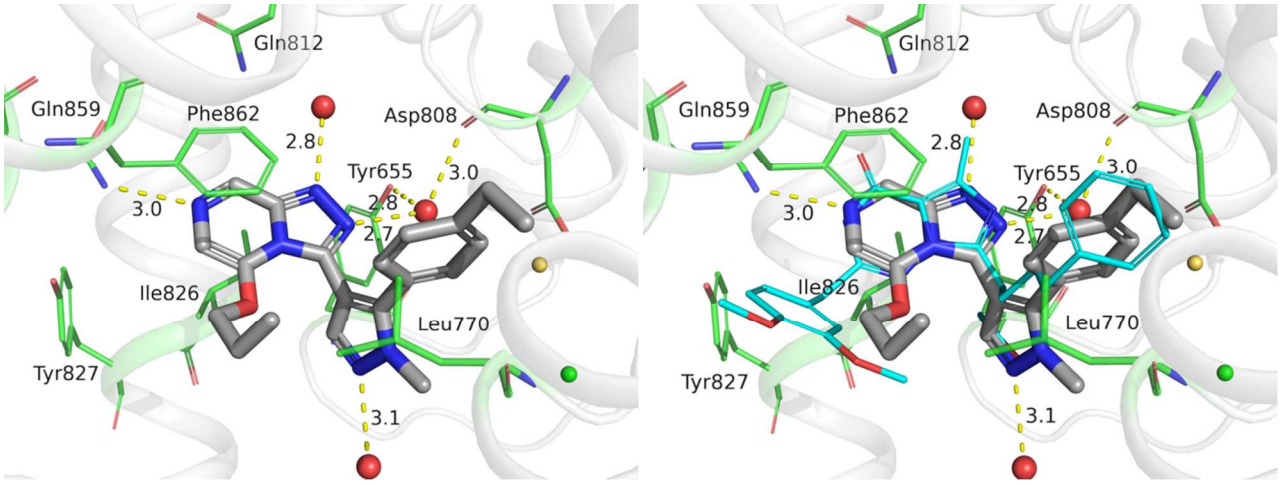

Figure 4. a) X-ray crystal structure of **39** bound to PDE2A. b) Overlap of **1** and **39** in PDE2A.

In terms of understanding the increase in potency observed when methylating the pyrazole, the methyl does not appear to make any specific interactions in the pocket nor does it appear to displace any water molecules. Dihedral angle scans were performed on three truncated phenyl pyrazole systems (**40**, **41**, and **42**, Figure 5), which suggest that the methyl on the pyrazole nitrogen has an effect on the orientation of the phenyl ring. The X-ray co-crystal structure of **39** with PDE2A reveals a preferred average dihedral angle of 67° in the bound conformation over the four structures in the asymmetric unit. The local minimum energy structures of **40** and the pyrazole tautomer **42** have dihedral angles of 35.3° and 28.6°, respectively, while that of **41** has a dihedral angle of 45.7° (see Supporting Information). This suggests that the methyl on the pyrazole ring causes the phenyl ring to adopt a conformation which is closer to that observed in the X-ray co-crystal structure, leading to a smaller conformational energy penalty upon binding. Optimization of the full systems and the dihedral scans of the truncated systems indicate that the conformational strain energy required to achieve the bound conformation for compounds without a methyl on the pyrazole, ~1.4 – 2.4 kcal/mol (depending on the tautomeric mixture), is at least twice that of those with a methyl on the pyrazole, ~0.6 kcal/mol.

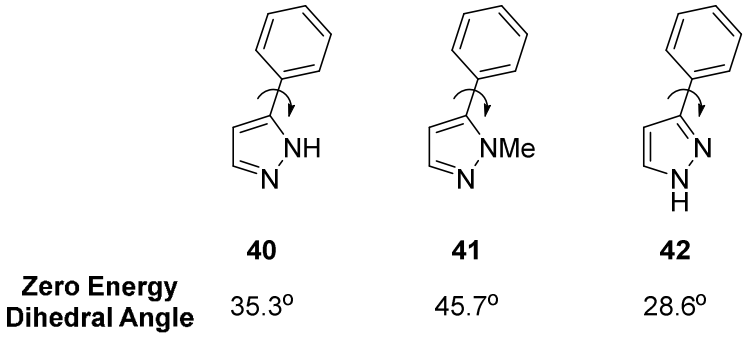

Figure 5. Truncated systems used to calculate dihedral angles in ground state.

Compound **39** was profiled more extensively for ADME properties and PDE selectivity (Table 10). The selectivity of this compound against other PDEs was exceptionally high, driven most likely by efficient filling of the PDE2A induced pocket. HLM Cl_{int} was high, but low MDR1 BA/AB efflux was observed. While the PDE2A potency was improved relative to **3**, the high HLM Cl_{int} negatively impacted estimated human dose predictions affording a value of >1438 mg/day.

Table 10. Comparison of PDE2A potency, selectivity and ADME profiles of **39** and **3**

Cpd. ID	**39**	**3**
PDE2A IC_{50} (nM)	7.1	390
PDE Selectivity	>2400x (1B/3B/4D/5A/6/7B/8B/9A/10A/11A)	<20x (1B/3A/7B/10A/11A); 29X (4D); 71x (5A); 69x (6); >200x (8B/9A)
HLM Cl_{int}*	>300	>287
MDR1 BA/AB	1.85	1.2
estimated human dose (mg/day)[a]	>1438	>46136

a) estimated human dose (mg/day) = 10 x PDE2A IC_{50} x HLM CL_{int} x 24 h x 70 kg x MDR1 BA/AB.

In order to address the high estimated human dose, improving PDE2A potency and reducing HLM Cl_{int} were targeted. Overlaying protein x-ray crystal structures of **4** and **39** showed that the heterocyclic cores aligned with one another regarding the substituents that projected into the ribose region, which were the isobutyl of **4** and aryl pyrazole of **39** (Figure 6a). A hybrid series was proposed which merged the pyrazolo[3,4-*d*]pyrimidine core with the aryl pyrazole side chain in **39** (Figure 6b).

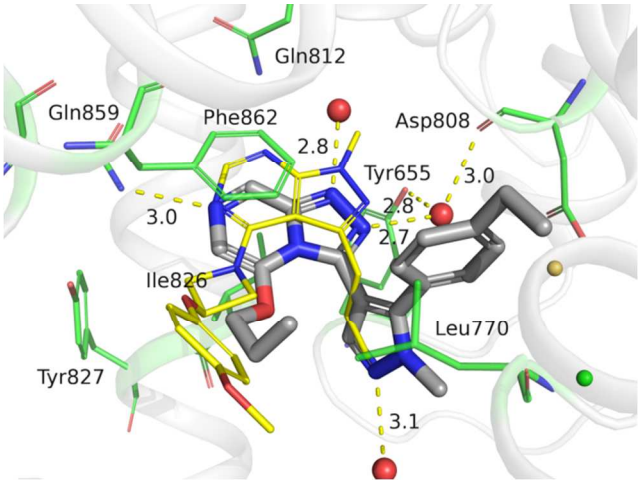

(a)

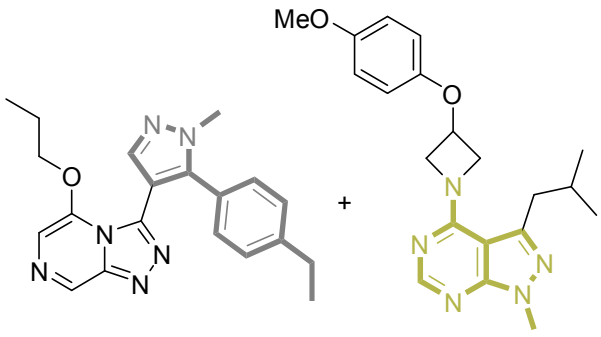

39 **4**

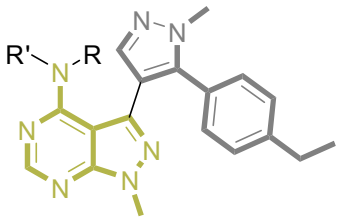

43

(b)

Figure 6. a) Overlap of **4** (yellow) and **39** (grey) in PDE2A. b) Merging **4** and **39** to yield a proposed hybrid series **43**.

In order to access compounds of general structure **43**, pyrazole boronate **44** was coupled with an aryl bromide (**45**) to afford **46** (Scheme 8). Formylation of **46** with dimethylformamide and phosphorous oxychloride yielded the 4-formyl pyrazole **47**. Low temperature lithiation of 4,6-dichloropyrimidine (**48**) at the 5-position followed by addition of **47** gave the carbinol **49**. Oxidation of **49** yielded the corresponding ketone **50** which could be reacted with an amine (HNRR') at room temperature to selectively provide the mono-amino product **51**. Subsequent reaction with methyl hydrazine afforded the target compounds of general structure **44**.

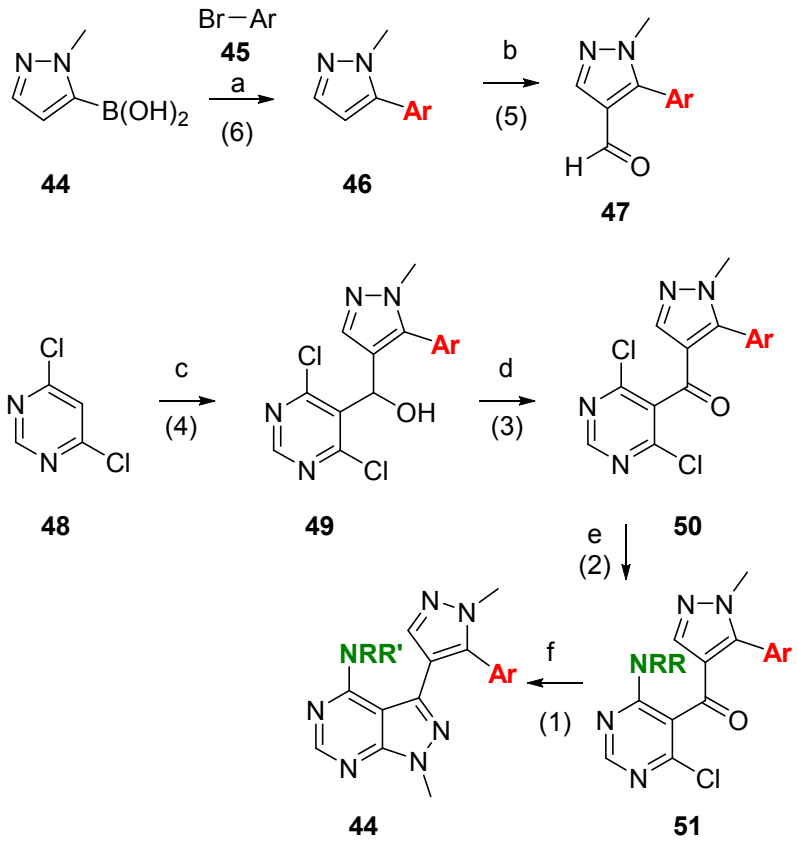

Scheme 8. a) $PdCl_2(PPh_3)_2$, $NaHCO_3$, DME, H_2O; b) DMF, $POCl_3$; c) i. **48**, LDA, THF, ii. **47** d) Dess-Martin periodinane; e) HNRR', MeCN; f) $MeNHNH_2$, pyridine.

Initial analogs with varied amines were prepared via a 2-step parallel chemistry protocol (**50** → **51** → **44**, Scheme 8). Trends for potency were demonstrated in this initial library with azetidine and 3-substituted azetidines providing the most potent PDE2A inhibitory activity (Table 11, **52-54**), comparable to or better than **39**. With lower clogP relative to **39** (ca. 1 unit), HLM Cl_{int} was reduced for these compound while maintaining low MDR1 BA/AB efflux which reduced the estimated human dose for **52** and **53** (160 and 337 mg/day, respectively). The polar methyl carbamate of **54** also showed reduced HLM Cl_{int}. However, with significant MDR1 BA/AB efflux, the estimated human dose increased (954 mg/day). Overall, LE and LipE values were also in a desirable range, especially for **52** (LE = 0.43, LipE = 6). The reduced conformational flexibility of **52** (RB = 4) most likely resulted in a low energy ground state that is similar to the PDE2A enzyme bound conformation, obviating an entropic penalty for binding, which is associated with the more flexible **1**. Pyrrolidines (**55-56**) provided slightly less activity than azetidines, but had higher human dose due to greater MDR1 BA/AB efflux. Six-membered ring amines (**57-58**) showed significantly less PDE2A activity.

Table 11. Representative parallel synthesis compounds varying 5-amino substituent

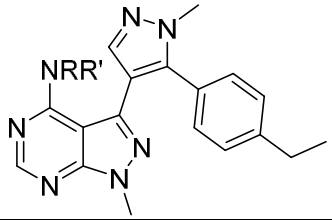

Cpd. ID	-NRR	PDE2A IC_{50} (nM)[a]	HLM Cl_{int}	MDR1 BA/AB	Estimated human dose (mg/day)[b]	clogP	LE	LipE

52	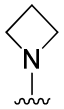	2.0	150	1.4	160	2.7	0.43	6
53	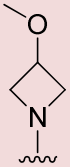	5.8	77	1.9	337	2.9	0.38	5.4
54	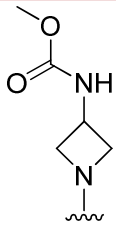	3.6	42	14	954	2.8	0.36	5.6
55	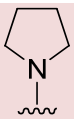	7.8[c]	200	3.1	1859	3.3	0.39	4.8
56	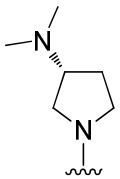	4.9	55	5.4	642	2.9	0.36	5.5
57	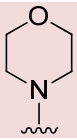	423.0	149	2.2	55,657	2.5	0.30	3.9
58	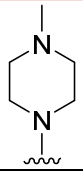	1407.0	60	6.2	222,323	2.9	0.26	3.0

a) PDE2A IC_{50} data is from library compounds. *b*) estimated human dose (mg/day) = 10 x PDE2A IC_{50} x HLM, Cl_{int} x 1440 min x 70 kg x (MDR1 BA/AB). c) PDE2A IC_{50} is the geometric mean of two independent IC_{50} measurements.

An x-ray crystal structure of **56** bound to PDE2A was successfully solved (Figure 7). Consistent with the PDE2A x-ray crystal structure of **4**, the pyrazolopyrimidine core made the same polar and non-polar interactions with the protein and the 1-methyl-5-arylpyrazole moiety resided in a similar position as in **39**. While azetidine and pyrrolidine were accommodated at the 4-position of the pyrazolopyrimidine, it is possible that the bulkier six-membered ring systems

such as morpholine and piperazine cannot fit as well and make unfavorable contacts with side-chains lining the bottom and sides of the binding pocket (Ile-826, Phe-830, Met-847).

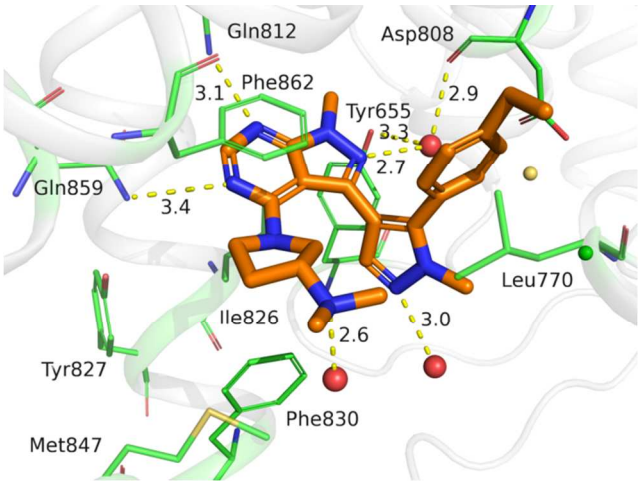

Figure 7. X-ray crystal structure of **56** bound to PDE2A

52 made via parallel synthesis was resynthesized on larger scale and more fully profiled. The PDE2A IC_{50} for this resynthesized material was equivalent to the compound made via parallel synthesis. In an analogous manner to **39**, selectivity against other PDE families was >3000x, providing further support that efficient binding to the induced pocket in PDE2A could be a general approach to minimizing off-target PDE activity.

The focus was nexted placed on exploring changes to the pyrazole 5-aryl group to reduce HLM Cl_{int} while maintaining low MDR1 BA/AB. The route in Scheme 8 was used to synthesize other substituted phenyl derivatives. An alternative route was developed (Scheme 9) to allow the incorporation of heterocycles which were low-yielding in the original method. Selective S_NAr of azetidine on **59** proceeded in high yield to afford **60**. The heteroaryl pyrazole moiety was constructed via Suzuki coupling between pyrazole boronic acid **61** and the halo-heterocycle **62** to give **63**. Direct iodination of **63** proceeded cleanly and in high yield to give **64**, which could be metallated with either *n*-BuLi or *i*-PrMgCl and then treated with **60** to yield the carbinol **65**.

Oxidation then gave the 4,6-dichloro-5-keto-pyrimidine **66** (similar to **51**) which readily reacted with methyl hydrazine to provide the target compounds **67**.

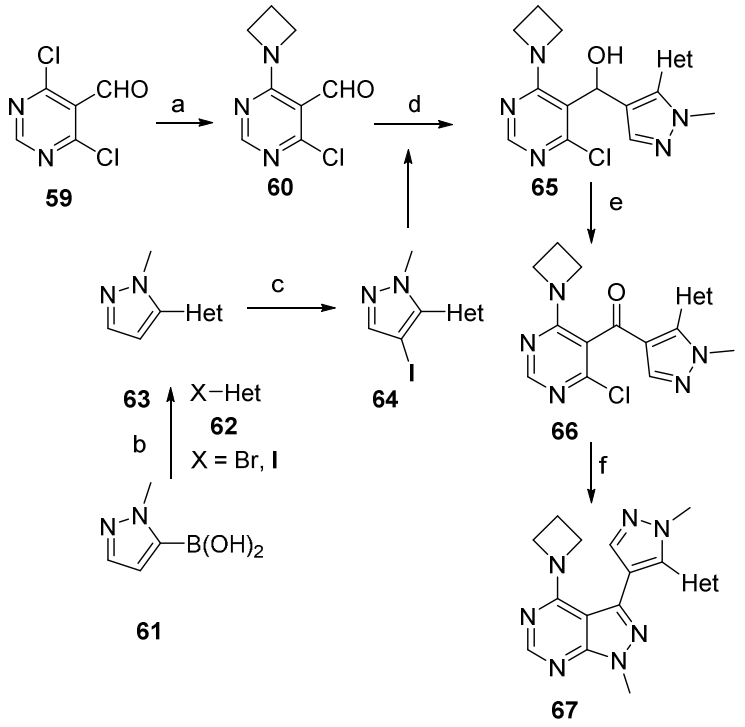

Scheme 9. Synthetic route to heteroaryl substituted pyrazole analogs **67**. a) azetidine, DIPEA, $CHCl_3$, 64%; b) $PdCl_2(PPh_3)_2$, Na_2CO_3, 1,2-DME, H_2O; c) NIS, AcOH; d) *n*-Butyl lithium or *i*-PrMgCl, THF; e) Dess-Martin periodinane, CH_2Cl_2; f) NH_2NHMe, pyridine.

Potency trends with regard to aryl para-substitution tracked with the triazolopyrazine results (compare Table 9 to Table 12). For example, adding a 4-methyl to the parent phenyl compound (**68** → **69**) gave an order of magnitude enhancement in potency and higher LE, both of which were further increased in the case of ethyl **(52).** Similarly, cyclopropyl (**70**) and trifluoromethyl (**71**, PF-05085727) also provided high potency. These more potent compounds maintained low MDR1 BA/AB with HLM Cl_{int} still in the moderate to high range, with **71** having an estimated human dose <100 mg/day. The replacement of phenyl with pyridine did reduce HLM Cl_{int} 2-3

fold when looking at matched pairs (**71** vs. **72**; **70** vs. **73**), but potency was reduced significantly (3-13 fold) which ultimately led to increased estimated human dose. Shifting from pyridine to the more polar pyrimidine (**73** → **74**) reduced HLM Cl_{int} 2-fold but afforded a 100-fold loss in potency along with increased MDR1 BA/AB efflux.

Table 12. SAR of pyrazole 5-aryl group

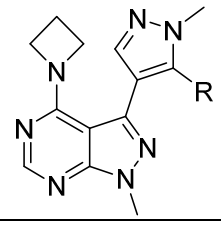

Cpd. ID	-R	PDE2A IC_{50} (nM)	HLM Cl_{int}	MDR1 BA/AB	estimated human dose[a] (mg/day)	clogP	LE	LipE
68	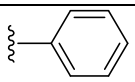	188.7	34	1.1	2512	1.7	0.35	4.6
69	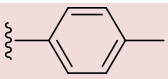	17.7[b]	47	1.8	546	2.2	0.40	5.5
52	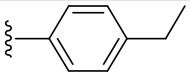	2.0	150	1.4	160	2.7	0.43	6
70	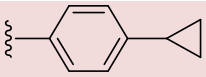	3.4	90	1.4	166	2.6	0.41	5.9
71	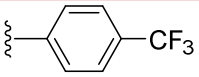	1.6	77	1.4	72	2.6	0.41	6.1
72	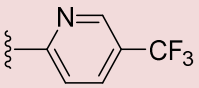	8.9	33	2.3	282	1.5	0.37	6.5
73	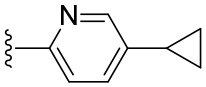	8.9	53	3.1	565	1.4	0.39	6.6
74	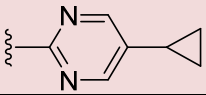	1012.7	28	5.6	60759	0.48	0.29	5.5

a) Estimated human dose (mg/day) = 10 x PDE2A IC_{50} x HLM, CL_{int} x 1440 min x 70 kg x (MDR1 BA/AB).
b) PDE2A IC_{50} is the geometric mean of two independent IC_{50} measurements.

In order to explore *in vivo* PDE2A inhibition, **71** was chosen to be profiled extensively to assess its potential for use as an *in vivo* tool. Key to choosing this compound was its lower rat liver

microsomal Cl_{int} (145 mL/min/kg) as compared to other low estimated human dose compounds such as **52** (707 mL/min/kg) and **70** (>1000 mL/min/kg) which would be important in helping maximize exposure in the rodent-based *in vivo* models. Similar to **52**, the overall PDE selectivity remained high (>4000x) against all other isoforms (Table 13) and thus selective inhibition of PDE2A *in vivo* versus other PDEs would be readily attainable with **71**. Selectivity against a broad range of kinases (Figure 8) and in a CEREP selectivity panel (Figure 9) showed **71** to have no significant off-target activity, obviating concerns of pharmacology which would cloud interpretation of *in vivo* activity with **71** (see Supporting Information for full data tables). Minimal inhibition of representative cytochrome P450 enzymes (CYPs) was observed, suggesting a low risk for **71** to elicit drug-drug interactions. Plasma protein binding was moderate across species. Assessment of human ether-à-go-go-related gene (hERG) ion channel affinity was conducted by displacement of the known radiolabeled ligand dofetilide and showed minimal binding. Profiling **71** in a cellular toxicity assay using transformed human liver endothelial (THLE) cells showed weak activity with IC_{50} = 162 μM to induce cell death.[15]

Table 13. *In vitro* selectivity, ADME, and toxicology profile of **71**.

PDE2A IC_{50} (nM)	1.6
PDE Selectivity	>4000x (1B/3B/4D/5A/6/7B/8B/9A/10A/ 11A)
CYP[b] Inhibition (3 μM)	1A2 (16%), 2C8 (18%), 2C9 (7%), 2D6 (4%), 3A4 (30%)
Liver microsomal clearance (mL/min/kg)[a]	Human – 77 Rat – 145
Fu,p (Fu,b)	Human – 0.17 Rat – 0.32 (0.095)

	Mouse – 0.20
Dofetilide Ki	<10% inhib @ 10 μM
THLE IC_{50} (μM)	162

a) values represent the Clint, apparent scaled (mL/min/kg). b) CYP = Cytochrome P450;

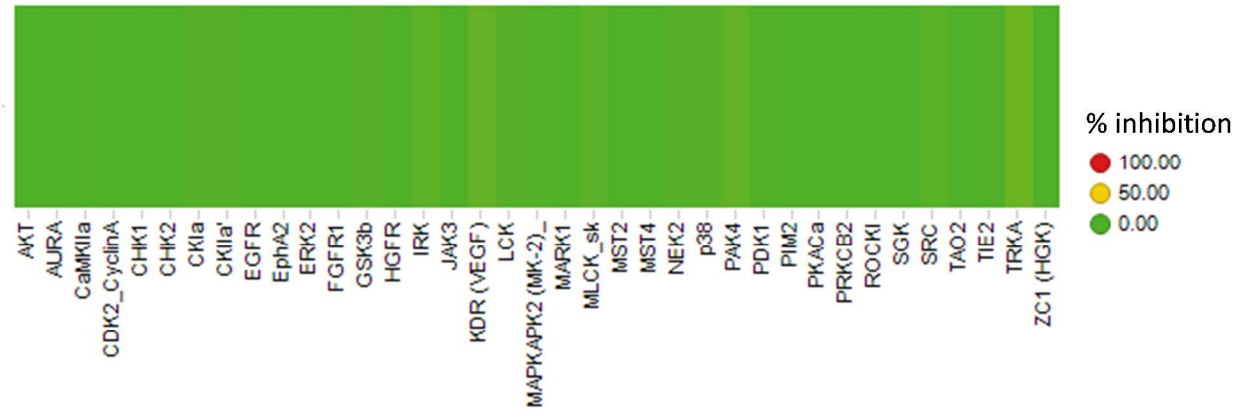

Figure 8. Activity of **71** in a kinase selectivity panel at a concentration of 10 μM (Invitrogen).

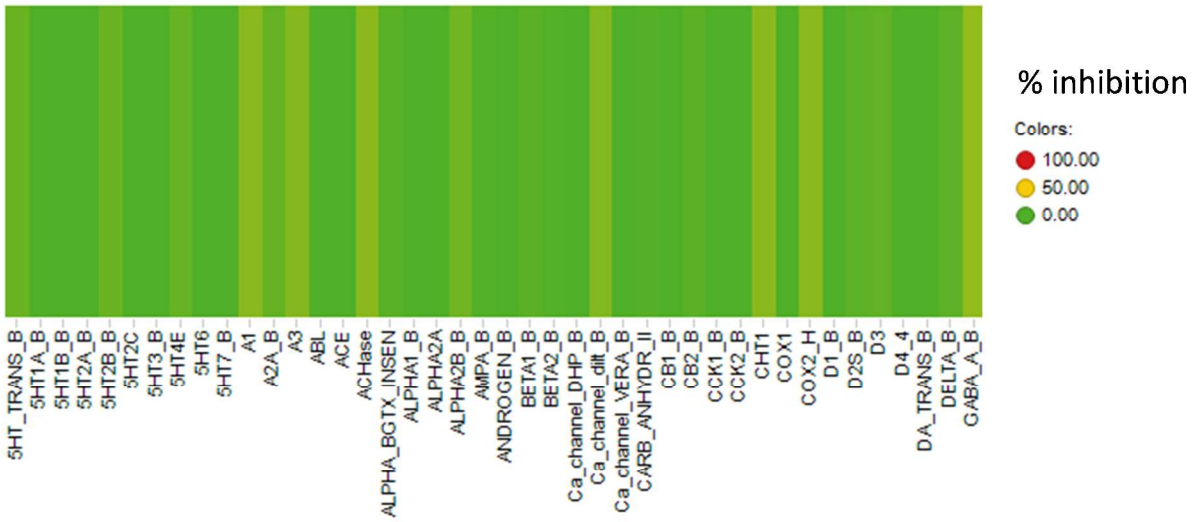

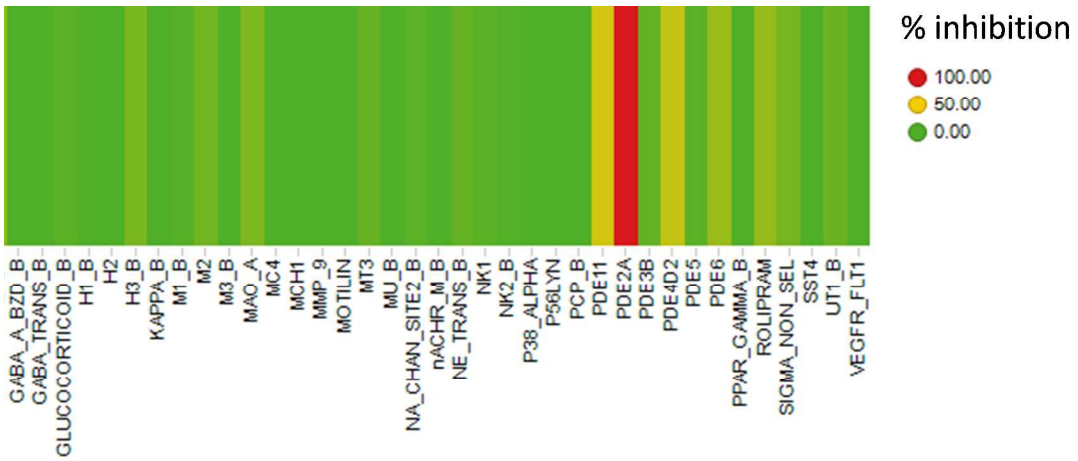

Figure 9. Activity of **71** in a selectivity panel at a concentration of 10 μM (CEREP).

In vivo subcutaneous (SC) administration of **71** to both mouse and rat gave C_{bu}/C_{pu} of ca. 0.27 and 0.37, respectively. C_{bu} was achieved which was >25-fold the PDE2A $IC_{50,}$ indicating significant target inhibition achieved *in vivo* in rodent brain (Table 14). In rat, CSF levels of **71** were also determined and were close to the C_{bu} (CSF/C_{bu} = 0.89).

Table 14. *In vivo* brain, plasma, and CSF exposure of **71** in mouse and rat following SC administration[a]

Species	SC Dose (mg/kg)	Total Brain (nM)	C_{bu}[b] (nM)	Total Plasma (nM)	C_{pu}[c] (nM)	C_{bu}/C_{pu}	CSF (nM)	CSF/ C_{bu}	C_{bu}/PDE2A IC_{50}
Mouse	3.2	452	43.0	798	160	0.27	--	--	26.9
Rat	3	950	90.2	776	248	0.37	79.9	0.87	56.4

a) Mouse n = 4, timepoint = 30 min post-dose; rat n = 3, timepoint = 30 min post-dose. *b*) Rat brain f_{ub} = 0.095: Mouse C_{bu} estimated using rat f_{ub} value. *c*) Rat plasma f_{up} = 0.32 and mouse f_{up} = 0.20.

An improved correlation between *in vitro* inhibition of PDE2A cGMP hydrolysis and target engagement of native PDE2A was sought via utilization of a radioligand. The high potency and selectivity of **71** along with its moderate protein binding would serve to minimize non-specific

tissue binding and made it an ideal candidate for radiolabeling. Treatment of **76**, a key intermediate in the synthesis of **71**, with hydrazine afforded *N*-1 des-methyl compound **77**. Treatment of **77** with base and CT_3-I afforded N-1 CT_3 compound **78** which following purification afforded a specific activity of 82 Ci/mmol as determined by mass spectrometry (Scheme 10).

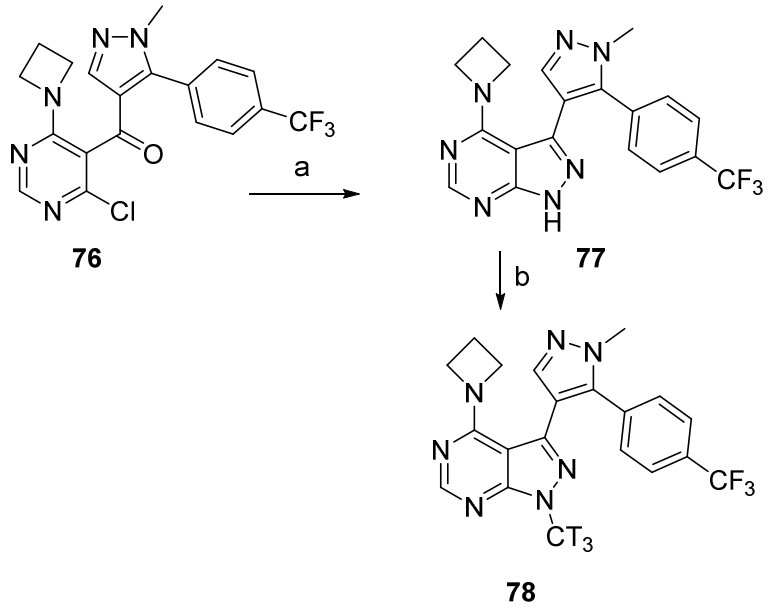

Scheme 10. Synthesis of *N*-1 CT_3 radioligand **78**. a) NH_2NH_2, THF, 56%; b) NaH, THF, CT_3I, HPLC purification.

A saturation radioligand binding assay was developed with **78** using striatal tissue from rat, dog and monkey, a brain region with high PDE2A expression. The binding constant (K_d) for **78** in striatal tissue was consistent across species (K_d = 2.8 – 3.2 nM) and was very similar to the *in vitro* IC_{50} for PDE2A cGMP hydrolysis demonstrated by **71** (IC_{50} = 2 nM), suggesting that the PDE2A enzyme assay was predictive of target engagement in brain tissue (Figure 10). Furthermore, the B_{max}, a measure of PDE2A enzyme concentration determined in this study, showed consistent protein levels across species (0.89 to 1.8 pmol/mg). The B_{max} value was sufficiently high to suggest that a positron emission tomography (PET) tracer could establish *in*

vivo target occupancy.[16] Indeed, this data was also used to support development of a PDE2A PET ligand which successfully demonstrated specific uptake in the striatum of monkeys.[17]

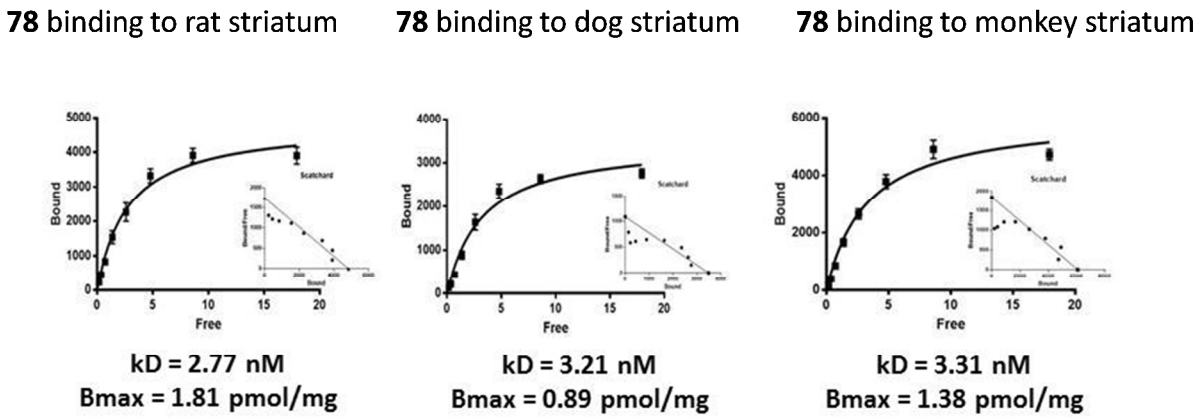

Figure 10. Saturation binding assay data in rat, dog and monkey striatal tissue using **78** as radioligand.

Administration of **71** in mice leads to an acute and exposure-dependent elevation in the accumulation of bulk levels of cGMP in cortex, striatum and hippocampus as measured by enzyme-linked immunosorbent assay (ELISA, Figure 11). [18, 19] Measurement of drug exposure in satellite animals was used to model the cGMP response across brain regions and resulted in a C_{bu} half effective concentration (EC_{50}) relative to the maximum effect (E_{max}) for cGMP accumulation of 70-136 nM and a 50% increase relative to baseline (E50) of 15-53 nM (Table 15). No cGMP changes were observed in cerebellum which lacks significant expression of PDE2A and serves as a reference region (not shown). No changes in cAMP or its downstream signaling effector phospho-cAMP response element-binding protein (p-CREB) were apparent in any brain region.[20] This suggests that the pool of cAMP regulated by PDE2A in these brain regions is relatively small and potentially regionally specialized, relative to the large endogenous pool of cAMP measured in our bulk biochemical studies.

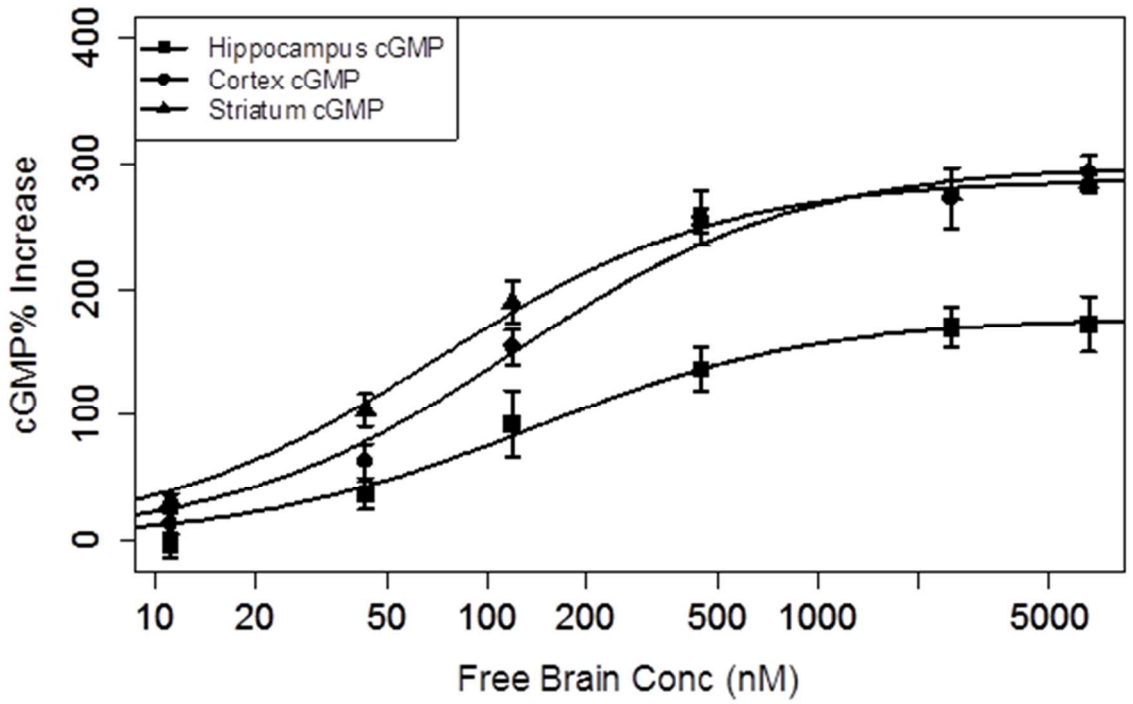

Figure 11. Mouse C_{bu} of **71** plotted against brain cGMP levels in different brain regions. cGMP = cyclic guanosine monophosphate

Table 15. Potency estimation of **71** for mouse brain cGMP %increase by brain region

Brain region	Striatum	Hippocampus	Cortex
EC_{50} (nM)[a]	70	136	120
Emax (%)[b]	288	178	299
E_{50} (nM)[c]	15	53	24

a) EC_{50} = half effective concentration. *b)* Emax = maximum effect. *c)* E_{50} = 50% increase relative to baseline.

Evaluating the behavioral consequences of PDE2A inhibition by **71** showed no effects on spontaneous locomotor activity or habituated locomotor activity in mice or rats (data not shown). **71** also showed no effect in selected positive symptom models of psychosis using rats, which included no significant attenuation of d-amphetamine or MK-801 induced hyperactivity and no

effect in the conditioned avoidance response model (data not shown). PDE2A protein is highly expressed in presynaptic synaptic compartment of glutamatergic principal neurons within the hippocampus and cortex[21] where it has been implicated in regulating presynaptic forms of short term synaptic plasticity[22] and in the induction of long term potentiation.[9] Furthermore, PDE2A inhibitors have been shown to potentiate NMDAR-stimulated cGMP accumulation in cultured neurons,[23,24] suggesting that inhibition of PDE2A may have the ability to reverse deficits in NMDA signaling cascades by enhancing cyclic nucleotide signaling cascades downstream of receptor activation. To evaluate the consequence of PDE2A inhibition on a cognitive task dependent upon NMDA receptors, a ketamine-disrupted working memory model in rats was used. Systemic administration of **71** (0.032 to 1 mg/kg, SC) significantly attenuated the working memory errors produced by ketamine (Figure 12).

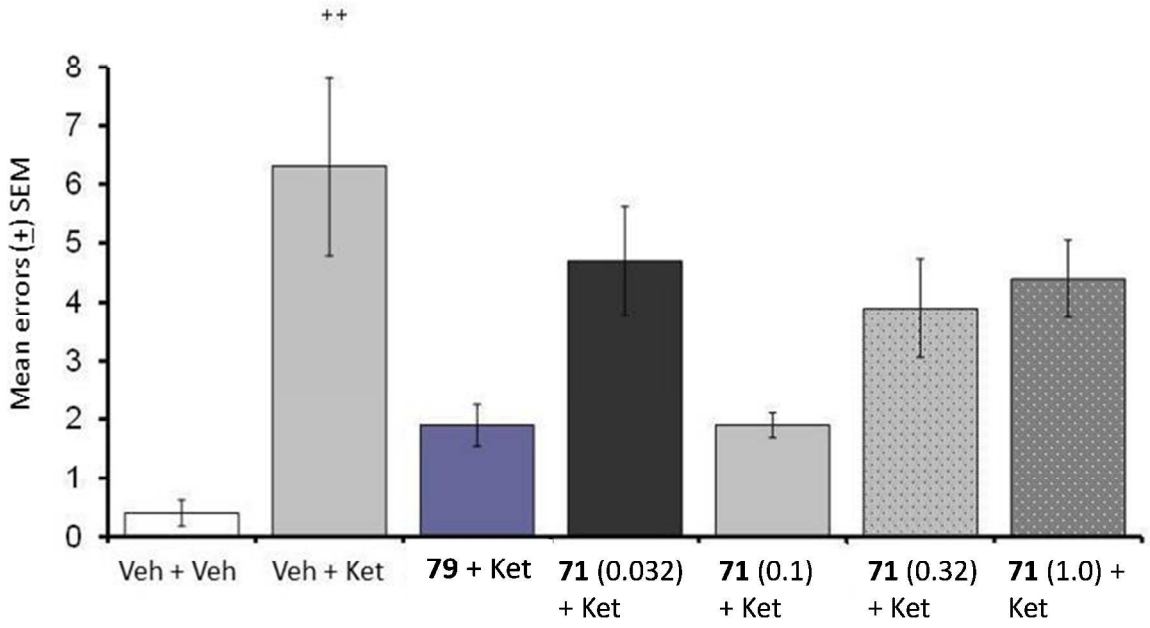

Figure 12. Effects of **71** on Ketamine-Disrupted Working Memory in LE Rats in Radial Arm Maze. Doses of **71** are in mg/kg. Ket = Ketamine; SEM = Standard error of the mean; Veh = Vehicle.

Based on measurement of exposure of **71** in satellite animals, the corresponding C_{bu} at the time of the 0.1 mg/kg dose was projected to be 2.3 nM and at the 0.32 mg/kg dose, 7.4 nM (Table 16).

Table 16. Rat C_{bu} of **71** at doses used in Radial Arm Maze

Dose (mg/kg)	0.1	0.32
C_{bu} (nM)	2.3	7.4

These effects were comparable to those produced by a positive control compound **79** (LY451646), which is a positive allosteric modulator of the α-amino-3-hydroxy-5-methyl-4-isoxazolepropionic (AMPA) receptor.[25] As compared to the ketamine-treated group, the 0.32 mg/kg doses of **71** also significantly improved several other performance indices including average time to maze completion, while the 0.10 and 0.32 mg/kg doses increased the percent correct choices on the maze (not shown). These data show that **71** afforded significant protection from the ketamine-induced working memory deficits on the rat RAM.

Dysfunction of the prefrontal cortex (PFC) is considered to be an important factor contributing to working memory-related decrease in cognitive performance of schizophrenia patients. [26] Administration of the NMDA receptor antagonist MK-801 has been shown to disrupt spontaneous neuronal activity and synaptic plasticity in the mPFC of anaesthetized rats and reversal of these changes have been observed with the positive allosteric modulator of the AMPA receptor (*R*)-*N*-(2-(4'-(2-(methylsulfonamido)ethyl)-[1,1'-biphenyl]-4-yl)propyl)propane-2-sulfonamide (LY451395).[27] Reversal of MK-801-induced disruptions in NMDA receptor signaling, detected with cortical electroencephalogram (EEG) recordings as changes in low frequency cortical delta oscillation and paired-pulse facilitation (PPF), were used as pharmacodynamic measures of PDE2A inhibition by **71** on glutamatergic transmission in cortex.

A single intravenous (IV) dose of MK-801 (0.07 mg/kg) consistently and significantly changed the characteristics of the cortical EEG from a low amplitude, highly regular 1.8 to 2.0 Hz signal (delta oscillation) to a slower, higher amplitude, less synchronous signal of 0.5 to 1.6 Hz for up to one hour post dose (Figure 13). PPF was simultaneously disrupted in these animals (data not shown). **71**, also given IV, was capable of maximally reversing 80% of the disruptive effects of MK-801 on both cortical EEG and PPF. The effect of reversal peaked at 30 minutes post IV dose of **71** and gradually diminished over time.

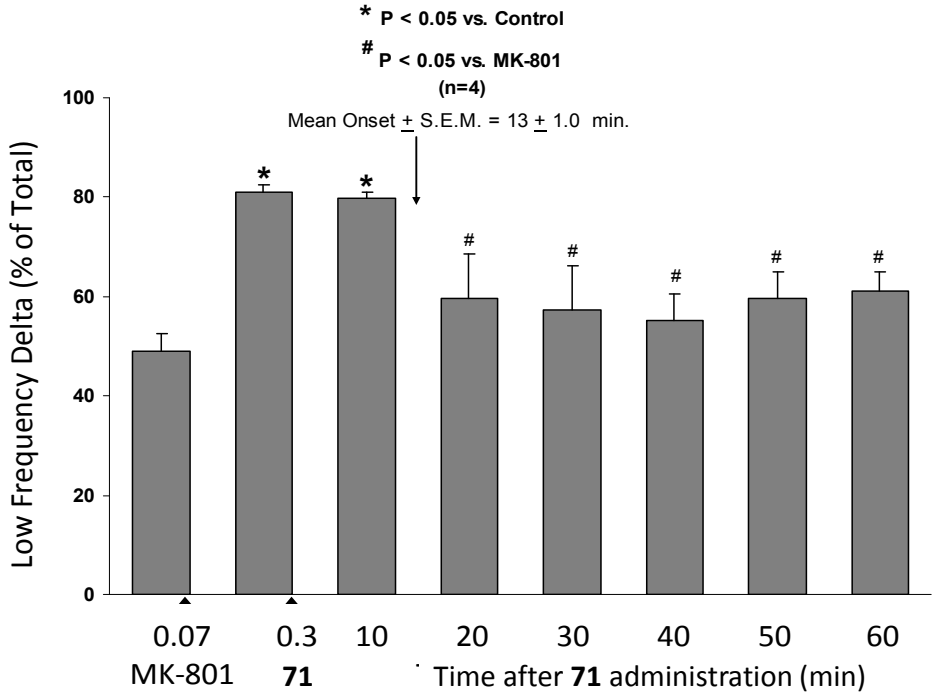

Figure 13. Timecourse of **71** (0.3 mg/kg, IV) effects on MK-801-induced changes in low frequency cortical oscillation activity

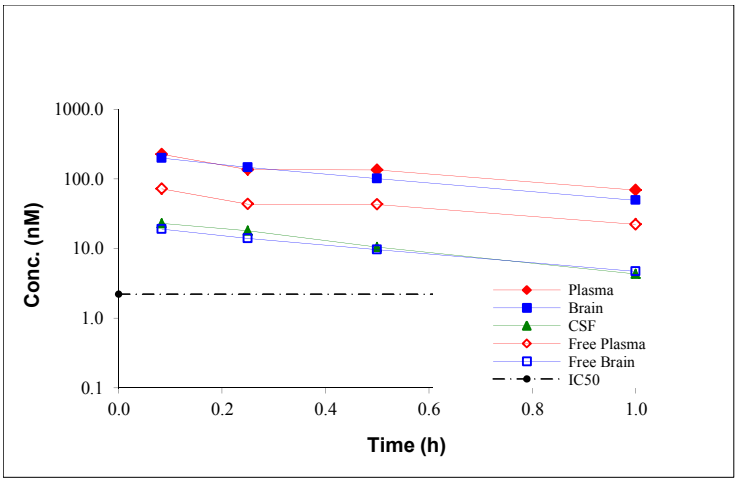

Figure 14. Rat exposure (0.3 mg/kg, IV) of **71**

Parallel neuro-pharmacokinetic studies were conducted to evaluate brain exposure of **71** over time (Figure 14) and to estimate **71** *in vivo* potency in cortical EEG through use of pharmacokinetic/pharmacodynamic (PK/PD) modeling (see Supporting Information). This model identified a linear relationship between **71** C_{bu} and reversal of the MK-801 effect. Based on the model, **71** was projected to provide a maximal reversal of 80% of the MK-801 induced local field potential disruption at steady state C_{bu} of 11 nM.

These studies indicate that specific inhibition of the PDE2A enzyme by **71** can significantly alleviate at least two measures of cortical disruption caused by NMDA antagonists at C_{bu} = 2.3 to 11 nM (Table 17). The corresponding calculated changes in brain cGMP at these C_{bu} levels show that low to moderate changes in cyclic nucleotides were also associated with the reversal of NMDA antagonist effects versus the maximal attainable brain cGMP increase.

Table 17. Comparison of calculated brain cGMP increases for **71** in mouse vs. rat *in vivo* efficacy C_{bu}

	Brain Region		
	Striatum	Hippocampus	Cortex

Assay	C_{bu} (nM)	Calculated % cGMP Increase		
RAM	2.3	9	3	6
RAM	7.4	28	9	17
Cortical EEG	11	39	13	25

C_{bu}= Unbound brain concentration; EEG = electroencephalogram; RAM = Radial arm maze.

An explanation for the lower levels of cyclic nucleotide increases providing efficacy in these models is that as previously mentioned, PDE2A exists as an inactive dimer and the NMDA antagonists used in the *in vivo* models could specifically activate PDE2A in discrete circuits that are sensitive to PDE2A inhibition. As a result, *in vivo* brain cGMP measurements may represent inhibition of a less active form of PDE2A that is broadly distributed and whose inhibition is primarily responsible for the observed biochemical changes. Using a more conservative estimate of measured values for the average, steady state C_{bu} from the reversal of MK-801-induced changes in cortical EEG (11 nM or ca. 6x PDE2A IC_{50}) and a C_{bu}/C_{pu} from rat studies of 0.36, the estimated human dose of 108 mg/day is very much in line with the estimates from *in vitro* data of 77 mg/day (Table 11), demonstrating that **71** is a viable lead series for optimization towards a clinical candidate.

Discussion and Conclusions

Using a combination of structure-based drug design, physicochemical property optimization, and strategic application of parallel chemistry, two unique screening hits, **2** and **3**, were merged to generate a potent and exceptionally PDE2A-selective series which culminated in the discovery of the tool compound **71**. The radioligand **78** demonstrated binding to PDE2A in brain tissue *in vitro* which was in line with its potency in an *in vitro* cell free system, building confidence in using the cell-free system to estimate target engagement *in vivo*. C_{bu}/C_{pu} was consistent in rodent

and CSF levels in rat tracked with the C_{bu}. Compound **71** demonstrated *in vivo* activity as evidenced by biochemical increases in brain cGMP accumulation in rodent brain regions expressing highest levels of PDE2A enzyme. Additionally, behavioral and electrophysiological changes due to two different NMDA antagonists were reversed at exposures where **71** would selectively inhibit PDE2A without activity at any other target. These data show that selective PDE2A inhibition in brain can potentiate pharmacologically-induced NMDA hypofunction *in vivo* and suggest a therapeutic role for brain penetrant PDE2A inhibitors in treating neurological and neuropychiatric disorders associated with NMDA hypofunction such as schizophrenia. Further characterization of this compound in translatable preclinical models of neuropsychiatric symptom domains should inform future clinical trial design. In order to support this research, **71** will be available for purchase from Millipore-Sigma (Catalog number PZ0355).

Experimental Methods

Research involving animals was performed in accordance with institutional guidelines as defined by Institutional Animal Care and Use Committee for U.S. institutions.

PDE2-A3 Scintillation Proximity Assay

Human PDE2A isoform sequences to be used for cloning were derived from NCBI accession entry NR_026572 for hPDE2A3, respectively. PDE2A isoform sequences were cloned into a pFastBac1 vector such that an amino terminal FLAG extension and appropriate protease cleavage sites would be available for subsequent purification steps. Full-length PDE2A3 enzyme was obtained from FLAG purification of sf21 insect cells using standard affinity purification procedures for this tag (anti-FLAG M2, Sigma Aldrich) or by crude lysate methods.

PDE2-A3 Assay Methodology

Test compounds were solubilized in 100% dimethyl sulphoxide and diluted to the required concentrations in 15% dimethyl sulphoxide/distilled H_2O at 5x final concentrations. Compounds were tested at 8 concentrations ranging from 0.316 μM to 0.0001 μM in triplicate. The activity of the test substances on human PDE2A3 was determined using the [3H]cGMP scintillation proximity assay format using 384 well plates. The PDE scintillation proximity assay (SPA) yttrium silicate beads (Perkin Elmer RPNQ0024) preferentially bind the linear nucleotide, GMP, compared to the cyclic nucleotide, cGMP. Using 3H-cGMP (Perkin Elmer NET337001MC) as the substrate in this reaction allows the product, 3H-GMP, to be detected using a Wallac Microbeta scintillation counter. The enzyme concentration for each isoform was determined by enzyme titration experiments to be in the linear range of the assay. The Michaelis constant (Km) of the enzyme was determined to be 12.8 μM for cGMP. The final substrate concentration used was at sub-Km levels so that IC_{50} values would approximate the K_i values. The reaction time was chosen with respect to the amount of time where 10-20% of substrate was hydrolyzed by the enzyme. The assay was validated using literature compounds as controls before testing the representative compounds of the present invention. The corresponding IC_{50} values of the compounds for the inhibition of PDE activities are determined from the concentration-effect curves by means of non-linear regression.

Phosphodiesterase Selectivity Assays

The phosphodiesterase (PDE) assays measure the conversion of 3', 5'-[^{3}H] cAMP to 5'-[^{3}H] AMP (for PDE 1B1, 3A1, 4D3, 7B, 8B and 10A1) or 3', 5'-[^{3}H] cGMP to 5'-[^{3}H] GMP (for PDE 5A1, 6 (Bovine), 9A1 and 11A4) by the relevant PDE enzyme subtype. Yttrium silicate (YSi) scintillation proximity (SPA) beads bind selectively to 5'-[^{3}H] AMP or 5'-[^{3}H] GMP, with the magnitude of radioactive counts being directly related to PDE enzymatic activity. The assay

was performed in white walled opaque bottom 384-well plates. 1 µl of compound in DMSO was added to each well. Enzyme solution was then added to each well in buffer (in mM: Trizma, 50 (pH7.5); $MgCl_2$, 1.3 mM) containing Brij 35 (0.01% (v/v)). For PDE1B1 the assay buffer additionally included $CaCl_2$ (30 mM) and calmodulin (25 U/ml). Subsequently, 20 µl of 3',5'-[^{3}H] cGMP (125 nM) or 20 µL of 3',5'-[^{3}H] cAMP (50 nM) was added to each well to start the reaction and the plate was incubated for 30 min at 25^{o}C. The reaction was terminated by the addition of 20 µl of PDE YSi SPA beads (Perkin Elmer). Following an additional 8 hour incubation period the plates were read on a MicroBeta radioactive plate counter (Perkin Elmer) to determine radioactive counts per well.

Data Analysis

Inhibition curves were plotted from individual experiments, and IC_{50} values were determined using a four parameter logistic fit. IC_{50} is defined as the concentration of the test article that produced a 50% inhibition of a maximal response. All PDE selectivity data is in the Supporting Information.

PDE2A Brain Tissue Binding Assay

Saturation binding experiments were conducting using membranes from dissected striatal regions of rat, dog and monkey). Initial tissue concentration curve studies were conducted and it was determined that 1.5 mg/mL for rat and 2.5 mg/mL for dog and monkey was ideal for each species, respectively. Frozen tissue was weighed into 50 mM Tris buffer (pH 7.4 at 4°C) containing 2.0 mM $MgCl_2$, homogenized using a Polytron and then spun in a centrifuge at 40,000 x g for 10 min. The pellet was re-suspended in assay buffer (50 mM Tris buffer @ pH 7.5 containing 1.3 mM $MgCl_2$). Incubations were initiated by the addition of 200 µl of pre-determined tissue concentration to 25 µl of increasing concentrations of **78**, along with 25 µl of

either DMSO buffer or 10 μM of **1** (a specific PDE2 inhibitor). After a 30 min incubation period at room temperature, assay samples were rapidly filtered through Unifilter-96 GF/BK PEI-coated filter plates and rinsed with ice-cold 50 mM Tris buffer (pH 7.4 at 4°C). Membrane bound **78** levels were determined by liquid scintillation counting of the filterplates in Ecolume. Once the Kd was determined, time course studies were conducted to ensure parameters were linear and at equilibrium by using a 30 min incubation.

Behavioral Assays

Male Long Evans rats from Charles River Laboratories (Kingston, NY) ranged between 200-225 g upon arrival and between 400-450 g during the study. Animals were individually housed in environmentally-controlled quarters (light/dark – 0600 h/1800 h) for one week prior to initiation of experiments.

Spontanous Locomotor activity

Locomotor activity was measured in 48 custom-made automated activity chambers (30 cm x 30 cm) housed in sound-attenuating cabinets and equipped with photocells and a metal touchplate. A single 15 watt bulb in each cabinet was controlled by a 24 hour timer which allows the behavioral chambers to be maintained on a 0400 h/1600 h light/dark cycle. Horizontal activity was measured as crossovers from one quadrant of the cage floor to another, while vertical locomotor activity (ie rears) was measured as the number of times an animal stood up on its hind legs against the walls of the chamber,making contact with the metal touchplate. Data were recorded, stored, and analyzed by a computer equipped with LabView software.

Radial Arm Maze

Animals were food-restricted (25-30 g rodent chow/day) beginning 7 days prior to the first day of exposure to the maze. The eight arm radial maze (Pathfinder Maze System, Lafayette Instrument

Co., Lafayette, IN) contained a food cup at the end of each arm, the contents of which were not visible from the central platform. The task required that the animals enter each arm to retrieve the food pellets and use spatial cues in the room in order to remember which arms of the maze they have previously entered. Permanent visual queues existed within each test room. During training, one reinforcement pellet was placed in the food cup at the end of each arm. Animals were placed on the maze facing away from the experimenter, facing the same arm at the start of each trial. The timer was started and each arm entry was recorded in sequence. An entry was defined as all four paws entering an arm of the maze. The animal was allowed to choose arms until all eight arms were entered and pellets were consumed, until 30 choices were made, or until 5 min had elapsed, which ever event occurred first. Entry into an arm previously chosen was counted as an error. If an animal failed to choose all eight arms in 5 min, the arms not chosen were also counted as errors. Animals were trained once a day on five days per week (Monday-Friday) and the training criterion was defined as 2 or fewer errors on 2 consecutive training days.

Maze Testing: Once the training criterion was met by all subjects (approximately 15 days of training), drug testing was initiated. On Mondays and Thursdays all animals were tested to identify those qualified for testing of experimental sybstances on Tuesdays and Fridays. No testing was performed on Wednesdays. Animals which committed two or fewer errors on qualifying days were randomly assigned to treatment groups and were subjected to drug testing by an experimenter who was blinded as to each animal's treatment. After each qualifying day, animals to be tested were again randomly assigned to treatment groups and were tested the following day. This procedure was repeated until the number for each group equaled at least 10, which typically took between 3 and 4 test days.

Electrophysiology assay: Cortical Delta Oscillation

Animals and surgical procedures

Male Sprague–Dawley rats (Harlan, USA; weighing 250–320 g) under urethane anesthesia @ 1.5 g/kg intraperitoneal (IP), were placed in a stereotaxic frame, where craniotomies were performed above the region of the medial prefrontal cortex (mPFC) and ipsilateral (CA)1/subiculum. Body temperature of the rat was maintained at 37°C with an electrical heating pad (Harvard Apparatus, USA). The femoral vein was cannulated for administration of test drugs. After the conclusion of the experiments animals were euthanized with an IV bolus of urethane. All surgical procedures were conducted in accordance with an approved animal use protocol in compliance with the Animal Welfare Act Regulations and with the Guide for the Care and Use of Laboratory Animals, National Institutes of Health guidelines.

Electrophysiological Recordings

Unilateral hippocampal EEG was recorded by a metal, monopolar macro electrode (Rhodes Medical Instruments, Inc., Model SNEX-300) placed in the mPFC region (co-ordinates: 3.4 mm anterior from the bregma, 0.6 mm lateral from the midline and 5.0 mm ventral) as described previously (Kiss et al, 2011). Field potentials were amplified, filtered (0.1-100 Hz), displayed and digitized at 2000 Hz for on-line and off-line analysis (Spike2 program; Cambridge Electronic Design, Cambridge, UK). Electrically evoked responses distinguished in the EEG and quantitative EEG analysis was performed by means of waveform averages and Fast Fourier Transformation, respectively (Spike2 program). Power spectrum density of the spontaneous EEG was computed in the delta, or 0-4 Hz frequency range over the same time periods used to measure the PPF responses. The EEG activity in normal rats under urethane anesthesia during baseline activity is a synchronous, sinusoidal oscillation which ranges from 1.8 to 2.4 cycles per

second (Hz). Following MK-801 administration, the cortical EEG shifts within the delta band to a less synchronous, higher amplitude signal of 0.5-1.8 Hz. Disruption of the cortical EEG following MK-801 injection was quantified by calculating the percentage of total power that occurred in the 0.5-1.8 Hz frequency range compared to the entire 0-4 Hz Delta band.

Paired-Pulse Stimulus, Waveform Averages, Data Analysis and Statistics

Twisted, stainless steel, bipolar stimulating electrodes were placed in the CA1/subiculum, (co-ordinates: 5.4 mm posterior from the bregma, 5.0 mm lateral and 8.0 mm ventral) (Kiss et al, 2011). Paired-pulse stimulation consisted of two square-pulses, duration: 0.1 ms, 0.6-2.5 mA, pair-pulse interval of 100 ms, inter-stimulus interval of 10 s generated continuously from a Master 8 stimulator (A.P.M.I., Jerusalem, Israel). The intensity of the stimulation was adjusted so that size of the P1 response was ~100 μV.

Brain cGMP measures

Brain tissue measurements of cGMP accumulation following drug administration were carried out as previously described (Schmidt et al., 2008).[28] CD-1 mice were sacrificed by focused microwave irradiation of the brain. Regions of interest were isolated and homogenized in 0.5 N HCL followed by centrifugation. Supernatant concentrations of cyclic nucleotides were measured using enzyme immunoassay kits (Cayman Chemical, Ann Arbor, MI). Data were analyzed using a one-way ANOVA followed by Fishers' PLSD test with the criterion for significance set at $p < 0.05$.

Neuropharmacokinetic Studies in Wistar-Hannover or Sprague-Dawley Rats and/or DRC Mice

The in-life portion of these studies were conducted at either Pfizer Inc. (Groton, CT) or Bioduro Inc. (Shanghai, China) while the bioanalytical portions of these studies were conducted at Pfizer Inc. (Groton, CT). Rats received single intravenous (IV) or subcutaneous (SC) doses of **71**. The IV dose was prepared as a solution in 5/5/90, DMSO/Cremaphor/saline or hydroxypropyl-beta-cyclodextrin acidified while the SC dose was prepared as a solution in 20% SBE-BCD +2ME 1N HCl in a volume of 1 mL/kg. Blood samples were collected via cardiac puncture in ethylenediaminetetraacetic acid (EDTA) treated tubes at designated times between 2 min and 24 h while whole brain and/or cerebrospinal fluid (CSF) samples were collected at the same time points as blood via terminal matrix samplings. Plasma was isolated after centrifugation and placed on wet ice, while CSF was collected into tubes via puncture of the cisterna magna and immediately placed on dry ice and brains were rinsed with saline and blotted dry before being placed on dry ice. Thawed whole brain samples were homogenized on ice with water and/or saline 4X the weight as the brain (1:4, w/v). All samples were stored at −80 °C prior to analysis.

Measurement of In Vitro Fractions Unbound

The *in vitro* unbound fractions of **71** were determined in mouse, rat, and human plasma, and in rat brain tissue homogenate using a 96-well equilibrium dialysis method described by Kalvass et al., with the following exceptions at Pfizer Inc. (Groton, CT). Plasma samples were obtained from BioReclamation (Chestertown, MD) and kept frozen until they were thawed and pH was adjusted to ~7.4 prior to dialysis. Mouse, rat, and human plasma was spiked with 1 μM of **71** and each matrix was dialyzed against an equal volume (150 μL) of phosphate buffer at 37 °C for 6 h. Following the incubations, equal volumes (50 μL) of plasma and buffer samples were collected and mixed with 50 μL of buffer or control plasma, respectively, for preparation of separate

mixed matrix samples. Following the incubations, 15 μL of plasma or 45 μL of buffer samples were collected and mixed with 15 or 45 μL of buffer or control plasma, respectively, for preparation of mixed matrix samples. All samples were then precipitated with internal standard in MeCN (200 μL), vortexed, and centrifuged. Supernatants were analyzed using an LC−MS/MS assay.

Brain homogenates were prepared from freshly harvested rat brains following dilution with a 4-fold volume of phosphate buffer and spiked with 5 μM **71**. The homogenate was dialyzed against an equal volume (150 μL) of phosphate buffer at 37 °C for 6 h. Following the incubation, equal volumes (50 μL) of brain homogenate and buffer samples were collected and mixed with 50 μL of buffer or control homogenate, respectively, for preparation of mixed matrix samples. All samples were then precipitated with internal standard in MeCN (200 μL), vortexed, and centrifuged. Supernatants were analyzed using an LC− MS/MS assay. A dilution factor of 5 was applied to the calculation of brain fraction unbound. The brain fraction unbound obtained in rat was used in calculating the unbound fraction of drug in both rat and mouse brain.

Computational Methods

Dihedral angle scans were performed on truncated systems comprised of the phenyl pyrazole with and without a methyl at the N1 position, as well as the NH pyrazole tautomer. The dihedral angle was increased from 0° to 360° in increments of 10° and each resultant structure was optimized at the B3LYP-D3/6-31+G** level of theory[29] followed by single-point energy calculations at the M06-2X/cc-PVDZ level of theory[30] in Jaguar (version 8.7, Schrödinger, LLC, New York, NY, 2015). Conformational strain energies were calculated as follows: 1) the tautomers (**40** and **42**) and **41** were overlaid with the bound conformation of Q5 from the X-ray co-crystal structure using ROCS (version 3.2.0.4: OpenEye Scientific Software, Santa Fe, NM.

http://www.eyesopen.com) [31] to do a flexible molecular superposition, 2) the dihedral angle was adjusted to the optimal angle from the DFT scan (0° and 30° for the tautomers (**40** and **42**) and 40° for **41**) or constrained to the X-ray co-crystal structure angle (67°), and 3) the energies were calculated at the M06-2X/cc-PVDZ//B3LYP-D3/6-31+G** level of theory. Conformational energy penalties were estimated by subtracting the relative energy at the local minima dihedral angle for the tautomers (**40** and **42**) and **41** from their respective energies at the dihedral angle of the X-ray co-crystal structure, based on Fig. 8.

Protein X-ray crystallography

The catalytic domain of human PDE2A was recombinantly expressed, purified and co-crystallized with 3-isobutyl-1-methylxanthine (IBMX) as previously described.[6] Complexes with other inhibitors were obtained either by soaking (for **3, 4** and **39**) or by co-crystallization (for **1** and **56**). The reservoir solution was used to make a saturated solution of the desired inhibitor for soaking, and one or two crystals of the IBMX complex were soaked in this solution for 2-24 h. Co-crystals with **1** were obtained from the same conditions as the original co-crystals with IBMX, and **39** yielded the best co-crystals in drops that contained a different precipitant (20-25% PEG 8000).

Crystals were flash-frozen in liquid nitrogen, after being briefly dipped in a cryoprotectant solution consisting of the soaking/crystallization buffer supplemented with 25% glycerol.

X-ray diffraction data were collected at 100 K with radiation of wavelength 1.0 Å at the Advanced Photon Source at Argonne National Laboratory, beam line 17ID and were integrated and scaled with programs of the HKL2000 package.[32] Subsequent data manipulations, including

refinement were carried out using the CCP4 suite of programs.[33] All the structures were solved by molecular replacement using the IBMX complex structure (PDB id 3ITU) as the search model. All-atom refinement was done either with Refmac5[34] or autoBUSTER .[35] Details of data collection and refinement statistics are given in the Supplementary Information.

Use of the IMCA-CAT beamline 17- ID at the Advanced Photon Source was supported by the companies of the Industrial Macromolecular Crystallography Association through a contract with Hauptman-Woodward Medical Research Institute. Use of the Advanced Photon Source was supported by the U.S. Department of Energy, Office of Science, Office of Basic Energy Sciences, under Contract No. DE-AC02-06CH11357."

Chemistry Experimental Section

Experiments were generally carried out under inert atmosphere (nitrogen or argon), particularly in cases where oxygen- or moisture-sensitive reagents or intermediates were employed. Commercial solvents and reagents were generally used without further purification, including anhydrous solvents where appropriate (generally Sure-Seal™ products from the Aldrich Chemical Company, Milwaukee, Wisconsin). Mass spectrometry (MS) data is reported from liquid chromatography-mass spectrometry (LCMS) or atmospheric pressure chemical ionization (APCI) instrumentation. Chemical shifts for nuclear magnetic resonance (NMR) data are expressed in parts per million (ppm, δ) referenced to residual peaks from the deuterated solvents employed, or to tetramethylsilane standard with multiplicities given as s (singlet), br (broad), d (doublet), t (triplet), dt (doublet of triplets), q (quintet), m (multiplet). Compound purity is determined by high performance liquid chromatography (HPLC) and all final test compounds were >95% purity. All final compounds were assessed for purity by HPLC via the following

general conditions: **Column**: Waters Atlantis dC18 4.6x50, 5u; Mobile phase A: 0.05% TFA in water (v/v); Mobile phase B: 0.05% TFA in MeCN (v/v); **Gradient**: 95.0% water/5.0% MeCN linear to 5% water/95% MeCN in 4.0min, HOLD at 5% water/95% MeCN to 5.0min. Flow: 2 mL/min.

3-Isobutyl-4-(isoindolin-2-yl)-1-methyl-1H-pyrazolo[3,4-d]pyrimidine (2)

Step 1: 2-(1-hydroxy-3-methylbutylidene)malononitrile (**7**): To a stirred solution of malononitrile (91.5 g, 1.38 mol) in anhydrous THF (2 L) was added sodium hydride (60% dispersion in mineral oil, 121 g, 3.04 mol) in portions below 10 ℃. The resultant mixture was stirred for 1 h, at which point 3-methylbutanoyl chloride (**6**, 200 g, 1.08 mol) was added dropwise while maintaining an internal temperature below 10 ℃. The resultant solution was stirred for 30 min at this temperature, and was then allowed warm to rt where it was stirred overnight. The reaction mixture was acidified with 2 M aqueous HCl to pH 2-3 and was extracted with EtOAc (2 L × 3). The organic layer was washed with brine (1 L) and concentrated to give 157.3 g (76%) of the title compound as an amber liquid. ^{1}H NMR (400 MHz, $CDCl_3$) δ 4.16 (s, 1H), 2.47 (d, 2H, J = 8 Hz), 2.12 (m, 1H), 1.04 (d, J = 6 Hz, 6 H).

Step 2: 2-(1-methoxy-3-methylbutylidene)malononitrile (**8**): Sodium bicarbonate (482 g, 6.03 mol) was added protionwise to a solution of compound **7** (100 g, 0.67 mol) in a mixture of dioxane (770 mL) and water (130 mL). Dimethyl sulfate (575 g, 4.15 mol) was added dropwise while cooling with an ice-bath. The resultant mixture was stirred at room temperature for 3 days. The mixture was filtered and the cake was partitioned between water (1x) and EtOAc (2x). The filtrate was concentrated under reduced pressure to remove dioxane and the aqueous residue was extracted with EtOAc (1 L×4). The combined organic layers were washed with brine (300 mL),

dried over Na_2SO_4 and concentrated to give crude product, which was purified by silica gel chromatography eluting with petroleum ether/EtOAc to afford 370 g (56%) of the title compound as a yellow liquid. ^{1}H NMR (400 MHz, $CDCl_3$) δ 4.14 (s, 1H), 3.95 (s, 3H), 2.54 (d, J = 10 Hz, 2H), 2.02 (m, 1H), 1.05 (d, *J* = 9.2 Hz, 6 H).

Step 3: 3-isobutyl-4-isocyano-1-methyl-1H-pyrazol-5-amine (**9**): To a stirred solution of compound **8** (110 g, 0.67 mol) in ethanol (800 mL) was added methyl hydrazine (61.8 g, 1.34 mol), and the resultant mixture was heated at 65 ˚C for 2 days. The mixture was concentrated and the residue was dissolved in EtOAc (300 mL), washed with water (100 mL) and brine (100 mL), dried over Na_2SO_4 and concentrated under reduced pressure. The crude product was purified by silica gel chromatography eluting with petroleum ether/EtOAc to afford 130 g (35%) of the title compound as a yellow liquid. ^{1}H NMR (400 MHz, $CDCl_3$) δ 3.58 (s, 3H), 2.46 (d, *J* = 7.2 Hz, 2H), 2.03 (m, 1H), 0.95 (d, *J* = 6.4 Hz, 6 H).

Step 4: 5-amino-3-isobutyl-1-methyl-1H-pyrazole-4-carboxamide (**10**): Compound **9** (147 g, 0.826 mol) was added to H_2SO_4 (650 mL) in portions below 10 ℃. After the addition, the resultant mixture was heated to 60 ℃ for 2 h. The reaction mixture was cooled to room temperature and poured into crushed ice. The mixture was carefully basified ammonium hydroxide to pH 9, while adding additional ice as needed. The mixture was left standing overnight, then was filtered. The resultant solid was dissolved in EtOAc (1 L), washed with brine (200 mL), dried over Na_2SO_4 and concentrated to give 55 g of the title compound. The filtrate from above was extracted with EtOAc (3 L×2). The organic layer was washed with brine (1 L), dried over Na_2SO_4 and concentrated to give an additional 55 g of the title compound for a combined yield of 110 g (68%). ^{1}H NMR (400 MHz, $CDCl_3$) δ 5.53 (brs, 2H), 5.28 (m, 2H), 3.48 (s, 3H), 2.45 (d, *J* = 9.6 Hz, 2H), 1.98 (m, 1H), 0.92 (d, *J* = 6.8 Hz, 6 H).

Step 5: 3-isobutyl-1-methyl-1,5-dihydro-4H-pyrazolo[3,4-d]pyrimidin-4-one (**11**): A solution of compound **10** (55 g, 0.28 mol) in formic acid (500 mL) was heated to reflux overnight. The mixture was then concentrated under reduced pressure and the residue was washed with MeOH (60 mL×2) and dried under vacuum to afford 41 g (71%) of the title compound as a white solid. ^{1}H NMR (400 MHz, $CDCl_3$) δ 12.15 (s, 1H), 7.91 (s, 1H), 3.90 (s, 3H), 2.78 (d, *J* = 7.2 Hz, 2H), 2.17 (m, 1H), 0.92 (d, *J* = 6.8 Hz, 6H). LC/MS (M+H): 207.

Step 6: 4-chloro-3-isobutyl-1-methyl-1H-pyrazolo[3,4-d]pyrimidine (**12**): Compound **11** (5 g, 2.41 mmol) was suspended in $POCl_3$ (35 mL) and the mixture was heated at 110 ^{o}C for 4 h. After cooling to rt, excess $POCl_3$ was removed under reduced pressure. To the residue was added dichloromethane (50 mL) and ice cold water (1 mL). The organic layer was separated and aqueous layer was extracted with dichloromethane (20 mL). The combined organic layer was dried over $MgSO_4$ and concentrated to give the crude title product, which was taken onto the next step without purification. ^{1}H NMR (400 MHz, $CDCl_3$) δ 8.72 (s, 1H), 4.11 (s, 3H), 2.99 (d, *J* = 8.0 Hz, 2H), 2.19 (m, 1H), 1.03 (d, *J* = 4.0 Hz, 6H). LC/MS = 225 (M+H).

Step 7: 3-isobutyl-4-(isoindolin-2-yl)-1-methyl-1H-pyrazolo[3,4-d]pyrimidine (2): To a solution of **12** (264 mg, 1.17 mmol) and isoindoline (340 mg, 2.86 mmol) in MeCN (5 mL) was added TEA (0.4 mL). The mixture was stirred overnight at room temperature. The solvent was removed in vacuo and the residue was purified by silica gel chromatography eluting with 4:6 EtOAc/hexane to afford 271 mg (75%) of the title product. ^{1}H NMR (400 MHz, CD_3OD) δ 8.39 (s, 1H), 7.33 (m, 4H), 5.19 (s, 4H), 3.99 (s, 3H), 3.01 (d, *J* = 7.2 Hz, 2 H), 2.01 (m, 1H), 0.95 (d, *J* = 6.8 Hz, 6H). LC/MS = 308 (M+H).

3-Isobutyl-4-(3-(4-methoxyphenoxy)azetidin-1-yl)-1-methyl-1H-pyrazolo[3,4-d]pyrimidine (4). To **12** (773 mg, 3.44 mmol) and 3-(4-methoxyphenoxy)azetidine (617 mg, 3.44 mmol) in THF (16 mL) and water (2 mL) was added K_2CO_3 (435 mg, 0.915 mmol). The mixture was stirred at rt overnight and the organic phase was removed, dried over $MgSO_4$, and concentrated. The crude residue was recrystallized from 2:8 EtOAc/heptane to afford 960 mg (76%) of the title compound as a white solid. ^{1}H NMR (400 MHz, CD_3OD) δ 8.39 (s, 1H), 6.86 (d, *J* = 8.0 Hz, 2H), 6.72 (d, *J* = 8.0 Hz, 2H), 5.05 (m, 1H), 4.77 (m, 2H), 4.42 (m, 2H), 3.96 (s, 3H), 3.78 (s, 3H), 2.76 (d, *J* = 8.0 Hz, 2H), 2.05 (m, 1H), 0.93 (d, *J* = 8.0 Hz, 6H). LC/MS = 368 (M+H).

3-Isobutyl-5-(2-methoxyphenethoxy)-[1,2,4]triazolo[4,3-a]pyrazine (3)

Step 1: 5-chloro-3-isobutyl-[1,2,4]triazolo[4,3-a]pyrazine (29a): To a solution of isovaleraldehyde (**18a**, 714 mg, 8.29 mmol) and 2-chloro-6-hydrazinylpyrazine (**28**, 1000 mg, 6.917 mmol) in dichloromethane (50 mL) was added (diacetoxyiodo)benzene (3.34 g, 10.4 mmol). The reaction solution was stirred at room temperature for 18 h. The reaction mixture was concentrated and purified by silica gel chromatography (Heptane/EtOAc 0-100% gradient) to afford the title compound in 84% yield (1220 mg, 5.79 mmol). ^{1}H NMR (400 MHz, $CDCl_3$) δ 9.21 (s, 1H), 7.81 (s, 1H), 3.36 (d, *J* = 7.02 Hz, 2H), 2.32 (td, *J* = 6.83, 13.66 Hz, 1H), 1.07 (d, *J* = 6.63 Hz, 6H).

Step 2: 3-isobutyl-5-(2-methoxyphenethoxy)-[1,2,4]triazolo[4,3-a]pyrazine (3): To a flame dried flask under a flow of nitrogen was added 2-(2-methoxyphenyl)ethan-1-ol (260 mg, 1.70 mmol). THF (5 ml) was added followed by addition of sodium hydride (60% dispersion in mineral oil, 71 mg, 1.78 mmol). The reaction was stirred at room temperature for 5 min. 5-

chloro-3-isobutyl-[1,2,4]triazolo[4,3-a]pyrazine (300 mg, 1.42 mmol) dissolved in THF (2 ml) was added dropwise and the reaction was stirred at room temperature for 2 h. The reaction was concentrated and the residue purified by silica gel chromatography (Heptane/EtOAc 100%/0% to 0%/100% gradient). Fractions collected to give the title compound in 58% yield (465 mg, 0.827 mmol). ^{1}H NMR (400 MHz, $CDCl_3$) δ 8.88 (s, 1H), 7.28-7.32 (m, 1H), 7.23 (s, 1H), 7.22 (d, *J* = 7.02 Hz, 1H), 6.87-6.99 (m, 2H), 4.52 (t, *J* = 7.02 Hz, 2H), 3.86 (s, 3H), 3.27 (t, *J* = 7.22 Hz, 2H), 3.16 (d, *J* = 7.02 Hz, 2H), 2.23 (td, *J* = 6.68, 13.56 Hz, 1H), 0.99 (d, *J* = 6.63 Hz, 6H). LC/MS = 327.3 (M+H).

Library Synthesis Protocol – Scheme 4

1. Prepare 0.40M aldehyde **18** in 1,2-dichloroethane (DCE).
2. Prepare 0.40M hydrazine **20** in DCE.
3. Prepare 0.20M iodobenzene diacetate in 1,2-dichloroethane (DCE)
4. Dispense 800µL of 0.40M aldehyde solution to the vials.
5. Dispense 800µL of 0.40M hydrazine solution to the vials.
6. Dispense 1250µL of 0.20M iodobenzene diacetate solution.
7. Cover with plastic sheets.
8. Vortex. Please make sure intermediates are in solution before proceeding.
9. Cover with plastic sheet.
10. Set in a fume hood for 2 h with the plastic sheets on.
11. Remove Solvents
12. Dispense 1600µL of DMSO to the vials.
13. Vortex until dissolved.
14. Purify by HPLC.

Resynthesis of library compound 22: 3-(3-(4-(trifluoromethyl)phenyl)-1H-pyrazol-4-yl)-[1,2,4]triazolo[4,3-a]pyrazine. To 2-hydrazinylpyrazine (**20**) (152 mg, 1.38 mmol), 5-(4-trifluoromethyl)phenyl)-1H-pyrazole-4-carbaldehyde (398 mg, 1.66 mmol), and diacetoxyiodobenzene (444 mg, 1.38 mmol) was added dichloromethane (5 mL). The reaction mixture was stirred at room temperature for 16 h. The reaction was then partitioned between dichloromethane and water. The organic layer was dried over anhydrous Na_2SO_4, filtered and concentrated. The residue was purified by silica gel chromatography (EtOAc/Methanol 0-10% gradient) to yield 45 mg (0.136 mmol, 9.9%) of the title compound. ^{1}H NMR (600 MHz, $DMSO_1$) δ 9.46 (d, *J* = 1.32 Hz, 1H), 8.54 (br. s., 1H), 8.19 (dd, *J* = 1.54, 4.61 Hz, 1H), 7.88 (d, *J* = 4.83 Hz, 1H), 7.75 (d, *J* = 7.91 Hz, 2H), 7.68 (br. s., 2H). LC/MS = 331.2 (M+H).

Library Synthesis Protocol – Scheme 5

Step 1. S_NAr by R_1OH

1. Prepare 1.2 M stock solution of core template in anhydrous THF.
2. Prepare 1.2 M stock solution of corresponding alcohols in anhydrous THF.
3. Prepare 1.2 M stock solution of KO-*t*-Bu in THF.
4. Dispense 500 µL (1.0 eqv., 600 µmol) of the corresponding alcohols solution from step 2 into an each single 6 ml tube in a 48-tubes plate.
5. Dispense 600 µL (1.2 equiv, 720 µmol) of KO-*t*-Bu solution from step 3 into the each test tube.
6. The tubes were closed, the reaction mixture was stirred using Vortex at room temp for 30 sec.

7. The new 48-tubes plate was prepared for the template solution
8. Dispense 500 µL (1.0 eqv., 600 µmol) of the core template solution into an each single 6 ml tube in a 48-tubes plate.
9. Open the tubes from step 6, transfer all the amount (1.1 mL) of the THF solution into the each test tube from step 8 portionwise, by 200 µL.
10. The tubes were closed, the reaction mixture was stirred using Vortex at room temp for 30 sec – 1 min.
11. Prepare 0.7 M stock solution of AcOH in DCM.
12. Dispense 900 µL (1.0 eqv., 630 µmol) of the AcOH solution from step 11 into the each test tube from step 10.
13. The reaction mixture was stirred using Vortex at room temp for 30 sec.
14. The solution from step 13 was evaporated in Zymark at ~40 °C for 4 h.

Step 2. Substitution by Hydrazine

15. The tubes with the products from step A (by 600 µmol) were distributed to the 48-tubes plate.
16. 500 µl of EtOH were added into the each tube.
17. 500 µl of hydrazine monohydrate were added into the each tube (the ratio of Hydrazine : EtOH = 1 : 1 is very important).
18. The tubes were closed, the reaction mixture was stirred using Vortex at room temp.
19. The reaction mixture was stirred at 80 °C for 4-5 h.
20. The reaction mixture was cooled to room temperature.
21. The solution from step 20 was evaporated in Zymark at ~50 °C for 4 h.
22. 2 mL of EtOAc were added into the each tube.

23. 500 µl of 5% NaCl aq. solution were added into the each tube.
24. The reaction mixture was stirred using Vortex for 20 sec.
25. Let the mixture to give 2 layers.
26. Transfer 2000µL of top organic layer to Celite column.
27. Do not transfer any water layer (very important).
28. Filter through Celite, collect the fraction.
29. Again, 2 mL of EtOAc were added into the each tube with the water layer.
30. The reaction mixture was stirred using Vortex for 20 sec.
31. Let the mixture to give 2 layers.
32. Transfer 2000µL of top organic layer to the same Celite column.
33. Do not transfer any water layer (very important).
34. Filter through Celite, collect the fraction.
35. Again, 2 mL of EtOAc were added into the each tube with the water layer..
36. The reaction mixture was stirred using Vortex for 20 sec.
37. Let the mixture to give 2 layers.
38. Transfer 2000µL of top organic layer to the same Celite column.
39. Do not transfer any water layer (very important)
40. Filter through Celite, collect the fraction.
41. Fractions from steps 28, 34 and 40 were combined and evaporated in Zymark at ~40 °C for 5 h.

Step 3. Hydrazone formation / Cyclization

42. The tubes with the products from step B (by 600 µmol, really ~100-150 µmol) were distributed to the 48-tubes plate.

43. 500 µl of MeCN were added into the each tube.
44. Prepare 0.3 M stock solution of corresponding aldehydes in anhydrous MeCN.
45. Dispense 500 µL (1.1-1.3 eqv., 150 µmol) of the aldehyde solution into an each single 6 ml tube in a 48-tubes plate.
46. 10 µL of AcOH were added into the each tube.
47. The tubes were closed, the reaction mixture was stirred using Vortex at room temp.
48. The reaction mixture was stirred at room temperature for 2 h.
49. Prepare 0.3 M stock solution of $PhI(OAc)_2$ (iodobenzene diacetate) in anhydrous MeCN.
50. Open the tubes, dispense 500 µL (1.2 eqv., 150 µmol) of the iodobenzene diacetate solution into the each test tube.
51. The tubes were closed, the reaction mixture was stirred using Vortex at room temp.
52. The reaction mixture was stirred at 80 °C for 2 h.

Library Synthesis Protocol – Scheme 6

Step 1: Suzuki Reaction

1. Prepare a solution of 5-iodo-1-methyl-1H-pyrazole **25** (0.1875 M, solution A) in DMF.
2. Prepare a solution of $Pd(dppf)Cl_2$ (0.0375 M, solution B) in DMF.
3. Dispense requisite aryl boronate (225 µmol, 1.5 eq) to 8 mL vials.
4. Dispense Cs_2CO_3 (97 mg, 300 µmol, 2.0 eq) to each vial.
5. Dispense 800 ul of solution A (150 µmol, 1.0 eq) to 8 mL vials.
6. Dispense 200 ul of solution B (7.5 µmol, 0.05 eq) to each vial under nitrogen atmosphere.
7. The reaction solution was bubbled with nitrogen gas for about one min.
8. Cap the vials and shake at 60 °C for 16 h.

9. Spot check by LC-MS.

10. The mixture from the vials was filtered and the filtrate was concentrated with a Speedvac.

11. The residue was purified by prep. TLC (EtOAc/petroleum ether = 1:3) to give substituted pyrazoles **26**.

Step 2: Iodination

12. Dispense substituted pyrazoles **26** to 8 mL vials.

13. Dispense NIS (N-iodosuccinimide, 23 mg, 105 μmol, 1.05 eq) to each vial.

14. Cap the vials and shake at 30 °C for 16 h.

15. Dispense another batch of NIS (13 mg, 50 μmol, 0.5 eq) to each vial.

16. Cap the vials and shake at 80 °C for 16 h.

17. Spot check by LC-MS.

18. The solvent was evaporated off by Speedvac.

19. Water (1.5 mL) was added.

20. The mixture was extracted with EtOAc (1.5 mL X 3). See **Library Synthesis Protocol – Scheme 5**, Steps 14-24.

21. The organic layer was collected, washed with saturated brine (1.5 mL), dried over Na_2SO_4 and was filtered.

22. The filtrate was concentrated to give crude substituted iodopyrazoles **27**, which were used for the next step without further purification.

Step 3: Aldehyde formation

23. The solvent DMF was bubbled with CO (g) to saturation before using.

24. Dispense $Pd(OAc)_2$ (1.1 mg, 5 μmol, 0.05 eq) to 8 mL vials containing the crude substituted iodopyrazoles **27**.

25. Dispense 1,1'-bis-diphenylphosphino-ferrocene (5.5 mg, 10 μmol, 0.1 eq) to each vial.

26. Dispense Et_3N (35 ul, 250 μmol, 2.5 eq) to each vial.

27. Dispense 1 mL of DMF saturated with CO (g) to each vial.

28. Dispense Et_3SiH (35 ul, 200 μmol, 2.0 eq) to each vial.

29. The reaction solution was bubbled with CO (g) for about one min at 0 °C.

30. Cap the vials and shake at 60 °C for 48 h.

31. Spot check by LC-MS.

32. The mixture was concentrated by Speedvac and the residue was purified by prep. TLC (EtOAc/petroleum ether = 1:1) to give title pyrazole aldehdyes

Steps 4/5: Hydrazone formation / Cyclization

33. Dispense 2-hydrazinyl-6-propoxypyrazine (**17a**, 10 mg, 60 μmol, 1.0 eq) to 8 mL vials containing the pyrazole aldehdyes

34. Dispense 300 ul of EtOH to each vial.

35. Cap the vials and shake at 80 °C for 1 h.

36. The reaction mixture was cooled to room temperature.

37. Dispense another 300 ul of EtOH to each vial.

38. Dispense (diacetoxyiodo)benzene (20 mg, 60 μmol, 1.0 eq) to each vial.

39. Cap the vials and shake at 30 °C for 16 h.

40. Spot check by LC-MS.

41. The reaction mixture was concentrated by Speedvac.

42. Purify by HPLC.

General Resynthesis Procedure for compounds prepared via Scheme 5 and 6 Library Synthesis Protocols: Compounds 30-39

Steps 1/2: Hydrazone formation / Cyclization

To a 2 dram vial was added 2-chloro-6-hydrazinylpyrazine (**28**, 1eq), the appropriate aldehyde (1.2eq), and dichloromethane (0.0875M). The reaction was stirred at room temperature for 5 min. (Diacetoxyiodo)benzene (1eq) was added and the reaction was stirred at room temperature for 18 h. Dess-Martin periodinane (1eq) was added and the reaction was allowed to stir at room temperature for 24 h. The reaction mixture was concentrated and subjected to a silica plug using 1:1 Heptane/EtOAc then 100% EtOAc. The eluent from 100% EtOAc wash was collected and carried forward crude.

Step 3: S_NAr by R_1OH

To a 2 dram vial was added the material isolated from step 1 in THF (0.0875M). To the reaction vessel was added the appropriate alcohol (R_1OH, 6 eq) followed by addition of sodium hydride (60% dispersion in mineral oil (3 eq)). The reaction mixture was stirred at room temperature for 3 h. The reaction was diluted with a 2:1 mixture of saturated aqueous NH_4Cl and water. The aqueous was extracted 3x with EtOAc. The organics were combined, dried over anhydrous magnesium sulfate, filtered and concentrated. The samples were purified via reverse phase HPLC (Methods A-D, below).

Purification Condtions

Method A: Compounds 31, **34**, **35**, **36**, **37**, **38**, **39**

Column: Waters XBridge C18 19x100, 5u; Mobile phase A: 0.03% NH_4OH in water (v/v); Mobile phase B: 0.03% NH_4OH in MeCN (v/v);

Gradient: 80.0% H_2O/20.0% MeCN linear to 40% H_2O/60% MeCN in 10.5min, 40% H_2O/60% MeCN linear to 0% H_2O/100% MeCN in 0.5min, HOLD at 0% H_2O/100% MeCN to 12.0min. Flow: 25 mL/min.

Method B: Compound 30

Column: Waters XBridge C18 19x100, 5u; Mobile phase A: 0.03% NH_4OH in water (v/v); Mobile phase B: 0.03% NH_4OH in MeCN (v/v);

Gradient: HOLD at 80.0% H_2O/20.0% MeCN for 1.0 min. 80.0% H_2O/20.0% MeCN linear to 60.0% H_2O/40.0% MeCN in 6.75min, linear to 0% H_2O/100% MeCN to 7.0 min. HOLD at 0% H_2O/100% MeCN from 7.0 to 8.0min. Flow: 30 mL/min.

Method C: Compound 33

(Column: Waters Sunfire C18 19x100, 5u; Mobile phase A: 0.05% trifluoroacetic acid (TFA) in water (v/v); Mobile phase B: 0.05% TFA in MeCN (v/v);

90.0% H_2O/10.0% MeCN linear to 50% H_2O/50% MeCN in 8.5min, 50% H_2O/50% MeCN linear to 0% H_2O/100% MeCN in 0.5min, HOLD at 0% H_2O/100% MeCN to 10.0min. Flow: 25 mL/min.

Method D: Compound 32

(Column: Waters Sunfire C18 19x100, 5u; Mobile phase A: 0.05% TFA in water (v/v); Mobile phase B: 0.05% TFA in MeCN (v/v);

75.0% H_2O/25.0% MeCN linear to 35% H_2O/65% MeCN in 8.5min, HOLD at 0% H_2O/100% MeCN to 10.0min. Flow: 25 mL/min.

Isolated yield, ^{1}H NMR and MS data for resynthesized library compounds from Schemes 5 and 6.

3-Isobutyl-5-propoxy-[1,2,4]triazolo[4,3-a]pyrazine (30): 20.4 mg, 8.7% yield. ^{1}H NMR (600 MHz, DMSO-d6) δ 8.89 (s, 1H), 7.44 (s, 1H), 4.32 (t, *J* = 6.37 Hz, 2H), 3.14 (d, *J* = 7.03 Hz, 2H), 2.15 (td, *J* = 6.92, 13.40 Hz, 1H), 1.88 (qd, *J* = 7.08, 13.89 Hz, 2H), 1.06 (t, *J* = 7.47 Hz, 3H), 0.93 (d, *J* = 6.59 Hz, 6H). LC/MS = 235.2 (M+H).

5-Propoxy-3-(3-(4-(trifluoromethyl)phenyl)-1H-pyrazol-4-yl)-[1,2,4]triazolo[4,3-a]pyrazine (31): 1.5 mg, 8.8% yield. ^{1}H NMR (600 MHz, DMSO-d6) δ 9.04 (s, 1H), 8.25 (br. s., 1H), 7.62 (br. s., 2H), 7.51-7.59 (m, 2H), 7.45 (s, 1H), 3.98 (br. s., 2H), 1.40 (br. s., 2H), 0.59 (br. s., 3H). LC/MS = 389.1 (M+H).

5-(2-Methoxyphenethoxy)-3-(3-(4-(trifluoromethyl)phenyl)-1H-pyrazol-4-yl)-[1,2,4]triazolo[4,3-a]pyrazine (32): 36.8 mg, 20.7% yield. ^{1}H NMR (400 MHz, cd_3od) δ 8.91 (s, 1H), 8.05 (s, 1H), 7.54-7.60 (m, 2H), 7.47-7.54 (m, 2H), 7.36 (s, 1H), 7.02-7.20 (m, 1H), 6.85 (d, *J* = 8.22 Hz, 1H), 6.64-6.73 (m, 2H), 4.19 (t, *J* = 6.26 Hz, 2H), 3.76 (s, 3H), 2.78 (t, *J* = 6.26 Hz, 2H). LC/MS = 481.2 (M+H).

5-Propoxy-3-(3-(p-tolyl)-1H-pyrazol-4-yl)-[1,2,4]triazolo[4,3-a]pyrazine (33): 13.4 mg, 9.6% yield. ^{1}H NMR (400 MHz, $CDCl_3$) δ 8.99 (s, 1H), 7.87 (s, 1H), 7.25 (d, *J* = 8.20 Hz, 2H), 7.13 (s, 1H), 7.04 (d, *J* = 7.80 Hz, 2H), 3.86 (t, *J* = 6.44 Hz, 2H), 2.28 (s, 3H), 1.52 (sxt, *J* = 7.02 Hz, 2H), 0.70 (t, *J* = 7.41 Hz, 3H). LC/MS = 335.2 (M+H).

3-(1-Methyl-5-(p-tolyl)-1H-pyrazol-4-yl)-5-propoxy-[1,2,4]triazolo[4,3-a]pyrazine (34): 4.4 mg, 9.2% yield. ^{1}H NMR (600 MHz, DMSO-d6) δ 8.94 (s, 1H), 7.79 (s, 1H), 7.44 (s, 1H), 7.20-7.25 (m, 2H), 7.16-7.20 (m, 2H), 4.15 (t, *J* = 6.15 Hz, 2H), 3.84 (s, 3H), 2.28 (s, 3H), 1.60 (qd, *J* = 6.88, 13.62 Hz, 2H), 0.71 (t, *J* = 7.25 Hz, 3H). LC/MS = 349.2 (M+H).

3-(1-Methyl-5-(4-(trifluoromethyl)phenyl)-1H-pyrazol-4-yl)-5-propoxy-[1,2,4]triazolo[4,3-a]pyrazine (35): 2.1 mg, 5.7% yield. ^{1}H NMR (600 MHz, DMSO-d6) δ 8.95 (s, 1H), 7.88 (s, 1H), 7.76 (d, *J* = 8.35 Hz, 2H), 7.61 (d, *J* = 7.91 Hz, 2H), 7.49 (s, 1H), 4.19 (t, *J* = 6.15 Hz, 2H), 3.88 (s, 3H), 3.31 (s, 7H), 1.57-1.69 (m, 2H), 0.73 (t, *J* = 7.47 Hz, 3H). LC/MS = 403.1 (M+H).

3-(1-Methyl-5-phenyl-1H-pyrazol-4-yl)-5-propoxy-[1,2,4]triazolo[4,3-a]pyrazine (36): 1.1 mg, 3.3% yield. ^{1}H NMR (600 MHz, DMSO-d6) δ 8.94 (s, 1H), 7.82 (s, 1H), 7.45 (s, 1H), 7.31-7.42 (m, 5H), 4.15 (t, *J* = 6.15 Hz, 2H), 3.85 (s, 3H), 1.54-1.64 (m, 2H), 0.71 (t, *J* = 7.47 Hz, 3H). LC/MS = 335.2 (M+H).

3-(1-Methyl-5-phenyl-1H-pyrazol-4-yl)-5-propoxy-[1,2,4]triazolo[4,3-a]pyrazine (37): 2.6 mg, 9.8% yield. ^{1}H NMR (600 MHz, DMSO-d6) δ 8.95 (s, 1H), 7.82 (s, 1H), 7.46 (s, 1H), 7.42 (dd, *J* = 5.49, 8.57 Hz, 2H), 7.23 (t, *J* = 8.79 Hz, 2H), 4.17 (t, *J* = 6.15 Hz, 2H), 3.84 (s, 3H), 1.62 (qd, *J* = 7.01, 13.67 Hz, 2H), 0.72 (t, *J* = 7.47 Hz, 3H). LC/MS = 353.2 (M+H).

3-(5-(4-Methoxyphenyl)-1-methyl-1H-pyrazol-4-yl)-5-propoxy-[1,2,4]triazolo[4,3-a]pyrazine (38): 2.4 mg, 7.6% yield. ^{1}H NMR (600 MHz, DMSO-d6) δ 8.95 (s, 1H), 7.88 (s, 1H), 7.76 (d, *J* = 8.35 Hz, 2H), 7.61 (d, *J* = 7.91 Hz, 2H), 7.49 (s, 1H), 4.19 (t, *J* = 6.15 Hz, 2H), 3.88 (s, 3H), 1.63 (qd, *J* = 6.88, 13.62 Hz, 2H), 0.73 (t, *J* = 7.47 Hz, 3H). LC/MS = 365.2 (M+H).

3-(5-(4-Ethylphenyl)-1-methyl-1H-pyrazol-4-yl)-5-propoxy-[1,2,4]triazolo[4,3-a]pyrazine (39): 4.1 mg, 7.0% yield. ^{1}H NMR (600 MHz, DMSO-d6) δ 8.94 (s, 1H), 7.79 (s, 1H), 7.45 (s, 1H), 7.25 (d, *J* = 8.35 Hz, 2H), 7.22 (d, *J* = 8.35 Hz, 2H), 4.15 (t, *J* = 6.15 Hz, 2H), 3.84 (s, 3H), 2.58 (d, *J* = 7.47 Hz, 2H), 1.59 (d, *J* = 7.03 Hz, 2H), 1.15 (t, *J* = 7.47 Hz, 3H), 0.70 (t, *J* = 7.47 Hz, 3H). LC/MS = 363.2 (M+H).

Representative synthesis of compounds of general structure 50

(4,6-Dichloropyrimidin-5-yl)(5-(4-ethylphenyl)-1-methyl-1H-pyrazol-4-yl)methanone (50a).

Step 1: 5-(4-ethylphenyl)-1-methyl-1H-pyrazole (46a)

A mixture of (1-methyl-1H-pyrazol-5-yl)boronic acid (42.8 g, 0.34 mol) and 1-bromo-4-ethylbenzene (63.0 g, 0.34 mol) in DME (1 L) and 2 M sodium carbonate (430 mL) was degassed and purged with nitrogen three times. Then $Pd(PPh_3)_2Cl_2$ (2.4 g, 3.4 mmol) was added and the mixture was purged with nitrogen twice. The reaction mixture was heated to reflux and stirred under nitrogen for 3 h. The mixture was cooled and DME was removed under reduced pressure. Water (500 mL) was added to the residue, then the mixture was extracted with CH_2Cl_2 (3 x 300 mL). the combined organic layers were washed with brine, dried over Na_2SO_4, and concentrated under reduced pressure. The residue was purified by column chromatography (EtOAc : petroleum ether 1:100) to afford 32.0 g (51%) of the title compound as a yellow liquid. ^{1}H NMR ($CDCl_3$, 400 MHz) δ 7.50 (d, *J* = 1.6 Hz, 1H), 7.34 (d, *J* = 6.4 Hz, 2H), 7.28 (d, *J* = 8 Hz, 2H), 6.28 (d, *J* = 1.8 Hz, 1 H), 3.89 (s, 3H), 2.70 (q, *J* = 7.6 Hz, 2H), 1.28 (t, *J* = 7.6 Hz, 3H).

Step 2: 5-(4-ethylphenyl)-1-methyl-1H-pyrazole-4-carbaldehyde (47a)

Dimethylformamide (200 mL) was cooled to 0 ^{o}C and treated with $POCl_3$ (50 g, 0.323 mmol). After the addition, the mixture was warmed to room temperature and stirred for 1 h. To the

solution was added **46a** and the reaction mixture was heated to 120 ^{o}C with stirring overnight. The mixture was cooled to RT at which point the $POCl_3$ and DMF were removed under reduced pressure. The residue was poured into ice-water (500 mL) and the mixture was carefully adjusted to pH = 8 with aqueous saturated sodium carbonate. The mixture was extracted with CH_2Cl_2 (4 x 200 mL). The combined organic layers were washed with brine, dried over Na_sSO_4, and filtered. The filtrate was concentrated under reduced pressure. Silica gel chromatography eluting with EtOAc/petroleum ether afforded 20.0 g (87%) of the title compound as a yellow solid. ^{1}H NMR ($CDCl_3$, 400 MHz) δ 9.60 (s, 1H), 8.03 (s, 1H), 7.37 (d, *J* = 8 Hz, 2H), 7.33 (d, *J* = 8 Hz, 2H), 3.81 (s, 3H), 2.74 (q, *J* = 7.6 Hz, 2H), 1.3 (t, *J* = 7.6 Hz, 3H).

Step 3: (4,6-dichloropyrimidin-5-yl)(5-(4-ethylphenyl)-1-methyl-1H-pyrazol-4-yl)methanol (49a)

n-Butyllithium (2.5 M in hexane, 94 mL, 0.234 mol) was added dropwise to a solution of diisopropylamine (33 mL, 0.234 mol) in THF (350 mL) at -70 ^{o}C. After stirring for 0.5 h, the solution was cooled to -90 ^{o}C and a solution of 4,6-dichloropyrimidine (34.8 g, 0.234 mol) in THF (200 mL) was added dropwise, maintaining the temperature between -70 to -90 ^{o}C, and the resultant solution was stirred for 1 h. To the mixture was added a solution of the aldehyde **47a** (25 g, 0.117 mol) in THF (200 mL) while maintaining an internal temperature between -70 and -90 ^{o}C. Stirring was continued at this temperature for 2 h following the addition. The reaction mixture was quenched with acetic acid (30 g), warmed to rt, and poured into water (600 mL). The organic phase was removed and the aqueous phase was extracted with EtOAc (2 x 250 mL). The combined organic layers were washed with brine, dried over Na_2SO_4, and concentrated. The residue was purified by silica gel chromatography eluting with EtOAc/petroleum ether afford 27.5 g (65%) of the title compound as a yellow solid. ^{1}H NMR ($CDCl_3$, 400 MHz) δ 8.50 (s,

1H), 7.63 (s, 1H), 7.26 (d, *J* = 8 Hz, 2H), 7.12 (d, *J* = 7.2 Hz, 2H), 6.26 (s, 1H), 3.68 (s, 3H), 2.66 (q, *J* = 7.6 Hz, 2H), 1.25 (t, *J* = 7.6 Hz, 3H).

Step 4: (4,6-dichloropyrimidin-5-yl)(5-(4-ethylphenyl)-1-methyl-1H-pyrazol-4-yl)methanone (50a)

To a mixture of **49a** (27.0 g, 74.4 mmol) and $CHCl_3$ (600 mL) was added Dess-Martin periodinane (47.3 g, 112 mmol) in portions at room temperature. After the addition, the reaction mixture was stirred at room temperature for 1 h. The reaction mixture was then filtered and the filtrate was washed sequentially with cold 0.5 M NaOH (700 mL) and brine. The solution was dried over Na_2SO_4, filtered, and concentrated under reduced pressure. Silica gel chromatography eluting with EtOAc/petroleum ether afforded 18.1 g (67%) of the title compound as a white solid. ^{1}H NMR ($CDCl_3$, 400 MHz) δ 8.44 (s, 1 H), 8.18 (s, 1H), 7.12 (m, 4H), 3.69 (s, 3H), 2.61 (q, *J* = 7.6 Hz, 2H), 1.22 (t, *J* = 7.6 Hz, 3H). LC/MS = 361.0 (M+H).

Library Protocol for Synthesis of Compounds in Table 8

1. Amines (HNR_1R_2, 100 μmoleach) were weighed into reaction vials (8 mL).
2. Diisopropyl ethylamine (DIEA) was added to each reaction vial (2 equiv, 200 μmol)
3. **50a** (5.0 mmol) was solubilized in MeCN/DMF (0.333 M final concentration) and distributed to the reaction vials (300 ul, 0.1 mmol., 1.0 eq.).
4. Shake at r.t. for 4 h.
5. Add DIEA to each vial (2 equiv, 200 μmol), then add 50 ul of methyl hydrazine.
6. Shake reaction vials for 18 h. overnight at 75 ^{o}C.
7. After cooling to room temperature, remove reaction vial caps and evaporate solvent. Add 2 mL 1:1 DCE/MeOH and solubilize reaction solids.

8. Filter solution through a solid-phase extraction (SPE) frit.
9. Evaporate solvent again from reaction vials.
10. Solubilize reaction solids again with 2 mL 1:1 DCE/MeOH. Load onto a Biotage ISOLUTE SCX SPE. Elute with 5 ml 1:1 DCE/MeOH, then switch to tared collection racks and elute with 6 ml 1 N TEA in MeOH.
11. Evaporate down the samples.
12. Solubilize crude reaction mixtures in 1 mL DMSO and submit to HPLC purification

Preparative HPLC Purification Methods

A. Column: Waters XBridge C18 19x100, 5u; Mobile phase A: 0.03% NH_4OH in water (v/v); Mobile phase B: 0.03% NH_4OH in MeCN (v/v).

B. Column: Waters Sunfire C18 19x100, 5u; Mobile phase A: 0.05% TFA in water (v/v); Mobile phase B: 0.05% TFA in MeCN (v/v).

C. Solvent Gradients for Compounds **52-59**

   a. **52**: 80.0% H_2O/20.0% MeCN linear to 45% H_2O/55% MeCN in 8.5min, 55% H_2O/50% MeCN linear to 0% H_2O/100% MeCN in 0.5min, HOLD at 0% H_2O/100% MeCN to 10.0min. Flow: 25 mL/min.

   b. **53**: 95.0% H_2O/5.0% MeCN linear to 5% H_2O/95% MeCN in 8.5min, HOLD at 0% H_2O/100% MeCN to 10.0min. Flow: 25 mL/min.

   c. **54**: 80.0% H_2O/20.0% MeCN linear to 50% H_2O/50% MeCN in 8.5min, 50% H_2O/50% MeCN linear to 0% H_2O/100% MeCN in 0.5min, HOLD at 0% H_2O/100% MeCN to 10.0min. Flow: 25 mL/min.

d. **55**: 95.0% H_2O/5.0% MeCN linear to 5% H_2O/95% MeCN in 8.5min, HOLD at 0% H_2O/100% MeCN to 10.0min. Flow: 25 mL/min.

e. **56**: 80.0% H_2O/20.0% MeCN linear to 50% H_2O/50% MeCN in 8.5min, 50% H_2O/50% MeCN linear to 0% H_2O/100% MeCN in 0.5min, HOLD at 0% H_2O/100% MeCN to 10.0min. Flow: 25 mL/min.

f. **57**: 95.0% H_2O/5.0% MeCN linear to 5% H_2O/95% MeCN in 8.5min, HOLD at 0% H_2O/100% MeCN to 10.0min. Flow: 25 mL/min.

g. **58**: 80.0% H_2O/20.0% MeCN linear to 50% H_2O/50% MeCN in 8.5min, 50% H_2O/50% MeCN linear to 0% H_2O/100% MeCN in 0.5min, HOLD at 0% H_2O/100% MeCN to 10.0min. Flow: 25 mL/min.

Assessment of purity via analytical scale HPLC

i. Column: Waters Atlantis C18 4.6×50mm, 5um; Mobile Phase A: 0.05% TFA in water (v/v); Mobile Phase B: 0.05% TFA in MeCN (v/v).

ii. Gradient: 95.0% H2O/5.0% MeCN linear to 5.0% H2O/95.0% MeCN in 4.0min, HOLD at 5.0% H2O/95.0% MeCNto 5.0min. Flow: 2 mL/min.

iii. **MS conditions:** MS mode: ESI+ ; scan range 160-1000 Daltons

Number	Prep HPLC Method	Observed MS (M+H)	QC Reten-tion Time (min)	Isolated Quantity (mg)
52	A	374.2668	2.08	6.4
53	A	404.276	2.18	30.2

54	A	447.3123	2.12	24.8
55	A	388.2807	2.13	12.8
56	A	431.3308	1.82	18.6
57	A	404.2774	2.37	20.8
58	A	417.3148	1.93	13.6

General Procedure A for resynthesis of compounds of generic structure **44** from **50**

Step 1: **50** (1 equivalent) dissolved in 20 volumes of MeCN (ml/gm) cooled to 0 ^{o}C was treated with diisopropylethyl amine (1.05 equivalents) and an amine (1.0 equivalents). The solution was stirred and was allowed to slowly warm to 23 °C overnight. LC/MS showed the desired mass for M + H. The solvent was removed in vacuo and the crude material could be taken directly into the next step or could be purified by silica gel chromatography.

Step 2: 51 (1 equivalent) from the previous step was dissolved in pyridine (10 volumes) and methyl hydrazine (10 equivalents) was added. The solution was heated to 85 ^{o}C for 16 h. After cooling to room temperature, the solvent was removed in vacuo and the crude material was purified by silica gel chromatography or precipitation from heptane. **Note: rotamers are often present with the azetidine which can lead to more complicated ^{1}H NMR spectra and absence of protons or less accurate integration of protons in certain instances.**

Synthesis via General Procedure A of 4-(azetidin-1-yl)-3-(5-(4-ethylphenyl)-1-methyl-1H-pyrazol-4-yl)-1-methyl-1H-pyrazolo[3,4-d]pyrimidine (52). 92% yield over two steps, 1.26 g (92% yield). Precipitated from heptane. ^{1}H NMR (400 MHz, $CDCl_3$) δ 8.32 (s, 1H), 7.67 (s, 1H), 7.28 (d, *J* = 8.0 Hz, 2H), 7.18 (d, *J* = 8.0 Hz, 2H), 4.00 (s, 3H), 3.92 (s, 3H), 2.64 (q, *J* = 7.61 Hz, 3H), 2.26 (td, *J* = 7.71, 15.42 Hz, 4H), 1.23 (t, *J* = 7.61 Hz, 3H). LC/MS = 374.2 (M+H).

4-(Azetidin-1-yl)-1-methyl-3-(1-methyl-5-phenyl-1H-pyrazol-4-yl)-1H-pyrazolo[3,4-d]pyrimidine (68)

Step 1: 1-methyl-5-phenyl-1H-pyrazole. Prepared similarly to **46a**. Purified by silica gel chromatography (4:1 heptane/EtOAc) to afford 1.2 g, 67% yield, of the title compound. ^{1}H NMR (400 MHz, $CDCl_3$) δ 3.91 (s, 3H), 6.33(d, 1H, *J* = 2Hz), 7.45 (m, 5H), 7.54 (d, 1H, *J* = 2Hz). LC/MS = 159 (M+H).

Step 2: 1-methyl-5-phenyl-1H-pyrazole-4-carbaldehyde. Prepared similarly to **47a**. Purified by silica gel chromatography (20:1 to 5:1 petroleum ether/EtOAc) to afford 420 mg, 59% yield, of the title compound. ^{1}H NMR (400 MHz, $CDCl_3$) δ 3.85 (s, 3H), 7.46 (m, 2H), 7.59 (m, 3H), 8.08 (s, 1H), 9.64(s, 1H). LC/MS = 187 (M+H).

Step 3: **(4,6-dichloropyrimidin-5-yl)(1-methyl-5-phenyl-1H-pyrazol-4-yl)methanol.** Prepared similarly to **49a**. Purification by silica gel chromatography (1:3 heptane/EtOAc) afforderd 59 mg, 32% yield, of the title compound. ^{1}H NMR (400 MHz, $CDCl_3$) δ 3.62 (s, 3H), 6.19 (s, 1H), 7.20 (m, 2H), 7.33 (m, 3H), 7.58 (s, 1H), 8.45 (s, 1H). LC/MS = 335 (M+H).

Step 4: (4,6-dichloropyrimidin-5-yl)(1-methyl-5-phenyl-1H-pyrazol-4-yl)methanone. Prepared similarly to **50a**. Crude material was triturated with EtOAc to afford 16 g, 80% yield,

of the title compound. ^{1}H NMR (400 MHz, $CDCl_3$) δ 3.71 (s, 3H), 7.23 (m, 2H), 7.37 (m, 3H), 8.19 (s, 1H), 8.49 (s, 1H). LC/MS = 333 (M+H).

Steps 5 / 6: 4-(azetidin-1-yl)-1-methyl-3-(1-methyl-5-phenyl-1H-pyrazol-4-yl)-1H-pyrazolo[3,4-d]pyrimidine (68). Prepared according to General Procedure A. Purified by silica gel chromatography (EtOAc / MeOH, 200:1 to 50:1); 75 mg, 82% yield. ^{1}H NMR (400 MHz, $CDCl_3$) δ 8.31 (s, 1H), 7.68 (s, 1H), 7.35 (m, 4H), 4.12 (d, *J* = 7.03 Hz, 1H), 3.98 (s, 3H), 3.95-3.85 (br s, 3H, azetidine N-CH_2 protons), 3.92 (s, 3H), 2.25 (quin, *J* = 7.71 Hz, 2H)). LC/MS = 346.1 (M+H).

4-(Azetidin-1-yl)-1-methyl-3-(1-methyl-5-(p-tolyl)-1H-pyrazol-4-yl)-1H-pyrazolo[3,4-d]pyrimidine (69)

Step 1: 5-(4-methylphenyl)-1-methyl-1H-pyrazole. Used same method as for **46a**. Purified by silica gel chromatography (100:1 petroleum ether/EtOAc) to afford 55.0 g, 73% yield, of the title compound as a yellow liquid. ^{1}H NMR (400 MHz, $CDCl_3$) δ 2.42 (s, 3H), 3.89 (s, 3H), 6.29 (d, *J* = 1.8 Hz, 1H), 7.29 (br AB quartet, J_{AB} = 8 Hz, 4H), 7.52 (d, *J* = 2.0 Hz, 1H).

Step 2: 1-methyl-5-(p-tolyl)-1H-pyrazole-4-carbaldehyde. Used same method as for **47a**. Purification by silica gel chromatography (100:1 to 30:1 petroleum ether/EtOAc) afforded 28.2 g, 81% yield, of the title compound as a yellow solid. ^{1}H NMR (400 MHz, $CDCl_3$) δ 2.46 (s, 3H), 3.81 (s, 3H), 7.33 (quartet, *J* = 8, 17 Hz, 4H), 8.04 (s, 1H), 9.60 (s, 1H).

Step 3: (4,6-dichloropyrimidin-5-yl)(1-methyl-5-(p-tolyl)-1H-pyrazol-4-yl)methanol. Used same method as for **49a**. Purification by recrystallization of crude material from EtOAc afforded 82.0 g, 78% yield, of the title compound as a white solid. ^{1}H NMR (400 MHz, $CDCI_3$) 2.39 (s, 3H), 3.72 (s, 3H), 6 26 (s, 1H), 7.17 (br dd, *J* = 8, 32 Hz, 4H), 7.66 (s, 1H), 8.55 (s, 1H).

Step 4: (4,6-dichloropyrimidin-5-yl)(1-methyl-5-(p-tolyl)-1H-pyrazol-4-yl)methanone. Used same method as for **50a.**. Purification of the crude product by recrystallization from MeOH afforded 31.3 g, 53% yield, of the title compound as a pale yellow solid. ^{1}H NMR (400 MHz, $CDCl_3$) δ 8.49 (s, 1H), 8.15 (s, 1H), 7.07-7.15 (br AB quartet, *J*„A=8 Hz, *J*„B=8 Hz, 4H), 3.69 (s, 3H), 2.33 (s, 3H). LC/MS = 346.9 (M+H).

Steps 5 and 6: Prepared according to General Procedure A. 4-(azetidin-1-yl)-1-methyl-3-(1-methyl-5-(p-tolyl)-1H-pyrazol-4-yl)-1H-pyrazolo[3,4-d]pyrimidine (69). Final compound purified via silica gel chromatography (Gradient: 0 to 30% MeOH in dichloromethane) to provide 200 mg (97% yield, two steps) of the title compound as a colorless oil. ^{1}H NMR (400 MHz, $CDCl_3$) δ 8.32 (s, 1H), 7.67 (s, 1H), 7.20 (br dd, *J* = 8.1, 33 Hz, 4H), 3.99 (s, 3H), 3.91 (s, 3H), 3.75-4.04 (br m, 4H), 2.34 (br s, 3H), 2.21-2.30 (m, 2H). LC/MS = 360.5 (M+H).

4-(Azetidin-1-yl)-3-(5-(4-cyclopropylphenyl)-1-methyl-1H-pyrazol-4-yl)-1-methyl-1H-pyrazolo[3,4-d]pyrimidine (70)

Step 1: 5-(4-cyclopropylphenyl)-1-methyl-1H-pyrazole. Used same procedure as for **46a**. Purification by silica gel chromatography (4:1 heptane/EtOAc) afforded 350 mg, 31% yield of the title compound. ^{1}H NMR (400 MHz, CD_3OD) δ 7.52 (s, 1H), 7.34 (d, *J* = 12 Hz, 2H), 7.18 (d, *J* = 8 Hz, 2H), 6.29 (s, 1H), 3.90 (s, 3H), 1.97 (m, 1H), 1.05 (m, 2H), 0.78 (m, 2H). LC/MS = 199 (M+H).

Step 2: 5-(4-cyclopropylphenyl)-1-methyl-1H-pyrazole-4-carbaldehyde. Used the same procedure as for **47a**. The final product was purified by silica gel chromatography eluted with petroleum ether/EtOAc (20:1 ~ 5:1) to afford 390 mg, 98% yield, of the title compound as an oil. ^{1}H NMR (400 MHz, CD_3OD) δ 9.61 (s, 1H), 8.05 (s, 1H), 7.25 (d, *J* = 12 Hz, 2H), 7.15 (d, *J* = 8 Hz, 2H,), 3.82 (s, 3H), 1.96 (m, 1H), 1.05 (m, 2H), 0.81 (m, 2H). LC/MS = 227 (M+H).

Step 3: (5-(4-cyclopropylphenyl)-1-methyl-1H-pyrazol-4-yl)(4,6-dichloropyrimidin-5-yl)methanol. Used same procedure as for **49a**. Purification by silica gel chromatography afforded 120 mg, 18% yield. ^{1}H NMR (400 MHz, CD_3OD) δ 8.56 (s, 1H), 7.64 (s, 1H), 7.25 (d, *J* = 12 Hz, 2H), 7.12 (d, *J* = 8 Hz, 2H), 6.26 (s, 1H), 3.83 (s, 3H), 1.97 (m, 1H), 1.08 (m, 2H), 0.75 (m, 2H). LC/MS = 377 (M+H).

Step 4: (5-(4-cyclopropylphenyl)-1-methyl-1H-pyrazol-4-yl)(4,6-dichloropyrimidin-5-yl)methanone. Used same procedure as for **50a**. Purification of crude material by triturating with EtOAc afforded 14 g, 70% yield, of the title compound. ^{1}H NMR (400 MHz, $CDCl_3$) δ 8.45 (s, 1H), 8.14 (s, 1H), 7.07 (d, *J* = 8 Hz, 2H), 6.96 (d, *J* = 8 Hz, 2H), 3.67 (s, 3H), 1.84 (m, 1H), 1.00 (m, 2H), 0.66 (m, 2H). LC/MS = 372.9 (M+H).

Steps 5 and 6: 4-(azetidin-1-yl)-3-(5-(4-cyclopropylphenyl)-1-methyl-1H-pyrazol-4-yl)-1-methyl-1H-pyrazolo[3,4-d]pyrimidine (70). Synthesized using General Procedure A. Purification by silica gel chromatography (200:1 to 50:1 EtOAc/MeOH) afforded a solid, 57 mg (0.148 mmol), 79% yield over two steps. Note: more complicated spectra due to rotamers. Integrations may not be accurate. ^{1}H NMR (400 MHz, $CDCl_3$) δ 8.27 (s, 1H), 7.62 (s, 1H), 7.19 (d, *J* = 8.2 Hz, 2H), 6.99 (d, *J* = 8.2 Hz, 2H), 4.08 (m, 1H), 3.95 (s, 3H), 3.92-3.75 (br m, 3H), 3.86 (s, 3H), 2.22 (m, 2H), 1.8 (m, 2H), 1.21 (t, *J* =7.12 Hz, 1.25 H), 0.95 (m, 1.9 H), 0.66 (m, 1.9 H). ^{13}C NMR (101 MHz, $CDCl_3$) δ 157.9, 154.8, 153.9, 145.0, 142.8, 140.1, 135.9, 129.3, 125.8, 125.7, 113.7, 100.9, 37.8, 33.8, 17.0, 15.2, 9.6. LC/MS = 386.1 (M+H).

4-(Azetidin-1-yl)-1-methyl-3-(1-methyl-5-(4-(trifluoromethyl)phenyl)-1H-pyrazol-4-yl)-1H-pyrazolo[3,4-d]pyrimidine (71)

Step 1: 1-methyl-5-(4-(trifluoromethyl)phenyl)-1H-pyrazole. Prepared similarly to **46a**. Purified by silica gel chromatography (4:1 heptane-EtOAc) to afford 1.4 g, 55 % yield, of the title compound as an oil. ^{1}H NMR (400 MHz, $CDCl_3$) δ 7.76 (d, *J* =12 Hz, 2H,), 7.57 (m, 3H), 6.39(d, *J* = 4 Hz, 1H,), 3.94 (s, 3H). LC/MS = 227 (M+H).

Step 2: 1-methyl-5-(4-(trifluoromethyl)phenyl)-1H-pyrazole-4-carbaldehyde. Prepared similarly to **47a**. Purification by silica gel chromatography (20:1 to 5:1 petroleum ether/EtOAc afforded 390 mg, 58% yield, of the title compound as a solid. ^{1}H NMR (400 MHz, $CDCl_3$) 9.68 (s, 1H) 8.09 (s, 1H), 7.86 (d, 2H, *J* = 8 Hz), 7.61 (d, 2H, *J* = 8 Hz), 3.86 (s, 3H). LC/MS = 255 (M+H).

Step 3: (4,6-dichloropyrimidin-5-yl)(1-methyl-5-(4-(trifluoromethyl)phenyl)-1H-pyrazol-4-yl)methanol. Prepared similarly to **49a**. Purification by silica gel chromatography (1:1 heptane/EtOAc) afforded 120 mg, 38% yield, of the title compound as a solid. ^{1}H NMR (400 MHz, $CDCl_3$) 8.51 (s, 1H), 7.65 (d, 2H, *J* = 8 Hz), 7.54 (s, 1H), 7.39 (d, 2H, *J* = 8 Hz), 6.14 (s, 1H), 3.66 (s, 3H). LC/MS = 403 (M+H).

Step 4: (4,6-dichloropyrimidin-5-yl)(1-methyl-5-phenyl-1H-pyrazol-4-yl)methanone. (4,6-dichloropyrimidin-5-yl)(1-methyl-5-(4-(trifluoromethyl)phenyl)-1H-pyrazol-4-yl)methanol (48.0 g, 0.119 mol) was dissolved in acetone (1 L). CrO_3 (31.7 g, 0.317 mol) was added. The reaction mixture was stirred at room temperature for 1 h. The solvent was evaporated. EtOAc and water were added to the residue. The organic layer was separated, washed with water, dried, and passed through a layer of silica gel. The residue was evaporated to a slurry. The formed crystals were filtered off and washed with ether. This afforded 35.0 g, 73% yield, of the title compound.

^{1}H NMR (400 MHz, $CDCl_3$) δ 8.59 (s, 1H), 8.07 (s, 1H), 7.70 (d, *J* = 8 Hz, 2H), 7.48 (d, *J* = 8 Hz, 2H), 3.77 (s, 3H). LC/MS = 401 (M+H).

Steps 5 and 6: 4-(azetidin-1-yl)-1-methyl-3-(1-methyl-5-(4-(trifluoromethyl)phenyl)-1H-pyrazol-4-yl)-1H-pyrazolo[3,4-d]pyrimidine (71). Synthesized using General Procedure A. Purification by silica gel chromatography (100:1 to 20:1 EtOAc/MeOH) afforded a solid, 4.1 g (9.92 mmol), 86% yield over two steps as a solid. ^{1}H NMR (400 MHz,$CDCl_3$) δ 7.63 (d, *J* = 8.00 Hz, 1H), 7.52 (d, *J* = 8.00 Hz, 1H), 3.98 (s, 3H), 3.92 (s, 3H), 3.89 (brs, ca. 4H), 2.27 (quin, *J* = 7.71 Hz, 2H). LC/MS = 414.4 (M+H).

4-(Azetidin-1-yl)-1-(methyl-t3)-3-(1-methyl-5-(4-(trifluoromethyl)phenyl)-1H-pyrazol-4-yl)-1H-pyrazolo[3,4-d]pyrimidine (78)

Step 1: 4-(azetidin-1-yl)-3-(1-methyl-5-(4-(trifluoromethyl)phenyl)-1H-pyrazol-4-yl)-1H-pyrazolo[3,4-d]pyrimidine (77). (4-(azetidin-1-yl)-6-chloropyrimidin-5-yl)(1-methyl-5-(4-(trifluoromethyl)phenyl)-1H-pyrazol-4-yl)methanone (intermediate prepared in the synthesis of **71**) (999 mg, 2.37 mmol) was dissolved in THF (10 mL), was cooled to 0 ^{o}C, and hydrazine (23.7 mmol, 23.7 mL, 1 M in THF) was added. The solution was allowed to slowly warm to room temperature and was stirred for 16 h. The solvent was removed *in vacuo* and the residue was purified by silica gel chromatography (heptane-EtOAc-MeOH, 100-9-1) to afford 529 mg, 56% yield, of the title compound as a solid. ^{1}H NMR (400 MHz, DMSO-d6) δ ppm 13.54 (s, 1 H), 8.18 (s, 1 H), 7.60 - 7.87 (m, 5 H), 3.89 (s, 3 H), 3.78 (br. s., 3 H), 2.19 (s, 2 H). LC/MS = 400.1, 402.3.

Step 2: 4-(azetidin-1-yl)-1-(methyl-t3)-3-(1-methyl-5-(4-(trifluoromethyl)phenyl)-1H-pyrazol-4-yl)-1H-pyrazolo[3,4-d]pyrimidine (78). A solution of 4-(azetidin-1-yl)-3-(1-methyl-5-(4-(trifluoromethyl)phenyl)-1H-pyrazol-4-yl)-1H-pyrazolo[3,4-d]pyrimidine (see above) (3.4

mg, 8.5 μmol, 2.7 eq) in 0.2 mL of DMF was treated with NaH (60% dispersion in mineral oil, 5.2 mg, 130 μmol, 42 eq) and stirred for 5 min at room temperature. The solution was transferred by syringe to a freshly opened 5 cc ampule containing 250 mCi of tritiated methyl iodide (80 Ci/mmol, 3.1 μmol, 1 eq, purchased from American Radiolabeled Chemicals, Inc., St. Louis, MO 63146) in 0.25 mL of DMF. After 15 min the reaction was diluted with EtOAc, washed twice with H_2O, concentrated *in vacuo* and reconstituted in EtOAc. Liquid scintillation counting (LSC) of the solution indicated the presence of 240 mCi of non-volatile radioactivity which was determined to be chemically and radiochemically impure **78** by HPLC (see HPLC method A below) and radio-TLC (see Radio TLC below).

Half of the crude product solution, 120 mCi, was concentrated and purified by normal phase flash cartridge chromatography (Thomson SINGLE StEP 4.7 g amine flash column, EtOAc eluant) to afford 105 mCi of radiochemically pure **78**. Remaining chemical impurities were removed by reconstitution of the product in 1 mL of 20% MeCN / 80% aq. 0.1% formic acid and purification by reverse phase flash cartridge chromatography (Thomson SINGLE StEP 5.5 g C18 flash column, 1 mL fractions, 20% MeCN / 80% aqueous 0.1% formic acid for 60 mL then linear gradient to 50% MeCN / 50% aq. 0.1% formic acid at 130 mL). The product fractions were combined, partially concentrated to remove MeCN, neutralized with sat. aq. $NaHCO_3$ and extracted with CH_2Cl_2. The organic layer was dried over anhydrous Na_2SO_4, concentrated *in vacuo* and the resulting residue was dissolved in EtOH for storage. LSC analysis of the EtOH solution indicated isolation of 55 mCi of **78**, which was found to be chemically and radiochemically pure by HPLC (see HPLC method B below) and have a specific activity of 82 Ci/mmol by MS (see MS method below).

HPLC method A:

Column: Zorbax SB-CN 4.6 x 150 mm, 5 micron

Column temperature: ambient

Flow rate: 1 mL/min

Detection: UV @ 210 nm, 254 nm and radiochemical by □-RAM

Mobile phase A: 0.1% aq. methanesulfonic acid

Mobile phase B: MeCN

Run time: 10 min

Gradient: initial 90% A, 7 min 10% A, 7.1 min 90% A

Radio-TLC: Thomson Amine plate eluting with EtOAc and AR-2000 radiometric detection

HPLC method B:

Column: Atlantis C18 2.1 x 50 mm, 5 micron

Column temperature: ambient

Flow rate: 1 mL/min

Detection: UV @ 210 nm and radiochemical by □-RAM

Mobile phase A: MeCN

Mobile phase B: H_2O/MeCN/formic acid (98/2/0.1)

Run time: 10 min

MS method information:

Flow rate: 1 mL/min

Mobile phase: H_2O/MeCN/formic acid (98/2/0.1)

Ionization source: ESI+

Scan range: 300-500

4-(Azetidin-1-yl)-1-methyl-3-(1-methyl-5-(5-(trifluoromethyl)pyridin-2-yl)-1H-pyrazol-4-yl)-1H-pyrazolo[3,4-d]pyrimidine (72)

Step 1: 2-(1-methyl-1H-pyrazol-5-yl)-5-(trifluoromethyl)pyridine. A mixture of (1-methyl-1H-pyrazol-5-yl)boronic acid (1.00 g, 7.94 mmol), 2-bromo-5-(trifluoromethyl)pyridine (1.79 g, 7.94 mmol), Bis(triphenylphosphine)palladium(II) dichloride (279 mg, 0.397 mmol), and sodium carbonate (3.37 g, 31.8 mmol) in dimethoxy ethane (30 mL), and water (3 mL) was heated at 90 °C overnight. THE mixture was cooled to RT, and the solvent was removed under vacuum. The residue was dissolved in water and extracted twice with EtOAc. The combined extracts were washed with brine, dried over anhydrous Na_2SO_4. Silica gel chromatography eluting with an EtOAc/heptanes gradient afforded 630 mg (35%) of the title compound. ^{1}H NMR (400 MHz, CD_3OD) δ 8.89 (br d, *J* = 2 Hz, 1H), 8.19-8.23 (m, 1H), 7.94 (br d, *J* = 8.2 Hz, 1H), 7.58 (d, *J* = 2.0 Hz, 1H), 6.60 (d, *J* = 2.2 Hz, 1H), 3.95 (s, 3H).

Step 2: 2-(4-iodo-1-methyl-1H-pyrazol-5-yl)-5-(trifluoromethyl)pyridine. To 2-(1-methyl-1H-pyrazol-5-yl)-5-(trifluoromethyl)pyridine (390 mg, 1.72 mmol) in acetic acid (4 mL) was added N-iodosuccinimide. The mixture was heated to 70 °C for 1 h. The solvent was removed under vacuum, and the crude material was chromatographed over silica gel to afford 524 mg (86%) of the title compound as a white crystalline solid. ^{1}H NMR (400 MHz, CD_3OD) δ 8.83 (br d, *J* = 2 Hz, 1H), 8.17 (br dd, *J* = 8, 2 Hz, 1H), 8.00 (br d, *J* = 8 Hz, 1H), 7.66 (s, 1H), 3.89 (s, 3H). LC/MS = 353. 8 (M+H).

4-(Azetidin-1-yl)-6-chloropyrimidine-5-carbaldehyde (61). A solution of 4,6-dichloropyrimidine-5-carbaldehyde (3.083 g, 17.17 mmol) and DIPEA (2.2g, 2.85 mL, 17.2

mmol) in chloroform (1.4 mL) cooled to 0 °C was treated with azetidine (1.0 g, 1.2 mL, 17 mmol) and then was allowed to warm slowly to room temperature where it was stirred for 16 h. The resulting reaction mixture was filtered to remove a precipitate that had formed, the solution was evaporated, and the residue was purified by silica gel chromatography eluting with a EtOAc / Heptane gradient. This afforded 2.2 grams of the title compound (11.1 mmol, 64% yield). ^{1}H NMR (400 MHz, CD_3OD) δ 10.25 (s, 1H), 8.27 (s, 1H), 8.06 (s, 1H), 4.25-4.10 (br s., 4H), 2.31-2.42 (m, 2H).

Step 3: (4-(Azetidin-1-yl)-6-chloropyrimidin-5-yl)(1-methyl-5-(5-(trifluoromethyl)pyridin-2-yl)-1H-pyrazol-4-yl)methanol. To a solution of 2-(4-iodo-1-methyl-1H-pyrazol-5-yl)-5-(trifluoromethyl)pyridine (50 mg, 0.14 mmol) in THF at -78 °C was added slowly dropwise nBuLi (0.074 mL of a 2.5 M solution in hexanes). The mixture was stirred for 1 h, and then a solution of 4-(azetidin-1-yl)-6-chloropyrimidine-5-carbaldehyde in THF (1 mL) was added. After 1.5 h, the mixture was diluted with water, warmed to rt, and extracted with EtOAc. After washing with brine, the organic material was dried over $MgSO_4$, filtered and concentrated. Silica gel chromatography eluting with 5:1:94 MeOH/Et_3N/dichloromethane afforded 40 mg (66%) of the title compound. ^{1}H NMR (400 MHz, CD_3OD) δ 8.89 (br d, J = 2 Hz, 1H), 8.19-8.23 (m, 1H), 7.94 (br d, J = 8.2 Hz, 1H), 7.58 (d, J = 2.0 Hz, 1H), 6.60 (d, J = 2.2 Hz, 1H), 3.95 (s, 3H).

Step 4: (4-(Azetidin-1-yl)-6-chloropyrimidin-5-yl)(1-methyl-5-(5-(trifluoromethyl)pyridin-2-yl)-1H-pyrazol-4-yl)methanone. To (4-(azetidin-1-yl)-6-chloropyrimidin-5-yl)(1-methyl-5-(5-(trifluoromethyl)pyridin-2-yl)-1H-pyrazol-4-yl)methanol (30 mg, 0.071 mmol) in dichloromethane (2 mL) in an ice bath was added Dess-Martin periodinane (33 mg, 0.078 mmol) After stirring for 1 h, the ice bath was removed and the mixture was stirred overnight. The mixture was diluted with dichloromethane and quenched with satd. $NaHCO_3$ (1 mL) and 1 M

sodium thiosulfate (1 mL). The organic portion was dried over anhydrous Na_2SO_4 and concentrated. Silica gel chromatography (95% EtOAc, 2.5% MeOH, 2.5% TEA) with a 0-100% Heptane gradient to afforded 29 mg (97%) of the title compound, containing minor impurities according to ^{1}H NMR analysis. The material was used in the next step without further purification. ^{1}H NMR (400 MHz, CD_3OD) δ 8.72 (br s, 1H), 8.00-8.13 (m, 3H), 7.89 (d, *J* = 8. 2 Hz, 1H), 3.99-4.07 (m, 4H), 3.78 (s, 3H), 2.30-2.39 (m, 2H). LC/MS = 423.1, 425.2 (M+H).

Step 5: 4-(Azetidin-1-yl)-1-methyl-3-(1-methyl-5-(5-(trifluoromethyl)pyridin-2-yl)-1H-pyrazol-4-yl)-1H-pyrazolo[3,4-d]pyrimidine (72). Prepared using the second step of General Procedure A. Purification by silica gel chromatography, 0-10% MeOH in EtOAc, afforded 2.6 mg, 7.5% yield, of the title compound. ^{1}H NMR (400 MHz, CD_3OD) δ 8.77-8.79 (m, 1H), 8.17 (s, 1H), 8.12-8.16 (m, 1H), 7.85 (d, *J* = 8.2 Hz, 1H), 7.80 (s, 1H), 3.98 (s, 3H), 3.94 (s, 3H), 3.79-4.04 (br m, 4H), 2.25-2.34 (m, 2H). LC/MS = 415.0 (M+H).

4-(Azetidin-1-yl)-3-(5-(5-cyclopropylpyridin-2-yl)-1-methyl-1H-pyrazol-4-yl)-1-methyl-1H-pyrazolo[3,4-d]pyrimidine (73)

Step 1: 5-Cyclopropyl-2-(1-methyl-1H-pyrazol-5-yl)pyridine. Used same procedure as for 2-(1-methyl-1H-pyrazol-5-yl)-5-(trifluoromethyl)pyridine (above). Obtained 1140 mg, 5.72 mmol, 46% yield. ^{1}H NMR (400 MHz, CD_3OD) δ 8.45 (d, *J* = 2.15 Hz, 1H), 7.53-7.57 (m, 1H), 7.46-7.50 (m, 1H), 7.45 (d, *J* = 2.15 Hz, 2H), 6.58 (d, *J* = 2.15 Hz, 1H), 4.07 (s, 3H), 1.98 (tt, *J* = 5.05, 8.51 Hz, 1H), 1.03-1.10 (m, 2H), 0.74-0.80 (m, 2H). LC/MS = 200.0 (M+H).

Step 2: 5-Cyclopropyl-2-(4-iodo-1-methyl-1H-pyrazol-5-yl)pyridine. Used same procedure as for 2-(4-iodo-1-methyl-1H-pyrazol-5-yl)-5-(trifluoromethyl)pyridine (above) which yielded

1.3 g (4 mmol, 84% yield) of a brown oil. ^{1}H NMR (400 MHz, CD_3OD) δ 8.51 (t, *J* = 1.56 Hz, 1H), 7.56-7.59 (m, 2H), 7.54-7.56 (m, 1H), 3.85-3.89 (m, 3H), 2.03 (tt, *J* = 5.05, 8.42 Hz, 1H), 1.05-1.15 (m, 2H), 0.77-0.86 (m, 2H). LC/MS = 325.9 (M+H).

Step 3: (4-(azetidin-1-yl)-6-chloropyrimidin-5-yl)(5-(5-cyclopropylpyridin-2-yl)-1-methyl-1H-pyrazol-4-yl)methanol. A solution of 5-cyclopropyl-2-(4-iodo-1-methyl-1H-pyrazol-5-yl)pyridine (430 mg, 1.32 mmol) in THF (10 mL) at -78 °C was treated dropwise with *n*-BuLi (1.45 mmol, 2.5 M in heptanes). After stirring for 1 hour a solution of the aldehyde **61** (261 mg, 1.32 mmol) in THF (4 mL) was added and the resulting orange solution was stirred for an additional 1.5 h. Water was added to quench the reaction, the mixture was warmed to room temperature, and the aqueous mixture was extracted with EtOAc (1 x 50 mL). The organic layer was dried over Na_2SO_4, was filtered, solvent was evaporated, and the crude material was purified by silica gel chromatography eluting with 5 : 1 : 94 MeOH / Et_3N / dichloromethane to afford the title compound, 167 mg (0.421 mmol, 32% yield). ^{1}H NMR (400 MHz, CD_3OD) δ 8.36 (d, *J* = 2.15 Hz, 1H), 7.83 (s, 1H), 7.49 (s, 1H), 7.37 (dd, *J* = 2.34, 8.20 Hz, 1H), 7.24 (d, *J* = 8.00 Hz, 1H), 6.28 (s, 1H), 4.22 (td, *J* = 7.76, 10.25 Hz, 2H), 3.91 (td, *J* = 7.81, 10.35 Hz, 2H), 3.74 (s, 3H), 2.10-2.22 (m, 2H), 1.90-2.00 (m, 1H), 1.02-1.11 (m, 2H), 0.72-0.80 (m, 2H). LC/MS = 397.1 (M+H).

Step 4: (4-(azetidin-1-yl)-6-chloropyrimidin-5-yl)(5-(5-cyclopropylpyridin-2-yl)-1-methyl-1H-pyrazol-4-yl)methanone). Prepared similarly to **50a.** Isolated 120 mg (0.42 mmol) of the title compound (72% yield). ^{1}H NMR (400 MHz, CD_3OD) δ 8.39 (d, *J* = 1.76 Hz, 1H), 8.02 (s, 1H), 7.93 (s, 1H), 7.31-7.45 (m, 2H), 4.01 (br. s., 4H), 3.73 (s, 3H), 2.30 (s, 2H), 1.90-2.02 (m, 1H), 1.03-1.14 (m, 2H), 0.74-0.82 (m, 2H). LC/MS = 395 (M+H).

Step 5: 4-(azetidin-1-yl)-3-(5-(5-cyclopropylpyridin-2-yl)-1-methyl-1H-pyrazol-4-yl)-1-methyl-1H-pyrazolo[3,4-d]pyrimidine (73). Prepared using the second step of General Procedure A. Purified by silica gel chromatography, using solvent A (90% EtOAc, 5% MeOH, 5% Et_3N), and solvent B (Heptane) with gradient 0-100% A. 50 mg (0.129 mmol, 42% yield). ^{1}H NMR (400 MHz, CD_3OD) δ 8.49 (d, *J* = 2.15 Hz, 1H), 8.12 (s, 1H), 7.67 (s, 1H), 7.23 (dd, *J* = 2.34, 8.20 Hz, 1H), 7.08 (d, *J* = 8.20 Hz, 1H), 4.03 (s, 3H), 3.94 (s, 3H), 3.84 (br s, 3H), 2.19 (quin, *J* = 7.76 Hz, 2H), 1.87-2.05 (m, 1H), 0.97-1.10 (m, 2H), 0.67-0.88 (m, 2H). LC/MS = 387.2 (M+H).

4-(azetidin-1-yl)-3-(5-(5-cyclopropylpyrimidin-2-yl)-1-methyl-1H-pyrazol-4-yl)-1-methyl-1H-pyrazolo[3,4-d]pyrimidine (74)

Step 1: 5-Cyclopropyl-2-(1-methyl-1H-pyrazol-5-yl)pyrimidine. (1-methyl-1H-pyrazol-5-yl)boronic acid (195 mg, 1.55 mmol), 2-chloro-5-cyclopropylpyrimidine (240 mg, 1.55 mmol), sodium carbonate (658 mg, 6.21 mmol), water (1 mL), and 1,2-dimethoxyethane (DME, 10 mL) were mixed and purged with nitrogen, then $Cl_2Pd(PPh_3)_2$ (55 mg, 0.078 mmol) was added and the mixture was heated at reflux for 16 h. Additional portions of boronic acid (50 mg, 0.4 mmol) and $Cl_2Pd(PPh_3)_2$ (10 mg, 0.014 mmol) were added and heating was continued for 3 days. After cooling to room temperature, DME was evaporated, the mixture was diluted with water and was extracted with EtOAc (2 x 200 mL). The organic layer was dried over Na_2SO_4, filtered, and evaporated. The crude mixture was purified by silica gel chromatography to afford the title compound (159 mg, 0.794 mmol, 51% yield) as a pale yellow oil. ^{1}H NMR (400 MHz, CD_3OD) δ 8.57 (s, 2H), 7.46 (d, *J* = 2.15 Hz, 1H), 6.96 (d, *J* = 2.1 Hz, 1H), 4.25 (s, 3H), 1.88-2.01 (m, 1H), 1.05-1.16 (m, 2H), 0.77-0.94 (m, 2H). LC/MS = 200.9 (M+H).

Step 2: 5-Cyclopropyl-2-(4-iodo-1-methyl-1H-pyrazol-5-yl)pyrimidine. 5-cyclopropyl-2-(1-methyl-1H-pyrazol-5-yl)pyrimidine (800 mg, 4.4 mmol) in acetic acid (20 mL) was treated with N-iodosuccinimide (1.090 gm, 4.62 mmol) at room temperature then was heated at 85 ^{o}C for 1h. After cooling to room temperature, the solvent was evaporated, the residue was dissolved in methylene chloride (2 mL) and was purified by silica gel chromatography (1:1 heptane-EtOAc) to afford to 1.3 g (3.99 mmol, 91% yield) of the title compound as a beige solid. ^{1}H NMR (400 MHz, CD_3OD) δ 8.66 (s, 2H), 7.56 (s, 1H), 4.06 (s, 3H), 1.95-2.05 (m, 1H), 1.15 (dd, *J* = 1.95, 8.39 Hz, 2H), 0.86-0.95 (m, 2H). LC/MS = 326.9 (M+H).

Step 3: (4-(Azetidin-1-yl)-6-chloropyrimidin-5-yl)(5-(5-cyclopropylpyrimidin-2-yl)-1-methyl-1H-pyrazol-4-yl)methanol. A solution of 5-cyclopropyl-2-(4-iodo-1-methyl-1H-pyrazol-5-yl)pyrimidine (485 mg, 1.49 mmol) in THF (10 mL) cooled to -78 ^{o}C was treated dropwise with *i*-PrMgCl (1.49 mmol, 0.74 mL, 2 M in THF). After stirring for 1h, the aldehyde **61** (294 mg, 1.49 mmol) in THF (1 mL) was added and the reaction solution was stirred for 1.5 h. Water was added to quench the reaction, the mixture was warmed to room temperature, and the aqueous mixture was extracted with EtOAc (1 x 50 mL). The organic layer was dried over Na_2SO_4 and concentrated. The crude material was purified by silica gel chromatography eluting with 5% of MeOH and 1% of Et_3N in dichloromethane to afford 370 mg (0.93 mmol, 62% yield). ^{1}H NMR (400 MHz, CD_3OD) δ 8.58 (s, 2H), 8.01 (s, 1H), 7.32 (s, 1H), 6.43 (s, 1H), 4.27-4.37 (m, 2H), 4.13 (s, 3H), 4.01-4.11 (m, 2H), 2.21 (quin, *J* = 7.76 Hz, 2H), 1.91-2.02 (m, 1H), 1.09-1.18 (m, 2H), 0.84-0.91 (m, 2H). LC/MS = 398.1 (M+H).

Step 4: (4-(Azetidin-1-yl)-6-chloropyrimidin-5-yl)(5-(5-cyclopropylpyrimidin-2-yl)-1-methyl-1H-pyrazol-4-yl)methanone. (4-(azetidin-1-yl)-6-chloropyrimidin-5-yl)(5-(5-cyclopropylpyrimidin-2-yl)-1-methyl-1H-pyrazol-4-yl)methanol (370 mg, 0.932 mmol) in

methylene chloride (10 mL) at 0 °C was treated portion wise with Dess-Martin periodinane (435 mg, 1.02 mmol). After 1 h the reaction mixture was allowed to warm to room temperature and was stirred for 16 h. The reaction mixture was diluted with methylene chloride, was quenched with saturated sodium bicarbonate (1 mL) and saturated sodium thiosulfate (1 mL), the organic layer was separated, dried over Na_2SO_4, filtered, and the solvent was evaporated. The crude material was purified by silica gel chromatography using solvent mix A (95% EtOAc, 2.5% MeOH, 2.5% Et_3N) in Heptane with a 0-100% gradient to give 267 mg (0.674 mmol) of the title compound (72% yield). ^{1}H NMR (400 MHz, CD_3OD) δ 8.48 (s, 2H), 8.05 (s, 1H), 7.95 (s, 1H), 4.82 (s, 3H), 4.00-4.23 (m, 4H), 3.86 (s, 3H), 2.33 (td, *J* = 7.71, 15.42 Hz, 2H), 1.86-2.01 (m, 1H), 1.10-1.19 (m, 2H), 0.76-0.96 (m, 2H). LC/MS = 396.1 (M+H).

Step 5: 4-(Azetidin-1-yl)-3-(5-(5-cyclopropylpyrimidin-2-yl)-1-methyl-1H-pyrazol-4-yl)-1-methyl-1H-pyrazolo[3,4-d]pyrimidine (74). (4-(azetidin-1-yl)-6-chloropyrimidin-5-yl)(5-(5-cyclopropylpyrimidin-2-yl)-1-methyl-1H-pyrazol-4-yl)methanone (267 mg, 0.674 mmol) in 1,4-dioxane (2.25 mL) at room temperature was treated with methyl hydrazine (95 mg, 109 Na_2SO_4, 2.0 mmol) and the solution was stirred for 1 h. The solvent was evaporated and the residue was purified by silica gel chromatography using a gradient 100%A : 0%B to 0%A : 100%B - A (heptane) : B (90% EtOAc, 5% MeOH, 5% Et_3N) – to afford the title compound in 64% yield, 167 mg (0.431 mmol). ^{1}H NMR (400 MHz, CD_3OD) δ 8.41 (s, 2H), 8.16 (s, 1H), 7.67 (s, 1H), 4.21 (s, 3H), 4.03-4.10 (br m, 2H, a-azetidine N), 3.89 (s, 3H), 2.15 (quin, *J* = 7.76 Hz, 2H), 1.81-1.90 (m, 1H), 1.01-1.09 (m, 1H), 0.98-1.11 (m, 2H), 0.73-0.80 (m, 2H). LC/MS = 388.1 (M+H).

Supporting information:

PDE2A protein x-ray crystal structure data collection and refinement statistics; BAY-60-7550 (**1**) brain exposure in mice; Derivation of estimated human dose equation (Equation 1); number of replicates and standard error of the mean (SEM) for PDE2A IC_{50} data and compound purity by HPLC; impact of pyrazole methylation on dihedral angles; kinase inhibition data for **71**; CEREP Selectivity Data for **71** dosed at 10 uM; PDE Selectivity Data for **1**, **2**, **3**, **4**, **39**, **52**, and **71**; table of rat IV pharmacokinetic data for **71** from Figure 14; PK/PD modeling of **71** in MK-801 disruption of Cortical Delta Oscillation in rat

PDB ID Codes: 5U7D (**1**), 5U7I (**4**), 5U7J (**3**), 5U7K (**39**), 5U7L (**56**). Authors will release the atomic coordinates and experimental data upon article publication

Corresponding Author Information: chris.j.helal@pfizer.com, 860-715-5064

Present/Current Author Addresses:

Michael D. Forman: Michael.forman@yahoo.com Bayer Crop Science

Mihaly Hajos: mihaly.hajos@yale.edu, Dept. of Comparative Medicine, Yale School of Medicine, 310 Cedar St., BML 330, P.O. Box 208016, New Haven CT 06520-8016

William E. Hoffman: wehoffma@gmail.com 10520 SE 42nd CT, Belleview FL, 34420, (353) 347-5464

Zhijun Kang: zkang@mdanderson.org IACS, 3SCR3, MD Anderson, 1881 East Road, Houston, TX 77054, 713-792-8558

Robin J. Kleiman: robin.kleiman@childrens.harvard.edu Boston Children's Hospital, CLSB 13070, 300 Longwood Avenue, Boston, MA 02115, 617 919 6303

Jiemin Lu: lujamie402@yahoo.com 2623 Misty Grove Dr, Manvel, Texas 77578

Noha Maklad: nmaklad@shire.com 300 Shire Way, Lexington, MA 02421 (781) 482-1651

Laura McDowell: laura.mcdowell@novartis.com Emeryville Campus, 5300 Chiron Way, Emeryville, CA 94608-2916 (510) 879-9568

Hirokazu Ueno: hirokazu_ueno@ajinomoto.com, Coordination & Management Group, R&D Planning Dept., AJINOMOTO CO., INC., 15-1 Kyobashi, Tokyo, JAPAN, 104-8315., TEL : +81-3-5250-8134

Acknowledgements: We would like to thank Stephen Jenkinson for the generation of the PDE selectivity data, Lois Chenard for generation of compounds in Table 10, Justin Bellenger for the HPLC purification of compounds in Table 10, and Kevin Parris and Artem Evdokimov for their help with final refinement of the x-ray structures.

Abbreviations Used: C_b, brain concentration; C_{bu}, brain unbound concentration; clogD, calculated logarithm of the partition coefficient at a specific pH; C_p, plasma concentration; C_{pu}, unbound plasma concentration; cpKa, calculated logarithm of the acid dissociation constant; DIS, diversity introduction step; DM, diversity monomer; EEG, electroencephalogram; Fu,b, fraction unbound in brain; Fu,p, fraction unbound in plasma; HLM Cl_{int}, human liver microsome intrinsic clearance (mL/min/kg); kD, dissociation constant; LipE, lipophilic ligand efficiency = $logIC_{50}$ – clogP; MDR BA/AB, ratio of basil to apical/apical to basil flux in cell overexpressing

the multi-drug resistant 1 transporter; mPFC, medial pre-frontal cortex; PFC, pre-frontal cortex; PPF, paired pulse facilitation; RAM, radial arm maze; TPSA, topological polar surface area.

(1) For a recent review of PDE10A inhibitors, see: Chappie, T. A.; Helal, C. J.; Hou, X. Current Landscape of Phosphodiesterase 10A (PDE10A) Inhibition. *J. Med. Chem.* **2012,** *55*, 7299-7331.

(2) Verhoest, P. R.; Chapin, D. S.; Corman, M.; Fonseca, K.; Harms, J. F.; Hou, X.; Marr, E. S.; Menniti, F. S.; Nelson, F.; O'Connor, R.; Pandit, J.; Proulx-LaFrance, C.; Schmidt, A. W.; Schmidt, C. J.; Suiciak, J. A.; Liras, S. Discovery of a Novel Class of Phosphodiesterase 10A Inhibitors and Identification of Clinical Candidate 2-[4-(1-Methyl-4-pyridin-4-yl-1H-pyrazol-3-yl)-phenoxymethyl]-quinoline (PF-2545920)(I) for the Treatment of Schizophrenia. *J. Med. Chem.* **2009,** *52*, 5188-5196.

(3) Verhoest, P. R.; Fonseca, K. R.; Hou, X.; Proulx-Lafrance, C.; Corman, M.; Helal, C. J.; Claffey, M. M.; Tuttle, J. B.; Coffman, K. J.; Liu, S.; Nelson, F. R.; Kleiman, R. J.; Menniti, F.

S.; Schmidt, C. J.; Vanasse-Frawley, M. A.; Liras, S. Design and Discovery of 6-[(3S,4S)-4-methyl-1-(pyrimidin-2-ylmethyl)pyrrolidin-3-yl]-1-(tetrahydro-2H-pyran-4-yl)-1,5-dihydro-4H-pyrazolo[3,4-d]pyrimidin-4-one (PF-04447943) a Selective Brain Penetrant PDE9A Inhibitor for the Treatment of Cognitive Disorders. *J. Med. Chem*. **2012**, *55*, 9045-9054.

(4) Claffey, M. M.; Helal, C. J.; Verhoest, P. R.; Kang, Z.; Bundesmann, M. W.; Hou, X.; Lui, S.; Kleiman, R. J.; Vanase-Frawley, M.; Schmidt, A. W.; Menniti, F.; Schmidt, C. J.; Hoffman, W. E.; Hajos, M.; McDowell, L.; O'Connor, R. E.; MacDougall-Murphy, M.; Fonseca, K. R.; Becker, S. L.; Nelson, F. R.; Liras, S. Application of Structure-Based Drug Design and Parallel Chemistry to Identify Selective, Brain Penetrant, *In Vivo* Active Phosphodiesterase 9A Inhibitors. *J. Med. Chem.* **2012**, *55*, 9055-9068.

(5) Boess, F. G.; Hendrix, M.; van der Staay, F.-J.; Erb, C.; Schreiber, R.; van Staveren, W.; de Vente, J.; Prickaerts, J.; Blokland, A.; Koenig, G. Inhibition of Phosphodiesterase 2 Increases Neuronal cGMP, Synaptic Plasticity and Memory Performance. *Neuropharmacology* **2004,** *47*, 1081-1092.

(6) Masood, A.; Huang, Y.; Hajjhussein, H.; Xiao, L.; Li, H.; Wang, W.; Hamza, A.; Zhan, C.-G.; O'Donnell, J. M. Anxiolytic Effects of Phosphodiesterase-2 Inhibitors Associated with Increased cGMP Signaling. *J. Pharmacol. Exp. Ther.* **2009,** *331*, 690-699.

(7) All reported PDE2A IC_{50} values are the geometric mean of at least three independent IC_{50} determinations unless otherwise noted. The PDE2A3 human splice variant was used for enzyme inhibition studies. PDE1, 3-11 IC_{50} values / % inhibition are the geometric mean of four independent assays. See Supporting Information for full data tables.

(8) Hopkins Andrew, L.; Groom Colin, R.; Alex, A. Ligand Efficiency: a Useful Metric for Lead Selection. *Drug Discovery Today* **2004,** *9*, 430-431.

(9) Edwards, M. P.; Price, D. A. Role of Physicochemical Properties and Ligand Lipophilicity Efficiency in Addressing Drug Safety Risks. *Annu. Rep. Med. Chem.* **2010,** *45*, 381-391.

(10) Feng, B.; Varma, M. V.; Costales, C.; Zhang, H.; Tremaine, L. *In vitro* and *in vivo* Approaches to Characterize Transporter-Mediated Disposition in Drug Discovery. *Expert Opin. Drug Discovery* **2014**, *9*, 873-890.

(11) Reneerkens, O. A. H.; Rutten, K.; Bollen, E.; Hage, T.; Blokland, A.; Steinbusch, H. W. M.; Prickaerts, J. Inhibition of Phoshodiesterase Type 2 or Type 10 Reverses Object Memory Deficits Induced by Scopolamine or MK-801. *Behav. Brain Res.* **2013**, *236*, 16-22.

(12) Zhu, J.; Yang, Q.; Dai, D.; Huang, Q. X-ray Crystal Structure of Phosphodiesterase 2 in Complex with a Highly Selective, Nanomolar Inhibitor Reveals a Binding-Induced Pocket Important for Selectivity, *J. Am. Chem. Soc*. **2013**, *135*, 11708-11711.

(13) Stepan, A. F.; Walker, D. P.; Bauman, J.; Price, D. A.; Baillie, T. A.; Kalgutkar, A. S.; Aleo, M. D. Structural Alert/Reactive Metabolite Concept as Applied in Medicinal Chemistry to Mitigate the Risk of Idiosyncratic Drug Toxicity: A Perspective Based on the Critical Examination of Trends in the Top 200 Drugs Marketed in the United States. *Chem. Res. Toxicol.* **2011,** *24*, 1345-1410.

(14) Zhang, K. Y. J.; Card, G. L.; Suzuki, Y.; Artis, D. R.; Fong, D.; Gillette, S.; Hsieh, D.; Neiman, J.; West, B. L.; Zhang, C.; Milburn, M. V.; Kim, S.-H.; Schlessinger, J.; Bollag, G. A

Glutamine Switch Mechanism for Nucleotide Selectivity by Phosphodiesterases. *Mol. Cell* **2004**, *15*, 279-286.

(15) Shah, F.; Louise-May, S.; Greene, N. Chemotypes Sensitivity and Predictivity of *in vivo* Outcomes for Cytotoxic Assays in THLE and HepG2 Cell Lines. *Bioorg. Med. Chem. Lett.,* **2014**, *24*, 2753-2757.

(16) Patel, S.; Gibson, R. In Vivo Site-Directed Radiotracers: Mini-Review. *Nucl. Med. Biol.* **2008**, *35*, 805-815.

(17) Zhang, L.; Villalobos, A.; Beck, E. M.; Bocan, T.; Chappie, T. A.; Chen, L.; Grimwood, S.; Heck, S. D.; Helal, C. J.; Hou, X.; Humphrey, J. M.; Lu, J.; Skaddan, M. B.; McCarthy, T. J.; Verhoest, P. R.; Wager, T. T.; Zasadny, K. Design and Selection Parameters to Accelerate the Discovery of Novel Central Nervous System Positron Emission Tomography (PET) Ligands and Their Application in the Development of a Novel Phosphodiesterase 2A PET Ligand. *J. Med. Chem.* **2013**, *56*, 4568-4579.

(18) Stephenson, D. T.; Coskran, T. M.; Wilhelms, M. B.; Adamowicz, W. O.; O'Donnell, M. M.; Muravnick, K. B.; Menniti, F. S.; Kleiman, R. J.; Morton, D. Immunohistochemical Localization of Phosphodiesterase 2A in Multiple Mammalian Species. *J. Histochem. Cytochem.* **2009**, *57*, 933-949.

(19) Padovan-Neto, F. E.; Sammut, S.; Chakroborty, S.; Dec, A. M.; Threlfell, S.; Campbell, P. W.; Mudrakola, V.; Harms, J. F.; Schmidt, C. J.; West, A. R. Facilitation of Corticostriatal Transmission Following Pharmacological Inhibition of Striatal Phosphodiesterase 10A: Role of

Nitric Oxide-Soluble Guanylyl Cyclase-cGMP Signaling Pathways. *J. Neurosci*. **2015**, *35*, 5781-5791.

(20) Frank, D. A., Greenberg, M. E. CREB: A Mediator of Long-Term Memory from Mollusks to Mammals. *Cell* **1994**, *79*, 5–8.

(21) Stephenson, D. T.; Coskran, T. M.; Kelly, M. P.; Kleiman, R. J.; Morton, D.; O'Neill, S. M.; Schmidt, C. J.; Weinberg, R. J.; Menniti, F. S. The Distribution of Phosphodiesterase 2A in the Rat Brain. *Neuroscience* **2012,** *226*, 145-155.

(22) Fernandez-Fernandez, D.; Rosenbrock, H.; Kroker, K. S. Inhibition of PDE2A, but Not PDE9A, Modulates Presynaptic Short-Term Plasticity Measured by Paired-Pulse Facilitation in the CA1 Region of the Hippocampus. *Synapse (Hoboken, NJ, U.S.)* **2015,** *69,* 484-496.

(23) Suvarna, N. U.; O'Donnell, J. M. Hydrolysis of N-Methyl-D-Aspartate Receptor-Stimulated cAMP and cGMP by PDE4 and PDE2 Phosphodiesterases in Primary Neuronal Cultures of Rat Cerebral Cortex and Hippocampus. *J. Pharmacol. Exp. Ther.* **2002,** *302,* 249-256.

(24) Hajjhussein, H.; Suvarna, N. U.; Gremillion, C.; Chandler, L. J.; O'Donnell, J. M. Changes in NMDA Receptor-Induced Cyclic Nucleotide Synthesis Regulate the Age-Dependent Increase in PDE4A Expression in Primary Cortical Cultures. *Brain Res.* **2007,** *1149,* 58-68.

(25) Roberts, B. M.; Holden, D. E.; Shaffer, C. L.; Seymour, P. A.; Menniti, F. S.; Schmidt, C. J.; Williams, G. V.; Castner, S. A. Prevention of Ketamine-Induced Working Memory

Impairments by AMPA Potentiators in a Nonhuman Primate Model of Cognitive Dysfunction. *Behav. Brain Res.* **2010**, *212*, 41-48.

(26) Kawashima, H.; Izaki, Y.; Grace, A. A.; Takita, M. Cooperativity Between Hippocampal-Prefrontal Short-Term Plasticity Through Associative Long-Term Potentiation. *Brain Res.* **2006**, *1109*, 37-44.

(27) Kiss, T.; Hoffmann, W. E.; Hajos, M. Delta Oscillation and Short-Term Plasticity in the Rat Medial Prefrontal Cortex: Modelling NMDA Hypofunction of Schizophrenia. *Int. J. Neuropsychopharmacol.* **2011**, *14*, 29-42.

(28) Schmidt, C. J.; Chapin, D. S.; Cianfrogna, J.; Corman, M. L.; Hajos, M.; Harms, J. F.; Hoffman, W. E.; Lebel, L. A.; McCarthy, S. A.; Nelson, F. R.; Proulx-LaFrance, C.; Majchrzak, M. J.; Ramirez, A. D.; Schmidt, K.; Seymour, P. A.; Siuciak, J. A.; Tingley, F. D., III; Williams, R. D.; Verhoest, P. R.; Menniti, F. S. Preclinical Characterization of Selective Phosphodiesterase 10A Inhibitors: a New Therapeutic Approach to the Treatment of Schizophrenia. *J. Pharmacol. Exp. Ther.* **2008,** *325,* 681-690.

(29) Grimme, S.; Antony, J.; Ehrlich, S.; Krieg, H. A Consistent and Accurate Ab Initio Parametrization of Density Functional Dispersion Correction (DFT-D) for the 94 Elements H-Pu. *J. Chem. Phys.* **2010,** *132,* 154104/1-154104/19.

(30) Zhao, Y.; Truhlar, D. G. The M06 Suite of Density Functionals for Main Group Thermochemistry, Thermochemical Kinetics, Noncovalent Interactions, Excited States, and Transition Elements: Two New Functionals and Systematic Testing of Four M06-Class Functionals and 12 Other Functionals. *Theor. Chem. Acc.* **2008,** *120,* 215-241.

(31) Hawkins, P. C. D.; Skillman, A. G.; Nicholls, A. Comparison of Shape-Matching and Docking as Virtual Screening Tools. *J. Med. Chem.* **2007,** *50,* 74-82.

(32) Otwinowski, Z.; Minor, W. Processing of X-ray Diffraction Data Collected in Oscillation Mode. *Methods in Enzymology*; Carter Jr., C.W.; Sweet, R. M., Eds.; Volume 276: Macromolecular Crystallography, Part A; Academic Press: New York, 1997. 307-326.

(33) Bailey, S. The CCP4 Suite: Programs for Protein Crystallography. *Acta Crystallogr., Section D: Biol. Crystallogr.* **1994**, *D50*, 760-763.

(34) Murshudov, G. N.; Vagin, A. A.; Dodson, E. J. Refinement of Macromolecular Structures by the Maximum-Likelihood Method. *Acta Crystallogr., Section D: Biol. Crystallogr.* **1997**, *D53*, 240-255.

(35) Software: Bricogne, G.; Blanc, E.; Brandl, M.; Flensburg, C.; Keller, P.; Paciorek, W.; Roversi, P.; Smart, O. S.; Vonrhein, C.; Womack, T. O. *BUSTER*, 2.11.5; Global Phasing Ltd.: Cambridge, UK, 2011.

Table of Contents graphic

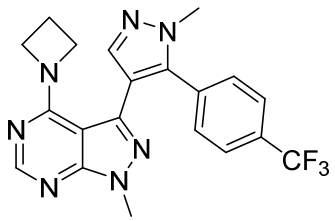

71

PDE2A IC_{50} = 2 nM
PDE1,3-11 selectivity >4000
HLM Cl_{int} = 85 ml/min/kg
MDR BA/AB = 1.4
C_{bu}/C_{pu} = 0.36 (rat)
C_{bu} cGMP EC50, striatum = 70 nM (mouse)
C_{bu} Ketamine RAM = 2.3 - 7 nM (rat)
C_{bu} MK-801 Cortical EEG = 11 nM (rat)